Helmut Wahanik

Advisor: Dan Marchesin IMPA
Co-advisor: Johannes Bruining TUDelft

Efeitos térmicos na injeção de CO_2 em aqüíferos subterrâneos profundos

Thermal effects in the injection of CO_2 in deep underground aquifers

Instituto de Matemática Pura e Aplicada

October 4, 2011

To my father Hans, my mother Esther Lucía and my siblings, Diana, Johanna, Adriana, Werner, and Christian.

Abstract

This work focuses on the physical and mathematical understanding as well as analytical tracking of buoyancy and temperature effects of carbon dioxide injection in deep underground aquifers. Our goal is achieved by applying the theory of hyperbolic conservation laws of continuum physics. We use Riemann solutions for understanding the evolution of wave patterns corresponding to a system of balance laws that takes into account buoyancy effects, energy conservation, and phase redistribution of the components that enforces local thermodynamic equilibrium. An iterative algorithm is applied for computing the vapor-liquid equilibrium of the carbon dioxide-water system. A particular model to describe the correct supercritical conditions for the vapor phase was chosen. Numerical methods for finding the wave curves associated to this system were implemented as computer codes reflecting our theoretical development.

Resumo

Este trabalho focaliza na compreensão física e matemática, bem como no acompanhamento analítico, dos efeitos de empuxo e dos efeitos térmicos provenientes da injeção de dióxido de carbono em aqüíferos subterrâneos profundos. Nosso objetivo é alcançado através da aplicação da teoria das leis de conservação hiperbólicas dos meios continuos. Usamos soluções de Riemann para compreender a evolução dos padrões de onda correspondentes a um sistema de leis de balanço que leva em conta os efeitos de empuxo, conservação de energia e redistribuição das componentes nas diversas fases, que impõe equilíbrio termodinâmico local. Um algoritmo iterativo é aplicado para calcular o equilíbrio entre o líquido e o vapor no sistema composto por dióxido de carbono e água. Um modelo específico foi escolhido para descrever as condições supercríticas corretas da fase vapor. Métodos numéricos foram implementados como códigos computacionais com o objetivo de encontrar as curvas de onda associadas a este sistema, refletindo a teoria desenvolvida para resolver o problema.

Acknowledgements

First I want to thank my advisor, Prof. Dan Marchesin for being supportive and cheerful at all times, and for all of his advice. I want to thank my co-advisor Prof. Hans Bruining, for his generosity in sharing with us his knowledge about transport in porous media and complex thermodynamic processes.

I want to thank Prof. André Nachbin, my initial advisor at IMPA, for his support during the early stages of my doctoral studies, and for introducing me to Applied Mathematics and Fluid Dynamics.

The efforts of a research group at IMPA enabled the design, implementation, and validation of our numerical codes for use in the RPn package. I want to thank Rodrigo Morante, for all his work and dedication in creating powerful computer programs, P. Rodríguez Bermúdez and Pablo Castañeda for his present efforts in coding and accelerating the flash algorithm, and for their work with the `Contour` algorithm. I want to thank also Daniel Albuquerque, Edson L. de Almeida, and Leandro Moreira for their work with the JAVA interface.

I am indebted to A.A. Eftekhari for his generous contribution in the model for phase equilibria of the CO_2-water system, and for the interesting discussions we had with respect to thermodynamics. His enthusiasm with our project has been essential for its success.

Thanks are due to Prof. Fred Furtado, for discussions about Riemann problems, Gibbs free energy minimization, and ideal mixing, to Prof. Vitor Matos, and Júlio D. Machado Silva for their comments on bifurcation theory for Riemann problems, and to Wanderson Lambert for early discussions on compositional flow in porous media.

Special thanks are due to Ankie Telles, Sérgio Pilotto and Sami Vaz, for their support at the Fluid Dynamics Laboratory.

This work was made possible by a Ph.D. Scholarship from CAPES.

I am grateful to Kirsty Morton and Schlumberger for their support in the completion of this work.

The hospitality of the Section of Geo-engineering at Delft University of Technology and the Instituto de Matemtica Pura e Aplicada is gratefully acknowledged.

Contents

Chapter 1
Introduction

Concern about global warming is generating interest in reducing the emissions of greenhouse gases such as carbon dioxide (CO_2). There are many ways of reducing CO_2 emissions. Two particular methods, on which we shall focus in this thesis, are the injection of CO_2 in saline aquifers and the replacement of cold water injection by mixed CO_2/water injection for geothermal energy recovery.

This work focuses on the physical and mathematical understanding as well as on the analytical tracking of buoyancy and temperature effects of CO_2 injection in deep underground aquifers such as saline aquifers and geothermal reservoirs. Our goal is achieved by applying the theory of hyperbolic conservation laws of continuum physics [14] to the transport of CO_2, H_2O and heat in porous media.

We use Riemann solutions for understanding the evolution of wave patterns corresponding to a system of balance laws that takes into account buoyancy effects, energy conservation, and phase redistribution of the components that enforces local thermodynamic equilibrium. An iterative substitution algorithm is applied for computing the vapor-liquid equilibrium (VLE) of the CO_2-H_2O system; a particular model to describe the correct supercritical conditions for the vapor phase is chosen. A family of numerical methods for finding the wave curves associated to this system has been implemented as a computer code reflecting our theoretical development.

There is a large body of engineering literature concerning the injection of carbon dioxide in aquifers. Practical examples are the injection of the separated carbon dioxide produced in the Sleipner gas field (Kongsjorden, Kåarstad et al. [34]; Zweigel, Arts et al. [99]) and the In Salah field in Algeria (Riddiford, Wright et al. [72]). In deep saline aquifers an important aspect to be taken into account is the transfer rate of carbon dioxide to the water phase, because the storage volume of dissolved supercritical carbon dioxide is much lower than gaseous carbon dioxide (R. Farajzadeh [19]; Gmelin's Handbuch [24]). There are only a few references that are concerned with the injection of CO_2 in geothermal reservoirs. Pruess coined the term CO_2-enhanced geothermal systems (EGS) for this type of storage process [66].

Injection of CO_2 in oil reservoirs also provides a mechanism for enhanced oil recovery (EOR) [36] and sequestration [59]. In reservoirs for which the pressure is above

the minimum miscibility pressure this mechanism can be effective [59]. Oil reservoirs are considered good storage locations because of their geological seals. Furthermore, oil fields are often well characterized. Other examples are gas reservoirs and unmineable coalbeds. Deep reservoirs are preferable because they allow the CO_2 to be injected in dense supercritical phase, thus occupying less volume [3, 59].

Supercritical carbon dioxide flow in brine aquifers is dominated by the buoyancy effects enhanced by the differences in the densities of CO_2 and brine (containing different proportions of dissolved salt) [27]. Gravity segregation caused by this difference will induce preferential flow at the top layers of the aquifer [59].[1] We are considering the case of high injection rate so that delay time, due to the cold CO_2 breakthrough at the bottom of the well, is relatively short. Moreover, our interest is confined to layers that are sufficiently thick so that heat exchange effects with the surrounding strata can be disregarded.

The evolution of buoyancy-driven currents have been analyzed by several authors. Norbotten et al. [56] found an analytical solution for the evolution of the CO_2-plume, providing an excellent match with numerical simulations. The physical mechanisms governing the segregation of the different fluids in the reservoir were analyzed by Riaz et al. [71]. Silin et al. [77] found two travelling-wave solutions describing two stable zones at the top and at the bottom of the vertical CO_2 plume, driven by buoyancy, viscous and capillary forces. In Chapter 2 we describe a mathematical model for fluid transport inside a slanted cylindrical core of porous rock representing a scenario of carbon dioxide migration in an aquifer.

In the context of fractional flow theory (Welge [94]), the isothermal horizontal flow of carbon dioxide and water was studied in [55]. In the latter work, compositional shock waves are calculated by finding lines tangent from the injection and initial states to the fractional flux function of the supercritical phase, *i.e.*, Oleinik's construction for scalar conservation laws [57]. In Chapter 3, based on the formulation of Bruining, Marchesin and Van Duijn [12] and Lambert, Marchesin and Bruining [40], we extend the formulation given in [55] by subdividing the flow into three different regions of thermodynamic equilibrium. These are the single phase supercritical configuration (spσ) (*i.e.*, a CO_2-rich supercritical fluid phase with dissolved H_2O; the single phase aqueous configuration (spa) (*i.e.*, a H_2O-rich liquid phase with dissolved CO_2, *i.e.*, "carbonated water") and the two phase configuration (tp); the latter consists of aqueous and supercritical phases subject to local thermodynamic equilibrium. In our formulation, the volumetric flow rate changes abruptly across shocks; this change was not observed in [55]. Shock waves are calculated first in the primary variables of the system, which are chosen among the composition of CO_2 (H_2O) in the supercritical (aqueous) fluid phase $\psi_{\sigma c}$ (ψ_{aw}), the vapor saturation s_σ (and the local temperature of the rock and fluids T for the case treated in Chapter 6, see [39, 40]). From the result we find how the secondary variable u, the seepage velocity, changes across the shock.

[1] Besides stratigraphic traps, other important trapping mechanisms are the dissolution into the water-rich phase and mineralization (adsorption). These mechanisms act in different spatial and temporal time scales [71].

The case corresponding to the vertical isothermal migration of CO_2 was solved in [25] describing a rising plume in a stratified reservoir. The flux entropy condition introduced in [32] is used for choosing the correct left and right flux states at permeability discontinuities. The injected fluid is pure supercritical CO_2, and the fluid initially in the reservoir is pure water. In a new approach, we consider a H_2O-rich aqueous phase in a slanted porous medium slab, and consider the flow subdivided into the different regions of thermodynamic equilibrium. Moreover, even with the inclusion of the gravity term inherited from Darcy's Law[2], the seepage velocity decouples from the other variables in the calculation of shock waves between different equilibrium regions. Unfortunately, it cannot be calculated secondarily across wave-curves, as in the horizontal case. Therefore we must calculate the wave-curves in all variables using the criterion for admissibility of shocks introduced by Liu [48] and Lax [42]. In future work, we intend to use the viscous profile criterion.

Riemann solutions for buoyancy-driven immiscible three-phase flow in porous media were studied by Rodríguez-Bermúdez and Marchesin [73] providing the wave patterns for the space-time evolution of three immiscible fluids with different densities placed in a very long and thin cylinder of porous rock insulated by an impermeable barrier. Such geometries may represent preferential paths for CO_2 migration in heavily fractured and highly heterogeneous reservoirs, such as the reservoir rock consisting of microbial carbonates in the Tupi oil field at the Santos basin off the coast of Brazil [18]. This work is a simplification of reality as no mass transfer between phases is considered.

Migration of carbon dioxide in brine is a particular type of compositional flow. Compositional models for flow in porous media are widely studied in Petroleum Engineering [36]. They describe flows in which the mass transfer of chemicals among phases, and possibly also temperature changes, need to be tracked. Bruining and Marchesin [10], Lambert, Marchesin and Bruining [40] and Lambert and Marchesin ([37], [39]) studied the injection of nitrogen and vapor into a porous medium containing water. The methodology used in these works can also be applied to understand the horizontal transport of CO_2, vapor and water in a cylinder of porous rock surrounded by an impermeable layer. This setting allows us to track the saturation and the heat in the flow, and thus understand the different underlying physical mechanisms. Moreover, the theory provides fundamental understanding of the non-isothermal flow of mixtures undergoing mass transfer among phases.

In order to take into account the heat effects related to the cold fluid injection and the dissolution of CO_2, we must understand the equilibrium of the different components in the phases that appear in the flow. In Chapter 4 we explain in a concise manner all thermodynamic concepts required for the calculation of phase equilibria in a language accessible both to mathematicians and engineers. From basic principles, we develop an alternative more mathematically oriented version of the derivations in Beattie (1948) [6]. Next the classic VLE substitution or flash algorithm is derived; we show how equilibrium states parametrize a 1-D manifold of states. One of our contributions in this thesis consists

[2] H. Darcy formulated this law based on his observations on the flow of water in sands [16].

of obtaining the partial derivatives of the compositions in the different phases up to any order; the results provide essential mathematical and physical information for applying the numerical algorithms presented in Appendix A to thermal or isothermal models of multicomponent multiphase flow in porous media.

The non-ideal behavior of the CO_2-water system has been extensively studied both theoretically and experimentally (Wiebe and Gaddy [97]; King, Mubarak et al. [33]; Bamberger, Sieder et al. [5]; Valtz, Chapoy et al. [90]; Koschel, Coxam et al. [35]). The thermodynamic models used for the prediction of vapor-liquid equilibrium have been reviewed by Orbey and Sandler [58]. Many efforts have been undertaken to find a comprehensive model for predicting the equilibrium composition and density of the different phases appearing in the CO_2-water system for a wide range of temperatures and pressures. Choosing a general model for the calculation of both phase equilibrium and physical properties of a non-ideal mixture would be optimal, but such a model is not yet available. In addition to accuracy, numerical methods for calculating fluid-phase equilibrium should have a relatively fast convergence speed in simulations. The flash substitution method (possibly combined with phase stability tests) is widely used for performing such calculations [50, 51]. Trangenstein [88] uses a minimization algorithm that takes advantage of the special structure of the Gibbs free energy to calculate the thermodynamic equilibrium among phases, which behaves well near critical points and phase boundaries. Moreover this algorithm is computationally faster than substitution algorithms. A tunneling algorithm was used by Nichita et al. [53] for calculating vapor-liquid, liquid-liquid, vapor-liquid-liquid and vapor-liquid-solid equilibrium.

In Chapter 5 we present the generous contribution to our work by A.A. Eftekhari from TUDelft, The Netherlands; a model was chosen and fitted to available experimental data to achieve accurate prediction of the VLE composition and density in each of the phases over a wide range of temperatures and pressures for the CO_2-H_2O system. A modified flash calculation with optimized mixing parameters was used for the computation of thermodynamic equilibrium. While the selected model can predict the composition of different phases very accurately, it can have weaknesses in the accurate prediction of other physical properties, e.g., liquid density. The final correction in the liquid density uses the volume shift parameter introduced in [61].

Aquifer sequestration of carbon dioxide can be combined with production of geothermal energy. The advantages of this process can be twofold: first, the coinjected CO_2 may lead to more efficient heat recovery and secondly, the carbon dioxide injected stays sequestered in the reservoir. In Chapter 6, using a 1-D model for compositional flow and based on the previously obtained VLE data, we investigate the concentration and temperature profiles that would occur in the absence of heat conduction from the surrounding rock in a scenario of mixed CO_2-water injection in a geothermal reservoir, see also Wahanik et al. [92]. Our analysis improves several features of the model studied by Lambert, Marchesin, and Bruining [39]; in particular, all components are present in all phases, and complex equilibrium processes are considered. Our physical data corresponds to a geothermal energy project proposed for heating the buildings of the Technical University

of Delft. There are numerous papers that describe injection of cold water in geothermal reservoirs; here we only mention the classical paper of Lauwerier [41].

Pruess [66] performed a numerical simulation to evaluate the mass flow and heat extraction rates from enhanced geothermal injection-production systems that are operated using either CO_2 or water as heat transmission fluid. There are strong effects of gravity on the mass flow and heat extraction due to the large contrast of CO_2 density at cold and hot conditions. Pritchett [64] examines the heat-sweeping effectiveness in a fractured reservoir with a low porosity. The results show, however, that the heat sweeping efficiency of water is better than that of CO_2 under these conditions [64]. The relative advantage of CO_2 injection in geothermal reservoirs, as a simultaneous storage method is not addressed in these papers.

After injection of the water/CO_2 mixture a complex interaction between physical transport and component redristribution (water and CO_2) occurs between the phases. In the analysis presented in Chapter 6 we do not deal with the presence of salt in the water.

Fractional flow theory is insufficient for solving thermal compositional models, therefore we use the wave curve method as described by Azevedo et al. [2] to determine the Riemann solution for the injection of two-phase mixtures of CO_2/water into porous rock saturated with hot water.

Riemann solutions provide the wave fronts found when studying piecewise constant initial value problems for hyperbolic systems of conservation laws. A complete study of physical phenomena modelled by such solutions is only possible through the implementation of numerical methods for the construction of wave curves for conservation laws.

In a first approach we designed a Matlab® package for finding such wave curves and several bifurcation loci. Prior to the incorporation of the complex VLE data this package used output data of the Quick Thermo method, based on ideal gas principles. The Quick method provides good qualitative equilibrium data, and was fundamental for the development of our Matlab® code. For its description see Appendix D.

Numerical methods were developed for the calculation of the wave curves. They are described in Appendix A. These methods were implemented in the n-dimensional Riemann Problem package (RPn), developed at the Fluid Dynamics Laboratory at IMPA for the creation of a state-of-the-art software in the style of a Computer-Aided-Design (CAD) package for wave curves. The first version of the RPn package, the Riemann Problem package, (RP), was developed since 1979 by E. Isaacson, D. Marchesin, P.J. Paes Leme, and B. Plohr together with many collaborators. The “Evolve”package was designed too by B. Plohr and D. Marchesin for exploring solutions of systems of reaction-convection diffusion equations. Many authors who contributed to the mathematical theory of immiscible three-phase flow utilized these packages. An extended survey of the theory can be found in [49].

The RP package was written initially in Fortran IV and was used for studying quadratic fluxes [76]. Next it was adapted for finding the wave curves for a model for three-phase flow in porous media [31], and was rewritten in Fortran 77. The RP package is a wave curve editor, and works as a CAD package. Besides its core features, it implements the

wave-curve algorithm as well as the viscous profile criterion for shock waves. The first major difficulty encountered in its development was the existence of non-local branches of the Hugoniot locus. Overcoming this difficulty allowed the development of the theory for non-strictly hyperbolic systems of conservation laws: this was required for studying umbilic points appearing in state space for such systems [31].[3]

The RPn is the next generation RP package and its aim is to analyse numerically wave curves for $n \times n$ systems of conservation laws. It has the capability of representing continuous changes in wave space from parameter variations. The numerical core of RPn is written in C++; its graphical interface and core administrator are written in Java. C++ [85] is an Object-Oriented-Programming (OOP) language well suited for building structured numerical algorithms. On the other hand Java [1] supports good graphical and interactive interfaces, portability as well as remote user processing. Our Matlab® code was also used for the verification of these C++ codes.

The numerical methods developed in this work for the study of non-gravitational compositional flow in porous media benefited from the decoupling of the seepage velocity from the other variables in the system of conservation laws. Indeed, we can find projections of the wave curves and their bifurcations in the space of primary variables and afterwards recover the secondary variables. This special feature suggested that several Fortran 77 routines from RP could be directly adapted for incorporation into the RPn package.

Also in Appendix A we describe new theoretical results for systems of conservation laws where the accumulation term is non-trivial, generalizing results of Lambert and Marchesin [37, 39].

[3] Several mathematical areas, such as differential topology, algebraic curve theory, ordinary differential equations, singularity theory, numerical analysis and optimization as well as scientific computing techniques, have been employed for the advance and application of the theory of Riemann solutions for conservation laws [14, 79]. Some of the applications of the theory are gas dynamics, water waves, combustion in porous media, and multiphase flow in porous media.

Chapter 2
The model

Here, we describe a mathematical model for fluid transport inside a thin slanted cylindrical core of porous rock representing a scenario of carbon dioxide migration in an aquifer. In an attempt to represent the observed features of compositional flow [12, 40, 39], we visualize the flow subdivided into three different regions of thermodynamic equilibrium, the spσ, spa and tp configurations, see Fig. 2.1.

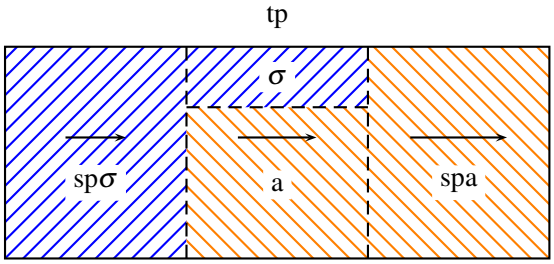

Fig. 2.1 Flow profile subdivided in three regions of thermodynamic equilibrium. The symbol "σ" stands for a CO_2-rich supercritical fluid phase, the symbol "a" represents a H_2O-rich aqueous phase, and the symbol "tp"indicates the region where the pores contain both a supercritical and aqueous phase in thermodynamic equilibrium. The abbreviation "sp"stands for "single phase". Injection occurs on the left and production on the right.

This consideration provides a new insight of the flow regime. Indeed, in the isothermal migration case treated in Chapter 3 we showed how the total volumetric flow rate u changes across discontinuities between the thermodynamic configurations of the flow. This was not observed in other analytical models of CO_2-H_2O porous media flow [55, 25]. A typical injection and initial condition is represented by a region of CO_2-rich supercritical fluid located behind a region of carbonated water. In our model we assume that thermodynamic equilibrium is reached instantaneously along the flow.

In our model we assume that each configuration is in local thermodynamic equilibrium, so we can use Gibbs phase rule, $f = c - p + 2$, where f represents Gibbs number of thermodynamic degrees of freedom, c and p are the number of chemical species and

phases, respectively. In our thermodynamic models the pressure has been fixed, and therefore the remaining number of thermodynamic degrees of freedom $f_{\text{P,T}}$ is reduced by 1.

The reservoir pressures and temperatures considered here are above the UCEP (*Upper Critical End Point*) of the CO_2-H_2O mixture, $(P_{\text{ucep}}, T_{\text{ucep}},)$. For pressures and temperatures above this point, a supercritical phase indistinguishable from gas and liquid substitutes the gas phase. Moreover, at a reference aquifer pressure of 100 [bar] [56], an isobaric thermal transition from a cold CO_2-rich phase to a CO_2-rich supercritical fluid phase would be continuous; this is explained from the fact that at these pressures these two states are found "above" the bubble point curve of the CO_2-H_2O system, see Spycher et al. [82].

In our model the rock porosity φ and permeability k are constant, see Table B.2. Gravity changes the flow: we will observe this effect during the calculation of the total Darcy velocity. We assume that pressure variations along the cylinder are so small that they do not affect the physical properties of the fluids, e.g., fluid density and viscosity.

The 1-D Darcy's law for slanted multiphase flow relates the pressure gradient and gravity acceleration with the seepage velocity:

$$u_\alpha = -\frac{kk_{r\alpha}}{\mu_\alpha}\left(\frac{\partial p_\alpha}{\partial x} + \rho_\alpha g_\beta\right), \qquad \alpha = \sigma, a, \tag{2.1}$$

The symbols "σ" ("a") stand for the supercritical fluid (aqueous) phases respectively. In Eq. (2.1), k is the absolute permeability of the porous medium, $k_{r\alpha}(s_\alpha)$ are the relative permeabilities of phases $\alpha = \sigma, a$, which will be considered functions of the saturation of the corresponding phases (see Eq. (B.3) in Appendix B); μ_α is the viscosity of phase α, the value of which depends on the local fluid temperature; p_α and ρ_α are the pressure and density of phase α. The capillary pressure is $p_c(s_\sigma) \equiv p_\sigma - p_a$. We use the abbreviation $g_\beta \equiv g\sin\beta$, where g is the gravity constant (Table B.2) and β is the angle of the slanted plane with the horizontal. The variable x represents the slanted coordinate of the flow, *i.e.*, $z = x\sin\beta$, where z is the vertical coordinate. Using Darcy's Law (2.1) we obtain:

$$u_\sigma = \frac{m_\sigma}{m_\sigma + m_a}u + k\frac{m_\sigma m_a}{m_\sigma + m_a}(\rho_a - \rho_\sigma)g_\beta - k\frac{m_\sigma m_a}{m_\sigma + m_a}\frac{\partial p_c}{\partial x}, \tag{2.2}$$

where the phase mobilities are defined by $m_\alpha \equiv k_{r\alpha}/\mu_\alpha$ for $\alpha = \sigma, a$. The fractional flow functions, which depend on saturation and temperature, are defined by:

$$f_\sigma = \frac{m_\sigma}{m_a + m_\sigma}, \qquad f_a = \frac{m_a}{m_a + m_\sigma}. \tag{2.3}$$

The total mobility is defined as $m = m_a + m_\sigma$. The saturations of the different phases add to 1. By Eq. (2.3) the same is true for f_σ and f_a. The effect of diffusive terms (related to capillary pressure, thermal conductivity, etc.) is to widen the evaporation front as well as other shocks, while the convergence of the characteristics tries to sharpen the fronts. The balance of these effects yields the front width, which is considered negligible compared to the cylinder length. Therefore we may disregard diffusive terms along the core. Repeating the procedure for the aqueous phase, from (2.2) one obtains:

$$u_\sigma = f_\sigma(s_\sigma)\big(u + km_a(\rho_a - \rho_\sigma)g_\beta\big), \quad u_a = f_a(s_a)\big(u + km_\sigma(\rho_\sigma - \rho_a)g_\beta\big). \tag{2.4}$$

We write the equations for the conservation of total mass of carbon dioxide (appearing in the supercritical fluid phase, as well as dissolved in liquid water) and water (appearing in the aqueous phase and dissolved in the CO_2-rich supercritical fluid phase) as:

$$\frac{\partial}{\partial t}\varphi\left(\rho_{\sigma c}s_\sigma + \rho_{ac}s_a\right) + \frac{\partial}{\partial x}\left(\rho_{\sigma c}u_\sigma + \rho_{ac}u_a\right) = 0, \tag{2.5}$$

$$\frac{\partial}{\partial t}\varphi\left(\rho_{\sigma w}s_\sigma + \rho_{aw}s_a\right) + \frac{\partial}{\partial x}\left(\rho_{\sigma w}u_\sigma + \rho_{aw}u_a\right) = 0. \tag{2.6}$$

where $\rho_{\sigma c}$ ($\rho_{\sigma w}$) [kg/m^3] denotes the (partial) density of carbon dioxide (water) in the supercritical fluid phase, and ρ_{ac} (ρ_{aw}) [kg/m^3] denotes the density of carbon dioxide (water) in the aqueous phase (these partial densities represent mass per unit volume of fluid; other authors prefer to write this systems in terms of the concentrations, *i.e.*, number of moles per unit volume of fluid; the two formulations are equivalent). Using (2.4), we can replace the system of equations (2.5), (2.6) by:

$$\frac{\partial}{\partial t}\varphi\left(\rho_{\sigma c}s_\sigma + \rho_{ac}s_a\right) + \frac{\partial}{\partial x}\Big(u(\rho_{\sigma c}f_\sigma + \rho_{ac}f_a) + (\rho_{\sigma c} - \rho_{ac})Z_\beta\Big) = 0, \tag{2.7}$$

$$\frac{\partial}{\partial t}\varphi\left(\rho_{\sigma w}s_\sigma + \rho_{aw}s_a\right) + \frac{\partial}{\partial x}\Big(u(\rho_{\sigma w}f_\sigma + \rho_{aw}f_a) + (\rho_{\sigma w} - \rho_{aw})Z_\beta\Big) = 0. \tag{2.8}$$

where $Z_\beta = kf_\sigma m_a(\rho_a - \rho_\sigma)g_\beta$.

In Chapter 3 we study a model for isothermal slanted migration. The number of thermodynamic degrees of freedom in each equilibrium configuration is given by the number of components minus the number of phases, as the temperature and pressure are fixed. Therefore in the spσ configuration we only have one degree of freedom, the partial composition of CO_2; for the spa configuration, analogously. In the tp configuration, we have none. We assume local volume conservation throughout the flow; this is applied for establishing mixing rules that will be used to relate the degrees of freedom of the equations (2.7) and (2.8) for single phase configurations.

For the isothermal case each configuration is described by two variables (V,u) where V denotes the supercritical carbon composition $\psi_{\sigma c}$ (see Chapter 3) for the spσ configuration, the aqueous H_2O composition ψ_{aw} for the spa configuration, and s_σ for the tp. In all cases, u is the seepage velocity. For horizontal flow, u decouples from the system, in the sense that it can be calculated along wave-curves from the values of V. In this case we say that V is a primary variable and u is a secondary variable. In the slanted case, u can still be calculated linearly across shock waves but not along wave-curves from the variable V. Therefore, the features of the special decoupling do not apply for the case of slanted migration.

2.1 Energy balance

We can include in our system an equation for the conservation of energy, which tracks temperature variations along the porous core. In this case, the temperature T is allowed to vary in all configurations. Each thermodynamic configuration appearing in the flow is described by three variables, denoted as $W = (V,u)$ where $V = (V_1,V_2)$. In the horizontal flow case, u can be found in terms of the primary variables along wave groups, [39] taking into account boundary conditions.

The equation for the conservation of energy is based on the conservation of enthalpy formulation [7, 8]. We neglect longitudinal heat conduction and heat losses to the surrounding rock. We ignore adiabatic compression and decompression effects. Thus the energy conservation equation is given by:

$$\frac{\partial}{\partial t}\varphi\left(\widehat{H}_r + H_\sigma s_\sigma + H_a s_a\right) + \frac{\partial}{\partial x}\left(H_\sigma u_\sigma + H_a u_a\right) = 0, \tag{2.9}$$

where we have $\widehat{H}_r = H_r/\varphi$, and H_r is the volumetric enthalpy density of the porous rock. Here we use the linearized expression $H_r = C_r(T - T_{\text{ref}}^{\text{rock}})$, where C_r (we denote $\widehat{C}_r = C_r/\varphi$) and $T_{\text{ref}}^{\text{rock}}$ in our examples are given in Table B.2, and H_σ, H_a are the volumetric enthalpy densities of the supercritical phase and of the aqueous phase, respectively (with units [J/m^3]). The volumetric enthalpy density of the supercritical CO_2-rich fluid phase and of the H_2O-aqueous phase are given by the approximate expressions $H_\sigma = \rho_{\sigma c} h_{\sigma C}$ and $H_a = \rho_{aw} h_W$, where $h_{\sigma C}$ [J/kg] is the specific carbon dioxide enthalpy (per unit mass) given by Span and Wagner (1996) [81], and h_W is the specific enthalpy function of water found in the 1967 IFC Formulation for Industrial Use (see [17]). Notice that these expressions embody the assumption that the contribution to the enthalpy in the corresponding phases comes essentially from their predominant components. Both of these enthalpies are obtained in the literature as numerical look-up tables, rather than as explicit functions. Therefore we fitted $h_{\sigma C}$ using Reinsch C^2-splines (Reinsch, 1967 [68]) for use in our Matlab package, and using B-splines [9] for use in the RPn package, and we easily found C_W that fitted the linear expression $h_W = C_W(T - T_{\text{ref}}^{\text{water}})$ using the Matlab® Curve Fitting Toolbox for usage in numerical codes (Chapter 6). The reference temperature $T_{\text{ref}}^{\text{water}}$ approximates the freezing point of pure water at 1 [bar] and was too found by a linear fitting process.

The water specific enthalpy h_W can also be fitted using Reinsch splines, although using them does not improve the resolution. For the numerical values of C_W and $T_{\text{ref}}^{\text{water}}$, see Table B.2 in Appendix B. Using (2.4) we can replace equation (2.9) by

$$\frac{\partial}{\partial t}\varphi\left(\widehat{H}_r + H_\sigma s_\sigma + H_a s_a\right) + \frac{\partial}{\partial x}\left(u(H_\sigma f_\sigma + H_a f_a) + (H_\sigma - H_a)Z_\beta\right) = 0. \tag{2.10}$$

A model for thermal flow including gravity effects is described by the balance equations (2.7), (2.8) and (2.10).

Remark 2.1. See Chapter 6 for the description of the domains of the tp configuration Ω_{tp} and for the spa Ω_{spa}.

2.2 Dimensionless equations

In this section we show the details for finding the dimensionless form of the system given by (2.7), (2.8) and (2.10). This process is essential to the successful application of numerical methods for finding fundamental waves, as the methods described in Appendix A and implemented in the RPn package. Indeed, the quantities conserved by the balance laws in this model differ by various orders of magnitude. For instance, the accumulation terms for the equations of balance of carbon dioxide and water are of the order of 10^3 [kg/m^3], but the accumulation term for the energy balance is of the order of 10^8 [J/m^3], introducing ill conditioning in matrices used in the numerical methods. Indeed, values for $\rho_{\sigma c}$ (ρ_{aw}) for reference reservoir conditions of $T_{res} = 323.15$ [K] and fixed pressure $P_{res} = 100.9$ [bar][1] are 389.23 (950.74) [kg/m^3] respectively and may vary from 879.28 (934.04) [kg/m^3] for 288 [K], and 118.73 (899.13) [kg/m^3] for 450 [K]. On the other hand, the enthalpy per unit volume of the rock ranges from 3.0131×10^7 [J/m^3] at 288 [K] and 3.5883×10^8 [J/m^3] at 450 [K]. The dimensionless form of the system is necessary for numerically robust quantification of the different mechanisms that govern the flow.

Let L_{ref} [m] be a reference length scale of the flow, U_{ref} [m/s] the reference total Darcy velocity, ρ_{ref} [kg/m^3] the reference density, K_{ref} [m^2] the reference absolute permeability, μ_{ref} [Pa· s] the reference viscosity, T_{ref} the reference temperature, and H_{ref} [J/m^3] the reference enthalpy per unit volume.

We define the dimensionless variables and constants as

$$\tilde{x} = x/L_{\text{ref}}, \qquad \tilde{t} = t/t_{\text{ref}}, \qquad \tilde{u} = u/U_{\text{ref}}, \tag{2.11}$$

$$\widetilde{\rho}_{\alpha i} = \rho_{\alpha i}/\rho_{\text{ref}}, \quad \widetilde{\mu}_{\alpha} = \mu_{\alpha}/\mu_{\text{ref}}, \qquad \widetilde{T} = \frac{(T - T_{\text{ref}}^{\text{water}})}{T_{\text{ref}}}, \tag{2.12}$$

$$\widetilde{\rho}_{\alpha} = \rho_{\alpha}/\rho_{\text{ref}}, \qquad \tilde{k} = k/K_{\text{ref}}, \qquad \widetilde{h}_{\iota} = h_{\iota}/h_{\text{ref}}, \tag{2.13}$$

where $i = c, w$, $\alpha = \sigma, a$, and $\iota = \sigma C, W$, and $t_{\text{ref}} := L/U_{\text{ref}}$. We define too the dimensionless mobilities as $\widetilde{m}_{\alpha} = m_{\alpha}\mu_{\text{ref}}$.

From these definitions we obtain $\frac{\partial}{\partial t} = \frac{1}{t_{\text{ref}}}\frac{\partial}{\partial \tilde{t}}$, $\frac{\partial}{\partial x} = \frac{1}{L_{\text{ref}}}\frac{\partial}{\partial \tilde{x}}$. We define

$$\widetilde{Z}_{\beta} = \frac{K_{\text{ref}} g \rho_{\text{ref}}}{\mu_{\text{ref}} U_{\text{ref}}} \left(\tilde{k} f_{\sigma} \widetilde{m}_{a} (\widetilde{\rho}_{\sigma} - \widetilde{\rho}_{a}) \widetilde{g}_{\beta} \right), \tag{2.14}$$

[1] In the Netherlands, there is a geothermal gradient of about 30°C/km leading to a temperature of around 323 [K] at a depth of 1000 m; geothermal pressure gradient is assumed to be hydrostatic with 10 [kPa/m].

where $\widetilde{g}_\beta = sin\ \beta$. Let $C_g := \frac{K_{\text{ref}} g \rho_{\text{ref}}}{\mu_{\text{ref}} U_{\text{ref}}}$.

If we substitute the dimensionless variables and the relations above into equations (2.7), (2.8) and (2.10) we obtain

$$\frac{\partial}{\partial \tilde{t}} \varphi \left(\widetilde{\rho}_{\sigma c} s_\sigma + \widetilde{\rho}_{ac} s_a\right) + \frac{\partial}{\partial \tilde{x}} \left(\tilde{u}(\widetilde{\rho}_{\sigma c} f_\sigma + \widetilde{\rho}_{ac} f_a) + C_g(\widetilde{\rho}_{\sigma c} - \widetilde{\rho}_{ac}) \widetilde{Z}_\beta \right) = 0, \tag{2.15}$$

$$\frac{\partial}{\partial \tilde{t}} \varphi \left(\widetilde{\rho}_{\sigma w} s_\sigma + \widetilde{\rho}_{aw} s_a\right) + \frac{\partial}{\partial \tilde{x}} \left(\tilde{u}(\widetilde{\rho}_{\sigma w} f_\sigma + \widetilde{\rho}_{aw} f_a) + C_g(\widetilde{\rho}_{\sigma w} - \widetilde{\rho}_{aw}) \widetilde{Z}_\beta \right) = 0, \tag{2.16}$$

$$\frac{\partial}{\partial \tilde{t}} \varphi \left(\widetilde{\widetilde{H}}_r + \widetilde{H}_\sigma s_\sigma + \widetilde{H}_a s_a\right) + \frac{\partial}{\partial x} \left(\tilde{u}(\widetilde{H}_\sigma f_\sigma + \widetilde{H}_a f_a) + C_g(\widetilde{H}_\sigma - \widetilde{H}_a) \widetilde{Z}_\beta \right) = 0. \tag{2.17}$$

In our model we choose reference values to fit the injection scenario studied. We focus on thermal flow profiles for small spatial scales which suggests that $L_{\text{ref}} \sim o(1)$ [m]. We use the reference permeability and Darcy velocity proposed by Nordbotten et al. [56]. The reference density of the system is given by the density of pure water at 1 [bar] and 293.15 [K]. The reference temperature is the critical temperature of the CO_2-H_2O system, T_{UCEP}. The reference viscosity correspond to carbon dioxide's at 100 [bar] and 323 [K]. The reference specific enthalpy of the components is given by the specific enthalpy of water at the critical temperature of the system *i.e.*, $h_{\text{ref}} = C_W(T_{\text{ref}} - T_{\text{ref}}^{\text{water}})$ given in [J/m^3]. For the numerical values of these reference constants see Table B.1, in Appendix B.

In the equations above the term C_g reflects gravitational effects. For the cases in which the total velocity is small we can set $U_{\text{ref}} = \frac{K_{\text{ref}} g \rho_{\text{ref}}}{\mu_{\text{ref}}}$, which would imply $C_g = 1$ in (2.17). For the value of C_g obtained from the reference values chosen in our model, see Table B.1 in Appendix B.

After dropping the symbol "$\sim$" we obtain the dimensionless form of the system (2.7)-(2.10)

$$\frac{\partial}{\partial t} \varphi \left(\rho_{\sigma c} s_\sigma + \rho_{ac} s_a\right) + \frac{\partial}{\partial x} \left(u(\rho_{\sigma c} f_\sigma + \rho_{ac} f_a) + C_g(\rho_{\sigma c} - \rho_{ac}) Z_\beta \right) = 0, \tag{2.18}$$

$$\frac{\partial}{\partial t} \varphi \left(\rho_{\sigma w} s_\sigma + \rho_{aw} s_a\right) + \frac{\partial}{\partial x} \left(u(\rho_{\sigma w} f_\sigma + \rho_{aw} f_a) + C_g(\rho_{\sigma w} - \rho_{aw}) Z_\beta \right) = 0, \tag{2.19}$$

$$\frac{\partial}{\partial t} \varphi \left(\widehat{H}_r + H_\sigma s_\sigma + H_a s_a\right) + \frac{\partial}{\partial x} \left(u(H_\sigma f_\sigma + H_a f_a) + C_g(H_\sigma - H_a) Z_\beta \right) = 0. \tag{2.20}$$

The numerical codes in Appendix A were applied to the system (2.18)-(2.20) with $Z_\beta = 0$ for finding the wave curves and their bifurcations in the tp configuration. For the results see Chapters 6 and Chapter 8.

Chapter 3
Isothermal migration with gravity

In this chapter we look for the basic wave structures and their bifurcations corresponding to a model for the evolution of isothermal fluid transport resulting from injection of pressurized CO_2 (*i.e.*, supercritical CO_2) with dissolved water in a slanted porous medium slab saturated with carbonated water.

When a CO_2-rich supercritical fluid phase is injected upstream of a H_2O-rich liquid phase, an intermediate region appears where carbon dioxide and water co-exist in two-phase equilibrium. The Riemann solution consists of a sequence of shocks, rarefactions and/or contact discontinuities including the three phase configurations in thermodynamic equilibrium: from left to right, spσ, tp, and spa. We follow the same methodology used in several previous works [12, 37, 39, 40] for finding the Riemann solution for the initial reservoir states, L and R, respectively in the spσ and spa configurations for the model of isothermal slanted flow given by the equations (2.7) and (2.8) detailed in Chapter 2, thus taking into account buoyancy effects. The assumption of isothermal flow has been introduced in order to illustrate large spatial and temporal scales of migration; together with local thermodynamic equilibrium this fully determines the tp configuration: the flow in this region is governed by the simple modification of the Buckley-Leverett conservation law with gravity:

$$\varphi \frac{\partial}{\partial t} s_\sigma + \frac{\partial}{\partial x} f_\sigma \left(u + k m_a (\rho_a - \rho_\sigma) g_\beta \right) = 0, \tag{3.1}$$

where k is the absolute permeability of the porous medium, m_a is the mobility of the aqueous phase, ρ_σ and ρ_a are the densities of the supercritical and aqueous phases, $g_\beta = g \sin\beta$, where g is the absolute value for the gravity acceleration, and β is the slope of the flow. In (3.1), u is constant along the two-phase region. The expression above permits us derive the principal difference between solving the Riemann problem for horizontal (β=0) and vertical flow: in the latter case the *shape* of the flux elucidates the existence of waves of negative speed: it is intuitively clear that a heavier H_2O-rich aqueous phase may drop over a lighter CO_2-rich supercritical fluid phase.

Due to thermodynamic constraints, the mass balance equations can be simplified considerably in each thermodynamical configuration, e.g. throughout the next sections we will see that u is spatially constant in every configuration and for each one the system of

balance laws reduces to a scalar conservation law of the type:

$$\frac{\partial}{\partial t}\mathbf{G}(V)+\frac{\partial}{\partial x}\big(u\mathbf{F}(V)+\mathbf{K}(V)\big)=0, \tag{3.2}$$

where V can be one of the following variables: supercritical fluid saturation s_σ, CO_2 composition in the supercritical fluid phase $\psi_{\sigma c}$, or H_2O composition in the aqueous phase ψ_{aw}; the flux term $\mathbf{K}$ includes the effects of gravity in the convection term of the conservation law.

This chapter is organized as follows. We will study first the wave curves in each region of thermodynamic equilibrium. Afterwards, we study the discontinuities occurring between different configurations. Finally, we find the Riemann solutions for a set of typical flow scenarios.

3.1 Phase configurations in equilibrium

There are three different phase configurations: a single-phase supercritical fluid configuration, spσ, which is a CO_2-rich phase with dissolved H_2O: the physical properties of this phase can be calculated [1] by appropriate equations of state (e.g. Redlich-Kwong [67], a polar version of Soave-Redlich-Kwong [74], Peng-Robinson [62]) which may include convenient modifications concerning mixtures; a two-phase configuration, tp, a mixture of two phases in thermodynamic equilibrium, one of liquid water with dissolved carbon dioxide, and the other one a CO_2-rich supercritical fluid phase with dissolved H_2O: in this case we use experimental data for the mutual solubilities of CO_2, (x_c), and H_2O, (y_w), provided by Bamberger et al (2000) [5]; and a single-phase aqueous configuration, spa, in which the pores contain liquid water with dissolved carbon dioxide.

Remark 3.1. We introduce the compositions of carbon dioxide in the supercritical fluid phase $\psi_{\sigma c}$ and of water in the aqueous phase ψ_{aw}, defined mathematically as

$$\psi_{\sigma c}=\rho_{\sigma c}/\rho_{\sigma C}, \qquad \psi_{aw}=\rho_{aw}/\rho_W, \tag{3.3}$$

where $\rho_{\sigma C}$ is the density of pure supercritical carbon dioxide, which can be found from experimental P-V-T values of CO_2 or can be predicted using a polar version of the Soave-Redlich-Kwong equation of state (C.8). For its numerical value see Table B.3; for a methodology for finding its value see Appendix C; ρ_W is the pure water density at 293.15 [K] and 1 [bar], for its value see Table B.2.

We assume local conservation of volume throughout the flow: this is applied for establishing mixing rules, where the artificial constants $\rho_{\sigma W}$ and ρ_{aC} are introduced; the first one represents an idealized density of pure water in the supercritical fluid phase; it

[1] The physical quantities used in this chapter will be calculated at the pressure and temperature of the reservoir $(P_{\text{ref}}, T_{\text{res}})$. For their values see Table B.3.

would be the density of the supercritical fluid phase if no solvent (*i.e.*, carbon dioxide) were present, but only solute (*i.e.*, H_2O). The description of ρ_{aC} is analogous but with the roles of H_2O and supercritical CO_2 interchanged.

Assuming ideal mixing rules, in Sections 3.1.1, 3.1.3 and 3.1.2 we will see that the unknowns of the system of PDE's above are a subset of $\psi_{\sigma c}$, ψ_{aw}, s_σ, and u; the phase configuration of the flow determines which unknowns are used.

3.1.1 Single-phase supercritical configuration - spσ

There are two chemical species (CO_2 and H_2O) and one supercritical fluid phase, *i.e.*, $c = 2$ and $p = 1$, so we only have one thermodynamic degree of freedom, which can be chosen to be the carbon composition in the supercritical fluid phase $\psi_{\sigma c} = \rho_{\sigma c}/\rho_{\sigma C}$. The composition of water in the supercritical fluid phase $\psi_{\sigma w}$ is defined as the quotient $\psi_{\sigma w} = \rho_{\sigma w}/\rho_{\sigma W}$, (see [10, 40] for the compositions of the nitrogen model). In this expression $\rho_{\sigma W}$ denotes the artificial partial density of pure water vapor "dissolved" in the CO_2-rich supercritical fluid phase: it has been introduced in order to obtain a consistent thermodynamic model for the supercritical fluid phase; at first it seems reasonable to carry out an approximation for its numerical value using the pure water vapor density ρ_{gW}. The latter can be found by the MSRK EOS using the pure water vapor pressure P_{gW} given by the Clausius-Clapeyron Law (Eq. (D.2) of Appendix D).

The compositions of the supercritical fluid phase, $\psi_{\sigma c}$ and $\psi_{\sigma w}$, can be related via a mixing rule. Based on the conservation of volume principle we may write the ansatz:

$$\psi_{\sigma c} + \psi_{\sigma w} = 1 + \varepsilon M_1(\psi_{\sigma c}, \psi_{\sigma w}) + \varepsilon^2 M_2(\psi_{\sigma c}, \psi_{\sigma w}) + \dots \tag{3.4}$$

It is reasonable to expect that the terms of $o(\varepsilon)$ in Eq. (3.4) create small distortions observed as weak shocks and short rarefactions in the wave train. The hypothesis $\varepsilon \equiv 0$ implies there are no volume contraction or expansion effects due to mixing so that the volumes of the components are additive. This hypothesis is called ideal mixing. The value of $\rho_{\sigma W}$ was found (see Table B.3) using (3.4) with $\varepsilon = 0$. This is explained in detail in Appendix C.

As we assume that $T \equiv T_{res}$ where T_{res} stands for the constant temperature of the reservoir, the quantities $\rho_{\sigma C}$ and $\rho_{\sigma W}$ are constant. Moreover, notice that in the tp configuration we have no degrees of freedom, thus the values of the compositions and corresponding densities are constant. Whenever it is necessary we will clarify whether the value of a density corresponds to the tp configuration, *e.g.*, to avoid confusion we will denote the CO_2 density in the supercritical fluid in the tp configuration as $\rho_{\sigma c}^{\mathrm{TP}}$.

3.1.1.1 Characteristic speed analysis

Let's include the ideal mixing rule hypotheses, *i.e.*, $\varepsilon \equiv 0$ in (3.4). Upon a division by the densities $\rho_{\sigma C}$, $\rho_{\sigma W}$, and using $f_\sigma = s_\sigma = 1$, $m_a = f_a = s_a = 0$, Eqs. (2.7)-(2.8) become:

$$\frac{\partial}{\partial t}\varphi\psi_{\sigma c} + \frac{\partial}{\partial x}u\psi_{\sigma c} = 0, \tag{3.5}$$

$$\frac{\partial}{\partial t}\varphi\psi_{\sigma w} + \frac{\partial}{\partial x}u\psi_{\sigma w} = 0. \tag{3.6}$$

From the mixing rule assumption, using the fact that the porosity is constant, adding the equations (3.5) and (3.6) we conclude that in the spσ configuration we have $\partial u/\partial x = 0$. Therefore u is constant along smooth scale-invariant solutions of (3.5)-(3.6), and across discontinuites appearing in weak solutions. In other words, composition changes have no volumetric effects in self-similar solutions of the system (3.5)-(3.6). Furthermore, the system (3.5)-(3.6) has a single finite and constant propagation speed. We conclude that the spσ configuration is governed by the linear advection equation

$$\frac{\partial}{\partial t}\psi_{\sigma c} + \lambda_\sigma \frac{\partial}{\partial x}\psi_{\sigma c} = 0, \quad \text{where} \quad \lambda_\sigma \equiv \frac{u_\sigma}{\varphi}. \tag{3.7}$$

There are no proper shocks and rarefactions whithin this region, just contact discontinuities C_σ with speed λ_σ, between states with compositions $\psi^-_{\sigma c}$ and $\psi^+_{\sigma c}$. The waves are described by $\psi^-_{\sigma c}$ if $x/t < \lambda_\sigma$ and $\psi^+_{\sigma c}$ if $x/t > \lambda_\sigma$.

The 2-parameter set of pairs $(\psi_{\sigma c}, u)$ characterizes the spσ configuration. They satisfy the physical restriction

$$1 \geq \psi_{\sigma c} \geq \Lambda_\sigma \equiv \rho^{\text{TP}}_{\sigma c}/\rho_{\sigma C} \tag{3.8}$$

Indeed, the CO_2-rich supercritical fluid phase becomes water-saturated at the H_2O concentration $\rho^{\text{TP}}_{\sigma w}$.

3.1.2 Single-phase aqueous configuration - spa

There are two chemical species (CO_2 and H_2O) and one aqueous fluid phase, *i.e.*, $c = 2$ and $p = 1$, so we only have one thermodynamic degree of freedom: the composition of H_2O in the aqueous phase denoted by ψ_{aw}, introduced in (3.3). We define the composition of carbon in the aqueous phase ψ_{ac} by the quotient $\psi_{ac} = \rho_{ac}/\rho_{aC}$, where ρ_{aC} denotes the artificial partial density of pure carbon dioxide "dissolved" in the H_2O-rich aqueous phase: it has been introduced in order to obtain a consistent thermodynamic model for the aqueous phase, and its value (see Table B.3) can be found using an ideal mixing hypotheses for the aqueous phase, *i.e.*, $\psi_{aw} + \psi_{ac} = 1$. The other unknown is u.

3.1.2.1 Characteristic speed analysis

Let's assume the ideal mixing hypotheses for the aqueous phase. Since $s_\sigma = 0$ and $s_a = 1$, using Eqs. (2.3) and (B.3) we have $f_\sigma = 0$ and $f_a = 1$; therefore after a division by the densities ρ_{aC}, ρ_W, Eqs. (2.5)-(2.6) become:

$$\frac{\partial}{\partial t}\varphi\psi_{ac} + \frac{\partial}{\partial x}u\psi_{ac} = 0, \tag{3.9}$$

$$\frac{\partial}{\partial t}\varphi\psi_{aw} + \frac{\partial}{\partial x}u\psi_{aw} = 0. \tag{3.10}$$

From the mixing rule assumption for the aqueous phase we also conclude that in the spa configuration we have $\partial u/\partial x = 0$. Therefore u is constant along smooth scale-invariant solutions of (3.9) and (3.10), and across discontinuites appearing in weak solutions. Furthermore, the system (3.9)-(3.10) has a single finite and constant speed of propagation.

We conclude that the spa configuration is governed by the linear advection equation

$$\frac{\partial}{\partial t}\psi_{aw} + \lambda_{\text{A}}\frac{\partial}{\partial x}\psi_{aw} = 0, \quad \text{with} \quad \lambda_{\text{A}} = \frac{u_{\text{A}}}{\varphi}, \tag{3.11}$$

where we use the notation u_{A} to indicate that the velocity u is spatially constant in the spa configuration.

We conclude that there are no proper shocks and rarefactions whithin this region, just contact discontinuities C_{A} with velocity λ_{A} between states with compositions ψ_{aw}^- and ψ_{aw}^+. The waves are described by ψ_{aw}^- if $x/t < \lambda_{\text{A}}$ and ψ_{aw}^+ if $x/t > \lambda_{\text{A}}$. From this we conclude that composition changes have no volumetric effects.

The 2-parameter set of pairs (ψ_{aw}, u) characterize the spa configuration. They satisfy the restriction

$$1 \geq \psi_{aw} \geq \Lambda_a \equiv \rho_{aw}^{\text{TP}}/\rho_W. \tag{3.12}$$

Indeed, the H_2O-rich aqueous phase becomes carbon-saturated at the CO_2 concentration ρ_{ac}^{TP}.

3.1.3 Two phase configuration tp

There are two chemical species (CO_2 and H_2O), $c = 2$, and two phases (supercritical fluid and liquid), *i.e.*, $p = 2$; so $f_{\text{P,T}} = 0$, thus there are no free thermodynamic variables. In this configuration, the compositions of carbon dioxide and water are determined by pressure and temperature, so they are fixed constants. The two variables to be determined are: supercritical fluid saturation and total Darcy velocity.

3.1.3.1 Characteristic speed analysis

In the tp configuration we can write Eqs. (2.7)-(2.8) as,

$$\frac{\partial}{\partial t}\varphi\left(s(\rho_{\sigma c}-\rho_{ac})+\rho_{ac}\right)+\frac{\partial}{\partial x}\Big(f\big(u+km_a(\rho_a-\rho_\sigma)g_\beta\big)\left(\rho_{\sigma c}-\rho_{ac}\right)+\rho_{ac}u\Big)=0,$$
$$\frac{\partial}{\partial t}\varphi\left(s(\rho_{\sigma w}-\rho_{aw})+\rho_{aw}\right)+\frac{\partial}{\partial x}\Big(f\big(u+km_a(\rho_a-\rho_\sigma)g_\beta\big)\left(\rho_{\sigma w}-\rho_{aw}\right)+\rho_{aw}u\Big)=0,$$

where f (*resp.* s) stands for f_σ (s_σ). We will use this notation in the rest of the chapter. We can write this system of equations as

$$\frac{\partial}{\partial t}\varphi s+\frac{\partial}{\partial x}\left(f\big(u+km_a(\rho_a-\rho_\sigma)g_\beta\big)+\frac{\rho_{ac}}{(\rho_{\sigma c}-\rho_{ac})}u\right)=0, \tag{3.13}$$
$$\frac{\partial}{\partial t}\varphi s+\frac{\partial}{\partial x}\left(f\big(u+km_a(\rho_a-\rho_\sigma)g_\beta\big)+\frac{\rho_{aw}}{(\rho_{\sigma w}-\rho_{aw})}u\right)=0. \tag{3.14}$$

Subtracting Eqs. (3.13) and (3.14) we obtain,

$$\frac{\partial}{\partial x}u\left(\frac{\rho_{ac}}{\rho_{\sigma c}-\rho_{ac}}-\frac{\rho_{\sigma w}}{\rho_{aw}-\rho_{\sigma w}}\right)=0. \tag{3.15}$$

Recalling that the partial densities are constants (found in Table B.3), we can verify the term inside of the parenthesis in Eq. (3.15) is different from zero. Therefore we conclude that $\partial u/\partial x=0$. Thus the total velocity u is constant along smooth scale-invariant solutions of (3.13)-(3.14), and across discontinuites appearing in weak solutions. Furthermore, this system has a single finite propagation speed, associated with the fractional flow with gravity function.

We conclude that the tp configuration is governed by the scalar conservation law

$$\frac{\partial}{\partial t}(\varphi s)+\frac{\partial}{\partial x}\Big(f\big(u^{\text{TP}}+km_a(\rho_a-\rho_\sigma)g_\beta\big)\Big)=0, \tag{3.16}$$

where we use the notation u^{TP} to indicate that the Darcy velocity u is constant in the tp configuration. The 2-parameter set of pairs (s,u) characterizes the tp configuration. We can now conclude that within this region we have saturation-discontinuities and saturation-rarefactions corresponding to the conservation law given by Eq. (3.16).

3.2 Shocks between configurations

The system of two balance laws (2.7)-(2.8) can be written in the compact form presented in (3.2): $\frac{\partial}{\partial t}\mathbf{G}+\frac{\partial}{\partial x}\big(u\mathbf{F}+\mathbf{K}\big)=0$.

There exist infinitesimal regions between different configurations where abrupt changes occur, giving rise to discontinuities. They are shocks in the flow, that satisfy the Rankine-Hugoniot relationship:

$$\upsilon[\mathbf{G}] = u^+\mathbf{F}^+ - u^-\mathbf{F}^- + \mathbf{K}^+ - \mathbf{K}^-, \tag{3.17}$$

where $W^- = (V^-, u^-)$ and $W^+ = (V^+, u^+)$ are the states on the left and the right side of the shock. The shock speed is $\upsilon = \upsilon(W^-, W^+)$; the accumulation term is $\mathbf{G}^\pm = \mathbf{G}(V^\pm)$, and $\mathbf{F}^\pm = \mathbf{F}(V^\pm)$, $\mathbf{K}^\pm = \mathbf{K}(V^\pm)$ at the left (right) of the shock; $[\mathbf{G}] = \mathbf{G}^+ - \mathbf{G}^-$. Notice that the accumulation and flux terms have different expressions at each side of the shock; indeed, these expressions depend on the thermodynamic configuration analyzed. For a fixed state W^-, the set of W^+ states satisfying Eq. (3.17) defines the Rankine-Hugoniot curve of W^-, which is denoted $RH(W^-)$. We call the shock curve the set of W^+ that satisfy Eq. (3.17) and an admissibility criterion, where we assume that the shock speed is decreasing from the $(-)$ state, which is Liu's criterion, see [46, 47]. The admissibility criterion selects discontinuities that are physical. We call the contact discontinuity curve the set of $W^+ \in RH(W^-)$ such that $\lambda(W^-)$=$\lambda(W^+)$; λ stands for the characteristic speed of the system.

We will proceed as follows: we will evaluate the expression (3.17) for the physically admissible discontinuities, *i.e.*, the shock between the spσ and tp configurations, and the shock between the spa and tp configurations. In both cases we will find an expresssion for the corresponding speeds in terms of W^- and W^+. The Riemann solution consists of an ensemble of both discontinuities together with a wave sequence built using the conservation law (3.1).

3.2.1 Evaporation Shock

In this section we study shocks with states $W^- = (\psi^-_{\sigma c}, u^-)$ in the spσ configuration and $W^+ = (s^+, u^+)$ along the tp configuration. If the left (*resp.* right) states of a shock wave are W^- (W^+), then from a fixed observation position in the porous rock, we may see a sudden evaporation of the liquid phase.

The quantities $\rho^+_{\sigma c}$, $\rho^+_{\sigma w}$, ρ^+_{ac}, ρ^+_{aw}, are constant in the tp configuration; their values are given in Table B.3. Applying the Rankine-Hugoniot relationship we obtain the speed of the evaporation shock,

$$\upsilon_{\text{e}} = \frac{u^+ n_1 - u^- \rho^-_{\sigma c} + g_1}{\varphi d_1}, \tag{3.18}$$

$$= \frac{u^+ n_2 - u^- \rho^-_{\sigma w} + g_2}{\varphi d_2}. \tag{3.19}$$

The terms $n_1, d_1, n_2, d_2, g_1, g_2$ are given in Appendix E.1. From Eq. (3.18) we have

$$u^- = \frac{u^+ n_1 - \upsilon_e \varphi d_1 + g_1}{\rho^-_{\sigma c}}. \tag{3.20}$$

Replacing (3.20) in (3.19) after some rearrangement of the terms we obtain,

$$\upsilon_e = \frac{u^+}{\varphi}\frac{f^+ - C_e}{s^+ - C_e} + \frac{f^+ k m_a^+ (\rho_a - \rho_\sigma) g_\beta}{\varphi\left(s^+ - C_e\right)}, \tag{3.21}$$

where

$$\begin{aligned} C_e &= \frac{\rho^+_{ac}\rho^-_{\sigma w} - \rho^+_{aw}\rho^-_{\sigma c}}{\rho^+_{ac}\rho^-_{\sigma w} - \rho^+_{aw}\rho^-_{\sigma c} + \rho^+_{\sigma w}\rho^-_{\sigma c} - \rho^+_{\sigma c}\rho^-_{\sigma w}}, \\ &= \frac{1}{1 - C^*_e}, \end{aligned} \tag{3.22}$$

with

$$C^*_e = \frac{\rho^+_{\sigma c}\rho^-_{\sigma w} - \rho^+_{\sigma w}\rho^-_{\sigma c}}{\rho^+_{ac}\rho^-_{\sigma w} - \rho^+_{aw}\rho^-_{\sigma c}}. \tag{3.23}$$

The term C_e depends on the values of the partial densities given by the $(-)$ state, and on the constant values of the partial densities for the region of two-phase equilibria, *i.e.*, it depends on the thermodynamic framework!

As it was observed before (see for instance Section 3.1.1 and Eq. (3.8), the concentration $\rho^-_{\sigma c}$ has a physically coherent value when it satisfies the inequality

$$\rho^{\text{TP}}_{\sigma c} \equiv \rho^+_{\sigma c} = 356.41 \leq \rho^-_{\sigma c} \leq \rho_{\sigma C} = 356.6 \quad [\text{kg/m}^3]. \tag{3.24}$$

This observation would be used for the construction of a physically correct solution for the Riemann problems for the evolution of the flow.

Notice that the expression for the shock speed (3.21) is split between the transport-driven shock speed (the first fraction in (3.21); in BrickRed), and the gravity-driven shock speed (the second fraction; in DarkBlue). In the horizontal case ($\beta = 0$) the shock speed consists only of the first term which represents the slope of the secant from the point (C_e, C_e) to a point over the graph of the fractional flow function.

Manipulations carried out over expression (3.21) take us to,

$$\begin{aligned} \upsilon_e &= \frac{f^+\left(u^+ + k m_a^+ (\rho_a - \rho_\sigma) g_\beta\right) - u^+ C_e}{\varphi\left(s^+ - C_e\right)}, \\ &= \frac{\mathrm{F}(s^+) - \left(u^+/\varphi\right) C_e}{\left(s^+ - C_e\right)}, \end{aligned} \tag{3.25}$$

where $\mathtt{F}^+ \equiv \left(f^+/\varphi\right)\left(u^+ + km_a^+(\rho_a - \rho_\sigma)g_\beta\right)$. The shock speed corresponds to the secant from the point $\left(C_\mathrm{e}, (u^+/\varphi)C_\mathrm{e}\right)$ to the graph of F, which corresponds to the flux of the conservation law (3.1).

In order to find numerically the shock speeds of the form (3.25), we must find the physically admissible values of C_e. Note that this can be done finding the dependence of C_e on $\rho^-_{\sigma c}$. Using the mixing rule (3.4) we can write $\rho^-_{\sigma w}$ as a function of $\rho^-_{\sigma c}$. A direct calculation shows that $C^*_\mathrm{e}(\rho^{\mathrm{TP}}_{\sigma c}) = 0$. This observation, and a direct computation of expression (3.23) using Matlab® show that C_e is an increasing function of $\rho^-_{\sigma c}$ and

$$1 = C_\mathrm{e}(\rho^{\mathrm{TP}}_{\sigma c}) \leq C_\mathrm{e}(\rho^-_{\sigma c}) \leq C_\mathrm{e}(\rho_{\sigma C}) = 1.0007. \tag{3.26}$$

This result is quite interesting! Inequality (3.26) will allow us to construct an Oleinik solution for the Riemann problem (3.39). An example of the construction of the shock (3.25) has been depicted in Fig. 3.2. In this figure we chose the secant to be tangent to the graph of F. Notice that $\mathtt{F}(s=1) = u^+/\varphi$. In Fig. 3.2 we also represent the line-segment corresponding to the physically admissible values of C_e belonging to the line passing through the origin with slope u^+/φ.

3.2.2 Condensation shock

The left state $W^- = (\psi^-_{aw}, u^-)$ is in the spa configuration. The right state $W^+ = (s^+, u^+)$ is in the tp configuration. Applying the Rankine-Hugoniot relationship we obtain

$$\upsilon_\mathrm{c} = \frac{u^+ n_1 - u^- \rho^-_{ac} + g_1}{\varphi d_3}, \tag{3.27}$$

$$= \frac{u^+ n_2 - u^- \rho^-_{aw} + g_2}{\varphi d_4}. \tag{3.28}$$

The terms $n_1, d_3, n_2, d_4, g_1, g_2$ are given in Appendix E.1.

In a similar way as it was done in Section 3.2.1 we find the value of u^- using Eq. (3.28). Indeed, we have

$$u^- = \frac{u^+ n_2 - \varphi d_4 \upsilon_\mathrm{c} + g_2}{\rho^-_{ac}}. \tag{3.29}$$

Replacing in Eq. (3.27) after some calculations we obtain

$$\upsilon_\mathrm{c} = \frac{u^+}{\varphi}\frac{f^+ - C_\mathrm{c}}{s^+ - C_\mathrm{c}} + \frac{f^+ km_a^+(\rho_a - \rho_\sigma)g_\beta}{\varphi\left(s^+ - C_\mathrm{c}\right)}, \tag{3.30}$$

where

$$C_{\mathrm{C}} = \frac{\rho_{ac}^{+}\rho_{aw}^{-} - \rho_{aw}^{+}\rho_{ac}^{-}}{\rho_{ac}^{+}\rho_{aw}^{-} - \rho_{aw}^{+}\rho_{ac}^{-} + \rho_{\sigma w}^{+}\rho_{ac}^{-} - \rho_{\sigma c}^{+}\rho_{aw}^{-}},$$

which can be written in the abbreviate form

$$= \frac{1}{1 + C_{\mathrm{C}}^{*}},$$

where

$$C_{\mathrm{C}}^{*} = \frac{\rho_{\sigma c}^{+}\rho_{aw}^{-} - \rho_{\sigma w}^{+}\rho_{ac}^{-}}{\rho_{ac}^{+}\rho_{aw}^{-} - \rho_{aw}^{+}\rho_{ac}^{-}}. \tag{3.31}$$

The concentration ρ_{aw}^{-} satisfies the inequality (compare with equation (3.12) of Section 3.1.2)

$$\rho_{aw}^{\mathrm{TP}} \equiv \rho_{aw}^{+} = 963.89 \leq \rho_{aw}^{-} \leq \rho_{W} = 998.2 \quad [\mathrm{kg/m^3}]. \tag{3.32}$$

Now we are interested in determining the variation of C_{C} depending on the choice of ρ_{aw}^{-}; for this we may use the mixing rule (3.3). A direct calculation shows that in the limit when ρ_{aw}^{-} approaches ρ_{aw}^{TP}, $C_{\mathrm{C}}^{*} \to \infty$. Numerical computations of expression (3.31) as a function of ρ_{aw}^{-} using Matlab® (the result has been depicted in Fig. 3.1) show that

$$-0.1605 = C_{\mathrm{C}}(\rho_{W}) \leq C_{\mathrm{C}}(\rho_{aw}^{-}) \leq C_{\mathrm{C}}(\rho_{aw}^{\mathrm{TP}}) = 0. \tag{3.33}$$

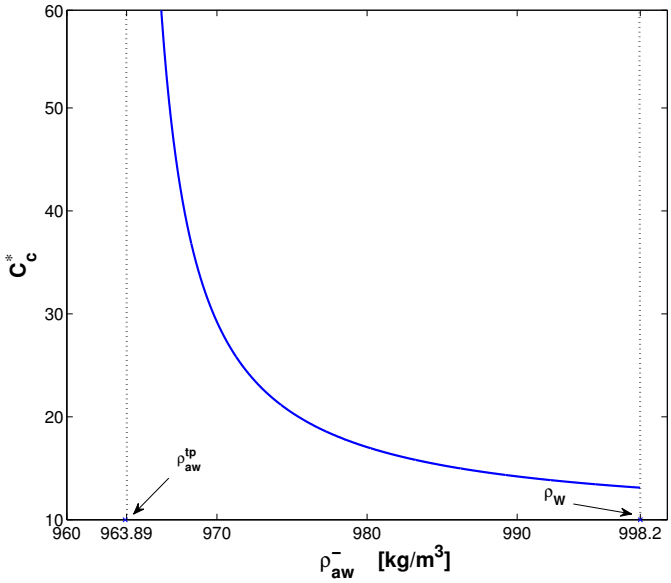

Fig. 3.1 C_c^* as a function of ρ_{aw}^{-}.

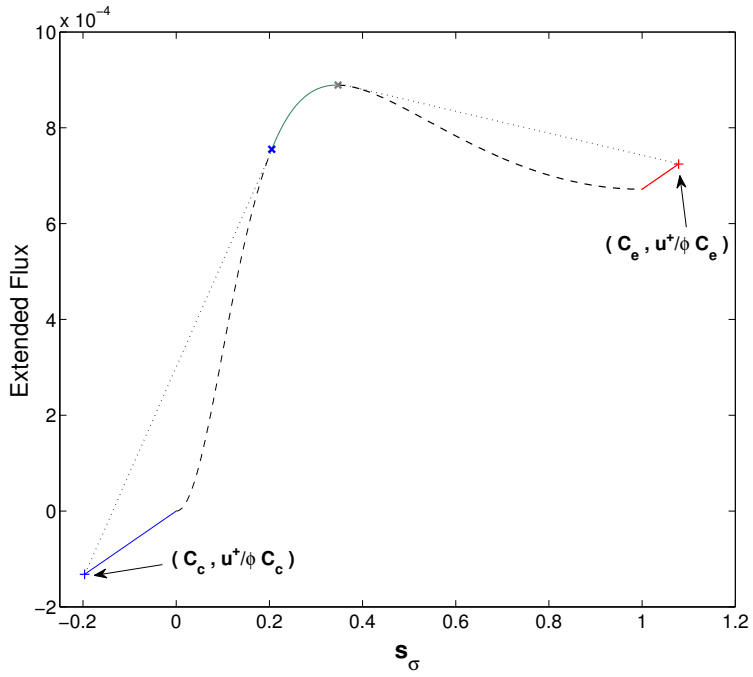

Fig. 3.2 Extended flux function Case $\beta = \pi/2$.

The interval (3.33) will show us how to construct the extension of the flux (3.1) as depicted in Fig. 3.2. In a similar way as was done in Section 3.2.1, we rearrange expression (3.30) to obtain

$$\upsilon_{\mathrm{C}} = \frac{\mathrm{F}(s^+) - \left(u^+/\varphi\right)C_{\mathrm{C}}}{\left(s^+ - C_{\mathrm{C}}\right)}. \tag{3.34}$$

The shock speed corresponds to the secant from the point $\left(C_{\mathrm{C}}, (u^+/\varphi)C_{\mathrm{C}}\right)$ to the graph of F. In Fig. 3.2 we show the construction of the solution for a "vapor–liquid displacement" problem; the fractional flow function with gravity (3.1) is "extended" with the C_{e} and C_{C} segments.

Remark 3.2. Notice that in the horizontal case, *i.e.*, when $\beta = 0$, the Rankine-Hugoniot shock condition (3.17) can be written as

$$\upsilon[\mathbf{G}] = u^+\mathbf{F}^+ - u^-\mathbf{F}^-, \tag{3.35}$$

which can be recast in matrix notation

$$\Pi(V^+)\begin{pmatrix}\upsilon\\ u^+\end{pmatrix} := \begin{pmatrix}[G_1] & (-F_1^+)\\ [G_2] & (-F_2^+)\end{pmatrix}\begin{pmatrix}\upsilon\\ u^+\end{pmatrix} = -u^-\begin{pmatrix}F_1^-\\ F_2^-\end{pmatrix}. \tag{3.36}$$

Notice that the RH Locus of a reference state $W^- = (V^-, u^-)$ can be found by choosing first a state $V^+ \neq V^-$ such that $\Pi(V^+)$ is invertible. Using such value we can immediately recover υ and u^+ from (3.36). The shock (W^-, W^+) satisfying the condition $\det(\Pi(V^+)) \neq 0$ will be called *non-degenerate*.

The later was just a particular case of a more general setting: indeed, (3.17) can be written in the form

$$\Pi(V^+)\begin{pmatrix}\upsilon\\ u^+\end{pmatrix} + \begin{pmatrix}K_1^+\\ K_2^+\end{pmatrix} = -u^-\begin{pmatrix}F_1^-\\ F_2^-\end{pmatrix} - \begin{pmatrix}K_1^-\\ K_2^-\end{pmatrix}, \tag{3.37}$$

which can be simplified when $\det(\Pi(V^+)) \neq 0$ to the form

$$\Pi(V^+)\begin{pmatrix}\upsilon + \widehat{K}_1^+\\ u^+ + \widehat{K}_2^+\end{pmatrix} = \begin{pmatrix}H_1^-\\ H_2^-\end{pmatrix}, \tag{3.38}$$

where $\begin{pmatrix}\widehat{K}_1^+\\ \widehat{K}_2^+\end{pmatrix} := \Pi^{-1}(V^+)\begin{pmatrix}K_1^+\\ K_2^+\end{pmatrix}$ and $\begin{pmatrix}H_1^-\\ H_2^-\end{pmatrix} := -u^-\begin{pmatrix}F_1^-\\ F_2^-\end{pmatrix} - \begin{pmatrix}K_1^-\\ K_2^-\end{pmatrix}$. We conclude that non-degenerate shocks can be first calculated by setting V^+, and then from (3.38) υ and u^+ are recovered.

From a Gaussian reduction of the system (3.37) we observe that for $V^+ \neq V^-$ for which $\det(\Pi(V+)) = 0$, and $[\mathbf{G}], \mathbf{F} \neq 0$, there exist constants π_1, π_2 such that $\upsilon = \frac{u^+ - u^-\pi_2}{\pi_1}$. In this chapter all shocks are non-degenerate.

3.3 Waves in Riemann Solutions for isothermal flow

Here we use the wave curve method for systems of type (3.2) as described in [2]. A comprehensive study of this method can be found in [31, 46, 79]. Mathematically, the evolution in time of the multiphase fluids contained in a slanted cylinder is modelled by the Riemann problem associated to Eqs. (2.4)-(2.6) with data:

$$\begin{cases} W^{\mathrm{L}} \equiv (V,u)^{\mathrm{L}} \text{ if } x<0,\ t=0,\\ W^{\mathrm{R}} \equiv (V,\cdot)^{\mathrm{R}} \text{ if } x>0,\ t=0. \end{cases} \tag{3.39}$$

In this case, the letter V stands for either $\psi_{\sigma c}$, ψ_{aw}, or s_σ. The velocity $u^{\mathrm{L}} > 0$ is specified in the left state. The $(\cdot)$ (dot) denotes that the total velocity u^{R} is not specified at the right state. In the next sections we will show that u^{R} can be obtained in terms of u^{L}, and the left and right values of V, combined with the construction of the wave-sequence corresponding to the Riemann solution of (3.39).

The characteristic speeds of the system can be either positive or negative. Therefore, in a first approach, this problem is regarded as an injection problem at $x = -\infty$. In the horizontal case all the characteristic speeds of the system have the same sign as u. and

therefore when u is positive, we can substitute (3.39) by the Riemann-Goursat problem $(V,u)^{\mathrm{L}}$ for $x=0$, $t>0$ and $(V,\cdot)^{\mathrm{R}}$ for $x>0$, $t=0$ which can be regarded as an injection problem at $x=0$.

A difficulty arises when including the effects of gravity during fluid transport: we observe a non-linear coupling of the total Darcy velocity u in the relation for equality between the characteristic speed and the shock speed between thermodynamic configurations. In order to solve (3.39) we must find simultaneously the unknown value of the seepage velocity downstream of the flow and the wave-sequence; this comes from a direct application of Oleinik's admissibility criterion. In the horizontal case, this dependence turns out to be linear, and therefore we can find the velocity u from the solution of the Riemann problem solved first in the set of primary variables, as introduced in [39] and which has been depicted in practical examples in [40] for the model of nitrogen and steam injection in porous media.

3.4 Solution for isothermal slanted flow

In this section we find the solution for a Riemann problem of the type (3.39) representing the evolution of injected supercritical fluid upstream of liquid in a slanted porous media slab. In particular we find the solution for a vapor-liquid displacement problem for the horizontal ($\beta=0$) and vertical ($\beta=\pi/2$) cases.

The migration regime is governed by the balance between the injection and buoyancy mechanisms. Indeed, the case where $C_g \ll 1$ (see Chapter 2, and [73]) is asymptotically equivalent to a horizontal regime. Hayek et al. [25] observed that the plume ascent is determined by the balance between the volumetric flow rate u and the mean ascent velocity G. The latter is given for our model as $G := k\overline{m}_a(\rho_a-\rho_\sigma)g$, where $\overline{m}_a$ is the averaged relative mobility of the aqueous phase

$$\overline{m}_a := \frac{1}{\mu_a}\int_0^1 k_{ra}(s)ds \tag{3.40}$$

The transport is injection-driven when $u \gg G$, and gravity driven when $u \ll G$. Gravity driven regimes are described essentially by cases where $\beta=\pi/2$ and $C_g \gg 1$. We study below the solution for an injection driven horizontal regime, and a "balanced" vertical regime; in particular we put $u^{\mathrm{L}}=G$ in the latter.

We will use mathematical and physical justifications for pasting together correctly the different pieces of the Riemann solutions, which are composed by a shock between the spσ and tp configuration (an Evaporation Shock), a Buckley-Leverett rarefaction wave in the tp configuration, and finally, a shock between the tp and spa configurations (*i.e.*, a reverse Condensation Shock). An interesting question that arises and that we answer is: does the total velocity change along these shocks? In order to find the value of u in

each of the thermodynamic configurations along wave curves, we solve a linear system of equations in the horizontal flow case and a non-linear equation in s_σ for the vertical case; the latter is justified by a direct application of Oleinik entropy condition for shocks between different configurations in equilibrium.

We do not present here the construction for the reverse case *i.e.*, the liquid-vapor-displacement problem, as it is analogous to the above.

3.4.1 Vapor-liquid migration

The Riemann problem is:

$$\begin{cases} W^{\mathrm{L}} \equiv (\psi_{\sigma c}, u)^{\mathrm{L}} \text{ if } x < 0,\ t = 0, \\ W^{\mathrm{R}} \equiv (\psi_{aw}, \cdot)^{\mathrm{R}} \text{ if } x > 0,\ t = 0. \end{cases} \tag{3.41}$$

i.e., the Left state is in the spσ configuration and the Right state is in the spa configuration. We write for instance $\rho^{\mathrm{L}}_{\sigma c} := \psi^{\mathrm{L}}_{\sigma c}\rho_{\sigma C}$.

Four different possibilities arise for the waves connecting the spσ and tp configurations, although only a shock wave followed by a s_σ-rarefaction in the tp configuration is the correct one; let's argue why: a single rarefaction wave and a rarefaction wave with an intermediate shock between both regions (*i.e.*, with a ray that satisfies the Rankine-Hugoniot relationship) are mathematically contradictory. Indeed, the spσ configuration is described by simple advection of characteristic speed λ_σ, see Eq. (3.7). We can modify the latter case placing the shock ray at the starting point of the rarefaction, *i.e.*, where we have a shock wave followed by a s_σ-rarefaction in the tp configuration, which makes perfect sense. This sequence is not parametrized by a composite curve. Finally, it is easy to see graphically that the last possibility, a Lax-shock *i.e.*, satisfying strict inequalities for Lax shock conditions, does not satisfy Oleinik's condition (construction of the Riemann solution using the convex hull), see Fig. 3.3.

In analogy with the last argument, we can show that a shock appears between the tp configuration and the spa configuration. It would be preceded by an s_σ-rarefaction in the tp configuration.

Let's assume that the initial conditions (3.41), are physically coherent, *i.e.*, we have

$$\rho^{\mathrm{TP}}_{\sigma c}/\rho_{\sigma C} \equiv 356.4089/356.6 \leq \psi^{\mathrm{L}}_{\sigma c} \leq 1, \tag{3.42}$$

$$\rho^{\mathrm{TP}}_{aw}/\rho_{W} \equiv 963.89/998.2 \leq \psi^{\mathrm{R}}_{aw} \leq 1. \tag{3.43}$$

Indeed, the vapor (liquid) is water (carbon)-saturated when present in the tp configuration. Notice now that if the initial conditions of the Riemann problem satisfy inequalities (3.42) and (3.43) then the corresponding densities $\rho^{\mathrm{L}}_{\sigma c}$ and ρ^{R}_{aw} would satisfy inequalities (3.24) and (3.32). This last result will allow us to construct a solution satisfying Oleinik's condition, Lax shock conditions

$$\lambda_\sigma > \upsilon_{\mathrm{e}}, \tag{3.44}$$
$$\upsilon_{\mathrm{c}} > \lambda_{\mathrm{A}}, \tag{3.45}$$

and agreeing with the expected physical framework.

As explained above, in order to start the construction of the Riemann solution, we must connect continuously an Evaporation Shock to a s_σ-rarefaction. Let's introduce

$$W^{\mathrm{TP,e}} = (s^{\mathrm{TP,e}}, u^{\mathrm{TP}}). \tag{3.46}$$

We must look for a point $W^{\mathrm{TP,e}}$ in the tp configuration as in (3.46) where the tp characteristic speed coincides with the shock speed υ_{e}, *i.e.*,

$$\mathrm{F}'(s^{\mathrm{TP,e}}) = \frac{\mathrm{F}(s^{\mathrm{TP,e}}) - \left(u^{\mathrm{TP}}/\varphi\right)C_{\mathrm{e}}}{\left(s^{\mathrm{TP,e}} - C_{\mathrm{e}}\right)}. \tag{3.47}$$

Notice that the total velocity u^{TP} is another unknown of this equation. We must find the solution set of the non-linear system of equations (3.20) and (3.47) for $s^{\mathrm{TP,e}}$ and u^{TP}, and use an appropriate criterion for choosing a solution from this set. This procedure simplifies in the case $\beta = 0$, described next. In order to complete the construction of the Riemann solution, a tp rarefaction must be connected continuously to a reverse Condensation shock representing the downstream water drying front. Let

$$W^{\mathrm{TP,c}} = (s^{\mathrm{TP,c}}, u^{\mathrm{TP}}). \tag{3.48}$$

Thus, we must look for a point $W^{\mathrm{TP,c}}$, in the tp configuration, where the tp characteristic speed coincides with the shock speed υ_{c}, *i.e.*,

$$\mathrm{F}'(s^{\mathrm{TP,c}}) = \frac{\mathrm{F}(s^{\mathrm{TP,c}}) - \left(u^{\mathrm{TP}}/\varphi\right)C_{\mathrm{c}}}{\left(s^{\mathrm{TP,c}} - C_{\mathrm{c}}\right)}. \tag{3.49}$$

Case A: $\beta = 0$

For the horizontal case Eq. (3.47) becomes independent of the total tp velocity and takes the form

$$f'(s^{\mathrm{TP,e}}) = \frac{f^{\mathrm{TP,e}} - C_{\mathrm{e}}}{s^{\mathrm{TP,e}} - C_{\mathrm{e}}}. \tag{3.50}$$

where $f^{\mathrm{TP,e}} := f(s^{\mathrm{TP,e}})$. We write Eq. (3.50) as a 4-th degree polynomial $\mathbb{P}_e(\cdot, C_{\mathrm{e}})$ in s_σ, whose coefficients are functions of C_{e}. See Appendix E.2.1. Using Matlab®'s polynomial root function, we find two roots inside the interval $[0,1]$. The largest root is the one required $s^{\mathrm{TP,e}}$. The smallest one, denoted as $s^{\mathrm{TP,e},*}$, is also the point where a faster secant is tangent to the extended flux and can be used for finding the solution for the water-carbon displacement problem.

Finally we are in position of finding the value of u^{TP} and verifying (3.44). From (3.20), after some calculations we have[2]

$$u^{\text{TP}} = u^{\text{L}} \left(\frac{\rho^{\text{L}}_{\sigma c}}{n_1 - f'(s^{\text{TP},\ominus}) \cdot d_1} \right). \tag{3.51}$$

The tangent condition for the reverse condensation shock is similar to Eq. (3.50) and is given by

$$f'(s^{\text{TP},\text{C}}) = \frac{f^{\text{TP},\text{C}} - C_{\text{C}}}{s^{\text{TP},\text{C}} - C_{\text{C}}}. \tag{3.52}$$

In order to solve (3.52) we find the roots of the polynomial $\mathbb{P}_c(\cdot) := \mathbb{P}_e(\cdot, C_{\text{C}})$: we obtain two roots in the interval $[0,1]$, the largest one is the one required and is denoted by $s^{\text{TP},\text{C}}$.; the smallest one, denoted as $s^{\text{TP},\text{C},*}$, is also a point where a slower secant is tangent to the extended flux and can be used for finding the Riemann solution for the water-displacing-carbon problem.

Notice that at this point we have already obtained the value of u^{TP} (from (3.51)) and $s^{\text{TP},\text{C}}$. Thus to complete the wave sequence it remains to find u^{R}. Indeed, from Eq. (3.28) we have[3]

$$u^{\text{R}} = u^{\text{TP}} \left(\frac{n_2 - f'(s^{\text{TP},\text{C}}) \cdot d_4}{\rho^{\text{R}}_{aw}} \right). \tag{3.53}$$

We computed an example taking a typical field value of the seepage velocity corresponding to an injection driven regime, as suggested by [56], *i.e.*, $u^{\text{L}} = 4.42 \times 10^{-3}$ [m/s], and we take $\rho^{\text{R}}_{aw} = \rho_W$. Considering all the physically admissible values for the composition of the supercritical fluid mixture, we obtain the corresponding range of values for u^{TP}, and u^{R}:

$$\begin{aligned} u^{\text{TP}}_{\sigma C} = 4.4198 \times 10^{-3} \leq u^{\text{TP}} \leq u^{\text{TP}}_{\sigma c,\text{tp}} = 4.42 \times 10^{-3} \quad [\text{m/s}], \\ u^{\text{R}}_{\sigma C} = 3.7593 \times 10^{-3} \leq u^{\text{R}} \leq u^{\text{R}}_{\sigma c,\text{tp}} = 3.7595 \times 10^{-3} \quad [\text{m/s}], \end{aligned}$$

where $u^{\kappa}_{\sigma c,\text{tp}}$, $\kappa = \text{TP}, \text{R}$, is the seepage velocity corresponding to configuration κ, found when taking $\rho^{\text{L}}_{\sigma c} = \rho^{\text{TP}}_{\sigma c}$, and $u^{\kappa}_{\sigma C}$ is the seepage velocity found when taking left state $\rho^{\text{L}}_{\sigma c} = \rho_{\sigma C}$.

Moreover the inequalities (3.44)-(3.45) were verified numerically and graphically. The Riemann solution for vapor-liquid displacement in the case $\beta = 0$ is illustrated in Fig. 3.3 for $\rho^{\text{L}}_{\sigma c} = \rho_{\sigma C}$ and $\rho^{\text{R}}_{aw} = \rho_W$, by using the extended flux approach.

[2] In the expressions for n_1 and d_1 the left state L substitutes the $(-)$ state and the right state TP substitutes the $(+)$ state.

[3] In the expressions for n_2 and d_4 the left state TP substitutes the $(-)$ state and the right state R substitutes the $(+)$ state.

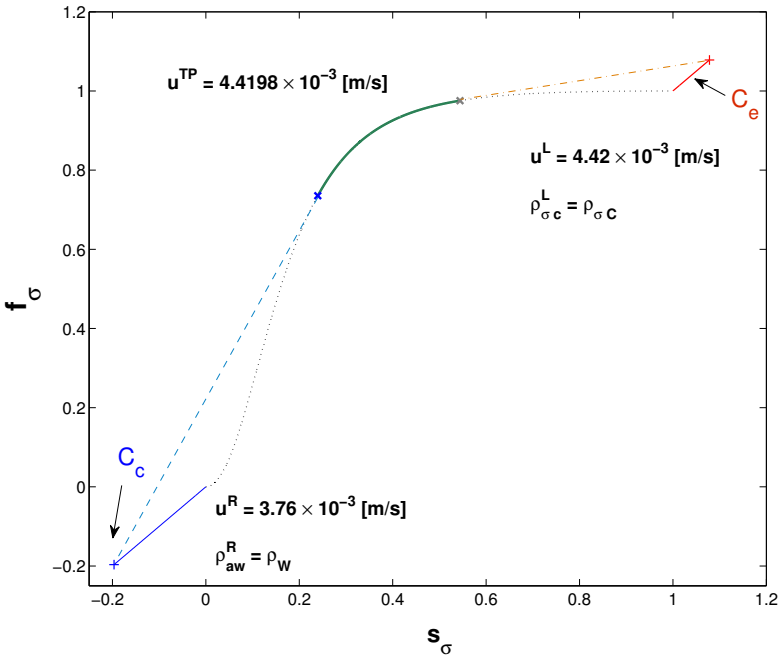

Fig. 3.3 Representation of the Riemann solution for vapor-liquid displacement for pure CO_2 injection in a horizontal reservoir core with pure water.

Case B: $\beta = \pi/2$

For this case we consider several left states $\rho^{\mathrm{L}}_{\sigma c}$ representing the composition of the supercritical fluid that is placed "behind" the aqueous phase in the slanted porous core, and we fix $\rho^{\mathrm{R}}_{aw} = \rho_W$. We study the regime where the convection term is balanced between the injection and gravity terms, *i.e.*, we take $u^{\mathrm{L}} = G$, see Table B.3 for the numerical value of G.

For vertical flow, the velocity u no longer decouples in (3.47). In this case, we must find $s^{\mathrm{TP,e}}$, and u^{TP} simultaneously from Eqs. (3.20) and (3.47) justified by Oleinik entropy condition applied to shocks between different configurations.

Equation (3.47) can be rewritten in terms of u^{TP} in the form

$$u^{\mathrm{TP}} = \frac{(fg^*)^{\mathrm{TP,e}} - \left(\frac{d}{ds}(fg^*)\right)^{\mathrm{TP,e}} \times (s^{\mathrm{TP,e}} - C_{\mathrm{e}})}{\left(\left(\frac{d}{ds}f\right)^{\mathrm{TP,e}} \times (s^{\mathrm{TP,e}} - C_{\mathrm{e}})\right) - (f^{\mathrm{TP,e}} - C_{\mathrm{e}})}. \tag{3.54}$$

After some calculations, from (3.20) we obtain another expression for u^{TP}:

$$u^{\mathrm{TP}} = \frac{u^{\mathrm{L}}\rho^{\mathrm{L}}_{\sigma c} - g_1 + \left(\frac{d}{ds}(fg^*)\right)^{\mathrm{TP,e}} d_1}{n_1 - \left(\frac{d}{ds}f\right)^{\mathrm{TP,e}}} \tag{3.55}$$

where g_1, d_1 and n_1 are given in Appendix E.1. From equations (3.54) and (3.55) we obtain a polynomial equation in $s := s_\sigma$, defined by $\mathbb{T}_e(\cdot, u^L, \rho^L_{\sigma c})$. We look for a real zero of $\mathbb{T}_e$ inside of the interval $[0,1]$ that satisfies the admissibility criteria. Afterwards we find the value of u^{TP} from Eq. (3.54) or (3.55).

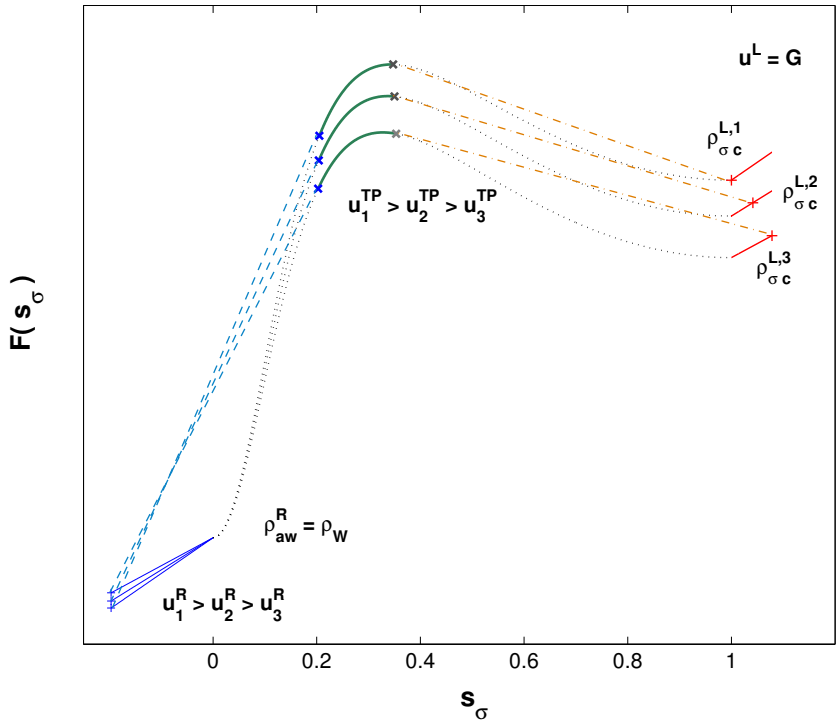

Fig. 3.4 Three Riemann problems for vertical migration, with $\rho^{L,1}_{\sigma c} = \rho^{TP}_{\sigma c}$, $\rho^{L,3}_{\sigma c} = \rho_{\sigma C}$, and $\rho^{L,2}_{\sigma c} = (\rho^{L,1}_{\sigma c} + \rho^{L,3}_{\sigma c})/2$. Observe that as the mass concentration of supercritical CO_2 decreases, the propagation fronts are faster and the volumetric flow rates become larger in the tp and spa configurations. The scale of this figure has been modified for visualization.

At the end of the s_σ-rarefaction wave, we find the point $s^{TP,C}$ by using the newly found Darcy velocity u^{TP} and Eq. (3.49). For doing so we solve Eq. (3.54) for $s^{TP,C}$ in place of $s^{TP,e}$, by replacing $C_e(\rho^L_{\sigma c})$ by $C_c(\rho^R_{aw})$. This is done by finding zeros (inside of the interval $[0,1]$) of a polynomial equation $\mathbb{Q}_c(\cdot, u^{TP})$ in s_σ found after carrying out some calculations on Eq. (3.54)), and by choosing the correct root. See Appendix E.2.2 for details.

Last we find the value of u^R by using equation (3.28) rewritten as

$$u^R = \frac{u^{TP}\left(n_2 - \left(\frac{d}{ds}f\right)^{TP,C} d_4\right) + g_2 - \left(\frac{d}{ds}(fg^*)\right)^{TP,C} d_4}{\rho^R_{aw}} \tag{3.56}$$

Notice that the value of u^{TP}, found from this set of rules, varies with the parameter $\rho^{\text{L}}_{\sigma c}$ and thus the fractional flux with gravity function changes continuously "from the left" .

The Riemann solution for vapor-liquid displacement for this case is illustrated in Fig. 3.4 for different vales of the "left" state, where we omit numerical values for convenience. In this figure the extended flux approach is used for the representation of the shocks between regions.

The inequalities (3.44)-(3.45) were easily verified numerically and graphically.

Chapter 4
Thermodynamic equilibrium between coexisting phases

In this chapter, first we present the concept of equilibrium of a closed thermodynamic system. We show how the minimization of the Gibbs free energy leads to the equilibrium of the system. An improved version of Beattie's [6] derivations for finding the explicit expression for the fugacity coefficient of a component in a closed heterogeneous multiphase multicomponent system is presented. Second, the classical equilibrium condition for finding minimae of the Gibbs free energy is presented.

We describe the classic substitution algorithm or flash calculation used for finding equilibrium states. We show how it is possible to obtain derivatives of the thermodynamic functions: this procedure is fundamental for implementing these algorithms in Riemann solvers.

Finally we show an example of the calculation of the partial fugacity coefficient for a vapor-liquid system.

4.1 Basics

We treat *thermodynamic systems* that correspond to heterogeneous bodies composed of homogeneous parts. Such systems will be considered to be *closed* where only heat and mechanical energy can be exchanged with the surroundings (unless stated otherwise, systems treated in this chapter are closed); in *open* systems there exists mass transfer between the system and the surroundings. Our interest is confined to large systems in which the individual molecules present in one phase are not affected by the molecules in the other phase, meaning that we exclude surface chemistry. Of course transfer between phases to achieve equilibrium will be considered. Without loss of generality we fix the mass of each chemical constituent in the system. An example is given by fixed amounts of carbon dioxide and water contained in a microscopical pore of the rock.

A *homogeneous* thermodynamic system displays uniform physical properties throughout. For instance a well stirred single-phase fluid contained in a closed vessel can be regarded as a homogeneous closed thermodynamic system (a body consisting of a single phase is not necessarily homogeneous). Furthermore a two-phase fluid contained in a

closed vessel is an example of a *heterogenous* closed system; it is a collection of homogeneous open systems: each phase can be regarded as a homogeneous open system and there exists mass transfer between phases.

The *thermodynamic state* of a system has been defined in the classic work by Fermi [21] in the language of Statistical Physics as the ensemble of all the dynamical states through which the system is rapidly passing. Indeed, there is an infinite number of patterns of molecular motion for which a system can have the same thermodynamic state. Therefore such a state cannot be studied in terms of physical properties at a molecular scale. In the language of classical thermodynamics we can study states using uniform intensive (independent of size or amount, e.g. temperature and pressure) or using extensive physical properties (e.g., volume and total number of moles) that depend on size and amount, see Fermi [21]. For a heterogenous closed system composed of various open systems (e.g., phases) we assume that the temperature and pressure are homogeneous throughout.

Consider a closed system composed of a given amount of moles of N different chemical compounds $\mathbf{n} = (n_i)$, for $i = 1, \ldots, N$. Assuming there is no mass exchange between the system and its surroundings, the thermodynamic state of a closed system (homogeneous or heterogeneous) is given by its uniform pressure P and temperature T, volume V, and composition $\mathbf{n}$. We assume that these quantities are related by an implicit relationship of the form

$$f(P, T, V, \mathbf{n}) = 0. \tag{4.1}$$

For heterogenous closed systems, relationship (4.1) is usually given empirically, for instance by the ideal gas law.

Consider a closed system contained in a cylinder having a movable piston of area a at one end. The pressure of the enclosed body against the walls of the cylinder is given by P, and therefore $P \cdot a$ is the force the body performs on the piston. If the piston shifts by a small distance dh, the infinitesimal amount of work dL performed by the body on its surroundings (through the piston) is

$$dL = Padh = PdV, \tag{4.2}$$

where dV is an infinitesimal variation of volume. Actually, this expression is valid in general, independently of the shape of the body.

The first law of thermodynamics states that an infinitesimal variation in the *internal energy* U of the system is given by

$$dU = -dL + dQ, \tag{4.3}$$

where dQ is the amount of heat exchanged by the system and its surroundings, see [21], [63], [78]. Note that the right side of (4.3) is not integrable exactly in general. Whenever the system performs work on its surroundings dL is positive; dQ is positive if the system receives heat from its surroundings.

Given the composition $\mathbf{n}$ of the system, we can define *transformations* of a closed system as paths in the space P-T-V representing a continuous succession of intermediate

thermodynamic states; such a system can be described by choosing any two out of the three variables P, T and V. *States of equilibrium* are defined as those for which physical properties do not vary as long as external conditions remain unchanged [21]. *Reversible transformations* are composed of successive intermediate states in thermodynamic equilibrium. The transitions between the successive states in a reversible transformation have to be performed infinitely slowly.

A basic concept in the second law of thermodynamics is the entropy.

Definition 4.1. We define the *entropy* of a state κ of the system as

$$S(\kappa) = \int_o^\kappa \frac{dQ}{T}, \tag{4.4}$$

where o is an arbitrary reference state in equilibrium, and the integral is taken over a reversible path.

Remark 4.1. Let κ and π be two states of the system. Then

$$S(\pi) - S(\kappa) \geq \int_\kappa^\pi \frac{dQ}{T}. \tag{4.5}$$

This inequality is valid when integrating along an irreversible path; the equality is valid for a reversible path. For an infinitesimal transformation we can write

$$dS \geq \frac{dQ}{T}; \tag{4.6}$$

the equality is valid when the transformation is reversible.

Details of the justification of the result above can be found in the work by Fermi [21]. Notice that the integral (4.4) is well defined because it is performed over a reversible path. Thus the entropy of the system for the state κ is independent of the previous history of the system. The same is true for the internal energy, volume, temperature and pressure of the system, it depends solely on the state κ. A *state function* is defined as a physical property that is independent of the previous history of the system, except that it depends on the final state.

Remark 4.2. We will assume except for $T = 0$ [K], that the internal energy and the entropy of a closed system are given by twice differentiable functions of T, P and V. We also assume that in the implicit relation (4.1) the variables T,P,V and $\mathbf{n}$, for instance represent V as a twice differentiable function of T and P for closed systems.

This implies as well that all state functions linearly defined from this two will be twice differentiable functions.

Definition 4.2. We define the *Helmholtz* energy of the system as

$$A \equiv U - TS. \tag{4.7}$$

Notice that the total differential for A is given by

$$dA = dU - TdS - SdT. \tag{4.8}$$

Let κ and π be the initial and final states of the system corresponding to an infinitesimal isothermal transformation of a thermodynamic system, held at temperature T. Therefore, for this transformation, from (4.8) we see that the variation of the Helmholtz energy is given by

$$dA = dU - TdS. \tag{4.9}$$

From the *first law* given by Eq. (4.3) we have

$$dA = -dL + dQ - TdS. \tag{4.10}$$

After application of inequality (4.6), Eq. (4.10) reduces to

$$dA \leq -dL. \tag{4.11}$$

From Eq. (4.11) we conclude that the absolute value of the decrease in the Helmholtz energy of the system is an upper limit for the work performed by the system. The equality sign holds if the transformation is reversible. Consider the case where there is no thermal insulation between the system and the environment (*i.e.*, there exists thermal conduction and both the system and the environment are at *constant* temperature T). If the system is mechanically isolated (in the sense that no external work is done on the system or performed by it), dL vanishes. Consequently for a transformation, held in those conditions, with initial state κ and final state π we have

$$A(\pi) \leq A(\kappa). \tag{4.12}$$

In other words, the Helmholtz energy cannot increase during an infinitesimal transformation held at constant temperature of a mechanically isolated system. A compact way of stating this fact is

$$dA_{T,V} \leq 0. \tag{4.13}$$

The notation $d\mathscr{F}_{T,V}$ represents an infinitesimal change of the state function $\mathscr{F}$ for constant temperature and volume.

When the temperature and the volume of a system are kept constant, a strict minimum of the Helmholtz energy corresponds to a state of stable equilibrium. Indeed, from Eq. (4.12) any irreversible transformation at constant T and V caused by a deviation from the minimizing state would decrease the Helmholtz energy, which is impossible because the Helmholtz energy is already at a minimum.

We would like to use a state function that recognizes states of equilibrium for constant temperature and pressure (e.g., we wish to establish conditions for equilibrium for a two-phase system, for fixed pressure and temperature).

Definition 4.3. We define the *Gibbs* free energy as

$$G \equiv A + PV. \tag{4.14}$$

The total differential of the Gibbs energy is given by

$$dG = dA + PdV + VdP. \tag{4.15}$$

For an isothermal and isobaric transformation from an initial state κ to a final state π we can combine Eq. (4.2), inequality (4.11) and the total differential (4.15) to obtain

$$G(\pi) \leq G(\kappa), \tag{4.16}$$

or alternatively

$$dG_{T,P} \leq 0. \tag{4.17}$$

We conclude that if the temperature and the pressure of a system are kept constant, the state of the system for which the Gibbs energy is a strict minimum is a state of equilibrium.

4.2 An explicit formulation for the Gibbs Free Energy

As mentioned in Section 4.1, heterogeneous closed systems are composed of various homogeneous open systems. For a heterogeneous closed system composed of various homogeneous systems, if we disregard surface contact energy, the total Gibbs energy is given by the sum of the Gibbs energies of each one of its parts, e.g., phases, which are themselves homogeneous open systems. For a heterogenous closed system composed of several chemical components distributed among M different phases, the Gibbs energy can be written as

$$G = \sum_{\alpha} G^{\alpha}(T, P, \mathbf{n}^{\alpha}), \tag{4.18}$$

where $\alpha = 1, \ldots, M$ and $\mathbf{n}^{\alpha} = (n_i^{\alpha})$ (n_i^{α} represents the number of moles of component i in phase α, for $i = 1, \ldots, N$; here N is the number of different chemical compounds present in the whole closed system and M is the number of different phases). The volume of each phase V^{α} does not appear in Eq. (4.18) because we can find it implicitly using an appropriate relation of the form (4.1): for homogeneous systems such as a homogeneous vapor phase, (4.1) is well approximated by an *equation of state*, generally given by a cubic in the compressibility factor, whose coefficients are functions of temperature, pressure and composition.

Notice that the total differential of each term of the sum in expression (4.18) is

$$dG^{\alpha} = \left(\frac{\partial G^{\alpha}}{\partial T}\right)_{P,\mathbf{n}^{\alpha}} dT + \left(\frac{\partial G^{\alpha}}{\partial P}\right)_{T,\mathbf{n}^{\alpha}} dP + \sum_{i} \left(\frac{\partial G^{\alpha}}{\partial n_i^{\alpha}}\right)_{T,P,\mathbf{n}^{\alpha,i}} dn_i^{\alpha}. \tag{4.19}$$

The subscripts stand for the variables held constant during differentiation. However, $\mathbf{n}^{\alpha,i}$ refers to all the components of $\mathbf{n}^{\alpha}$ except for n_i^{α}, *i.e.*,

$$\mathbf{n}^{\alpha,i} = (n_1^{\alpha}, n_2^{\alpha}, \ldots, n_{i-1}^{\alpha}, n_{i+1}^{\alpha}, \ldots, n_{\mathrm{n}}^{\alpha}). \tag{4.20}$$

For each homogeneous open system indexed by α, the first two derivatives of equation (4.19) are equivalent to the partial derivatives of the corresponding Gibbs energy when regarded as a homogeneous closed system with chemical composition $\mathbf{n}^{\alpha}$. Using (4.2), (4.3), (4.8) and (4.15) it can be easily shown that they are given by

$$(\partial G^{\alpha}/\partial T)_{P,\mathbf{n}^{\alpha}} = -S^{\alpha}, \tag{4.21}$$
$$(\partial G^{\alpha}/\partial P)_{T,\mathbf{n}^{\alpha}} = V^{\alpha}. \tag{4.22}$$

Definition 4.4. We define the *Chemical Potential* for component i in phase α as

$$\mu_i^{\alpha} \equiv \left(\frac{\partial G^{\alpha}}{\partial n_i^{\alpha}}\right)_{T,P,\mathbf{n}^{\alpha,i}}. \tag{4.23}$$

Therefore using Eqs. (4.19)-(4.23) we can write

$$dG^{\alpha} = -S^{\alpha} dT + V^{\alpha} dP + \sum_{i} \mu_i^{\alpha} dn_i^{\alpha}. \tag{4.24}$$

Notice that at constant temperature and pressure this expression becomes

$$dG^{\alpha}_{T,P} = \sum_{i} \mu_i^{\alpha} dn_i^{\alpha}, \tag{4.25}$$

and from Eq. (4.18) we obtain

$$dG_{T,P} = \sum_{i,\alpha} \mu_i^{\alpha} dn_i^{\alpha}. \tag{4.26}$$

At this point we are interested in "integrating" expression (4.26). We use the approach given in [78].

Definition 4.5. We define the molar Gibbs energy, the molar entropy and the nonzero molar volume of phase α present in the system, given by $g^{\alpha} = G^{\alpha}/n^{\alpha}$, $s^{\alpha} = S^{\alpha}/n^{\alpha}$ and $v^{\alpha} = V^{\alpha}/n^{\alpha}$ respectively, where $n^{\alpha} = \sum_i n_i^{\alpha}$ is the (nonzero) total number of moles of all compounds in phase α. We introduce ξ_i^{α}, the *molar fraction* of component i in phase α, given by $\xi_i^{\alpha} = n_i^{\alpha}/n^{\alpha}$.

Applying the chain rule to $G^{\alpha} = n^{\alpha} g^{\alpha}$ and $n_i^{\alpha} = \xi_i^{\alpha} n^{\alpha}$ in Eq. (4.24) we obtain

$$n^\alpha dg^\alpha + g^\alpha dn^\alpha = n^\alpha(-s^\alpha dT + v^\alpha dP) + \sum_i \mu_i^\alpha \left(\xi_i^\alpha dn^\alpha + n^\alpha d\xi_i^\alpha\right), \tag{4.27}$$

Rearranging the terms in Eq. (4.27) we have

$$n^\alpha \left(dg^\alpha + s^\alpha dT - v^\alpha dP - \sum_i \mu_i^\alpha d\xi_i^\alpha \right) + dn^\alpha \left(g^\alpha - \sum_i \mu_i^\alpha \xi_i^\alpha \right) = 0. \tag{4.28}$$

The variables n^α, $\alpha = 1,\ldots,M$, determine the size of the system and can be chosen arbitrarily. We study arbitrary infinitesimal molar transformations of phase α, given by dn^α. Therefore n^α and dn^α are independent and arbitrary, see [78]. Therefore Eq. (4.28) can only be zero for all perturbations dn^α, dg^α, dT, dP and $d\xi_i^\alpha$ for all $i = 1,\ldots,N$, when both expressions inside parentheses are zero. We conclude for each phase

$$g^\alpha = \sum_i \mu_i^\alpha \xi_i^\alpha. \tag{4.29}$$

Multiplying (4.29) by n^α we have

$$G^\alpha = \sum_i \mu_i^\alpha n_i^\alpha. \tag{4.30}$$

Adding all terms in (4.30) we obtain

$$G = \sum_{i,\alpha} \mu_i^\alpha n_i^\alpha. \tag{4.31}$$

Therefore for constant temperature and pressure we can write

$$G_{T,P} = \sum_{i,\alpha} \mu_i^\alpha(\mathbf{n}^\alpha) n_i^\alpha. \tag{4.32}$$

For fixed temperature and pressure, (4.32) is the integral version of (4.26).

Remark 4.3. We differentiate (4.32) and compare the results with (4.24) to conclude that for an isothermal and isobaric transformation

$$\sum_i n_i^\alpha d\mu_i^\alpha = 0. \tag{4.33}$$

This is the *Gibbs-Duhem* equation. In Sections 4.4 and 4.5 we will use this identity.

4.3 Derivation of an explicit expression for the chemical potential

Our final objective is to find an explicit expression for the Gibbs energy of a heterogeneous closed thermodynamic system. Therefore we need to find an expression for the chemical potential μ_i^α of component i in each phase α depending on the physical variables P, T and the concentrations $\mathbf{C}^\alpha = (C_i^\alpha)$. These concentrations are defined as the number of moles $\mathbf{n}^\alpha = (n_i^\alpha)$ divided by the volume of phase α, V^α. To find these expressions for the chemical potential we will assemble the basic equations relating state functions of the thermodynamic model.

First, we find explicit expressions for the internal energy and entropy of a homogeneous system consisting of n moles of a single chemical component in a single phase. In the next step we derive similar expressions for the internal energy and entropy for single phase homogeneous mixtures (*i.e.*, with several chemical components). In the latter step we use special equilibrium assumptions introduced by Beattie [6]. Finally we derive the expression for the chemical potential.

4.3.1 Properties of single component systems

For independent variables T and V, and for an infinitesimal reversible transformation of the system, the change in internal energy U for a pure component closed homogeneous system is given by

$$dU = \left(\frac{\partial U}{\partial T}\right)_V dT + \left(\frac{\partial U}{\partial V}\right)_T dV. \tag{4.34}$$

The transformation is reversible, therefore from Eqs. (4.2), (4.3), and (4.6) we obtain

$$dS = \frac{1}{T}\left(\frac{\partial U}{\partial T}\right)_V dT + \frac{1}{T}\left(\left(\frac{\partial U}{\partial V}\right)_T + P\right) dV. \tag{4.35}$$

We conclude that the right hand side of (4.35) is the exact differential of the entropy (with independent variables T and V). Assuming that the entropy is twice continuously differentiable, from Schwartz theorem [45] its mixed derivatives are equal. Therefore comparing them and rearranging terms we obtain

$$\left(\frac{\partial U}{\partial V}\right)_T = T\left(\frac{\partial P}{\partial T}\right)_V - P. \tag{4.36}$$

Therefore Eq. (4.34) can be written as

$$dU = \left(\frac{\partial U}{\partial T}\right)_V dT + \left(T\left(\frac{\partial P}{\partial T}\right)_V - P\right) dV. \tag{4.37}$$

Replacing (4.36) in (4.35) we see that an infinitesimal variation of entropy is given by

$$dS = \frac{1}{T}\left(\frac{\partial U}{\partial T}\right)_V dT + \left(\frac{\partial P}{\partial T}\right)_V dV. \tag{4.38}$$

Consider a reference state (V_0, T_0) at $P_0 \equiv 1$ [atm]. We use 1 [atm] as a reference state because all the tables for instance in the Handbook of Chemistry and Physics [44] give the thermodynamic quantities with $P_0 = 1$[atm] as the reference state. For finding the internal energy and the entropy at a volume V and temperature T we take our system reversibly from the reference state above to a state of large volume V^* at constant temperature T_0 where the system behaves ideally. At volume V^* we change the temperature of the system reversibly from T_0 to T. Finally, we compress the system reversibly at constant temperature until it reaches the volume V (for each step described in the transformation above, the presssure can be recovered implicitly given an appropriate equation of state).

The stepwise *reversible* transformation described above can be summarized by the following steps

$$V_0 \xrightarrow{T_0} V^*, \tag{4.39}$$

$$T_0 \xrightarrow{V^*} T, \tag{4.40}$$

$$V^* \xrightarrow{T} V \tag{4.41}$$

where the arrow's superscripts denote the variable that has been fixed.

We integrate along the reversible transformation suggested above. From Eq. (4.37) the total variation of the internal energy along the transformations (4.39)-(4.41) is given by

$$U(V,T) - U(V_0,T_0) = \int_{V_0}^{V^*} \left(T\left(\frac{\partial P}{\partial T}\right)_V - P\right)(\upsilon, T_0)\, d\upsilon + \int_{T_0}^{T} nc_{\mathrm{v}}^*\, d\tau + \int_{V^*}^{V} \left(T\left(\frac{\partial P}{\partial T}\right)_V - P\right)(\upsilon, T)\, d\upsilon. \tag{4.42}$$

where

$$c_{\mathrm{v}}^*(T) := \frac{1}{n}\left(\frac{\partial U}{\partial T}\right)_V (V^*, T), \tag{4.43}$$

is the molar heat capacity at constant volume, for volume V^* and temperature T,a and τ and υ are integrating variables for the temperature T and the volume V. Analogously from (4.38) we calculate the total variation of the entropy S along the transformation (4.39)-(4.41)

$$S(V,T)-S(V_0,T_0)=\int_{V_0}^{V^*}\left(\left(\frac{\partial P}{\partial T}\right)_V-\frac{nR}{\upsilon}\right)(\upsilon,T_0)\,d\upsilon+\int_{T_0}^{T}\frac{nc_{\mathrm{v}}^*}{\tau}\,d\tau$$
$$+\int_{V^*}^{V}\left(\left(\frac{\partial P}{\partial T}\right)_V-\frac{nR}{\upsilon}\right)(\upsilon,T)\,d\upsilon+nR\ln\frac{V}{V_0}. \quad (4.44)$$

where we subtract and add the integral $\int_{V_0}^{V}\frac{nR}{\upsilon}\,d\upsilon$.

Let

$$nu^{0,*}:=U(V_0,T_0)-\int_{V_0}^{V^*}\left(P-T\left(\frac{\partial P}{\partial T}\right)_V\right)(\upsilon,T_0)\,d\upsilon+\int_{T_0}^{T}nc_{\mathrm{v}}^*\,d\tau, \quad (4.45)$$

$$ns^{0,*}:=S(V_0,T_0)-\int_{V_0}^{V^*}\left(\frac{nR}{\upsilon}-\left(\frac{\partial P}{\partial T}\right)_V\right)(\upsilon,T_0)\,d\upsilon+\int_{T_0}^{T}\frac{nc_{\mathrm{v}}^*}{\tau}\,d\tau+nR\ln\frac{T}{T_0} \quad (4.46)$$
$$-nR\ln\frac{V_0}{1[\mathrm{m}^3]}.$$

Remark 4.4. The intermediate path corresponds to the interval $V^*\times[T_0,T]$, where $V_0\ll V^*$. The order of magnitude of V_0 will be fixed on the rest of this chapter and will be chosen in such a way that states belonging to the segment $[V_0,V^*]\times T$ are above the *dew curve* (or condensation curve) of the fluid mixture and correspond to thermodynamical states at low pressures. Therefore the ideal gas law can be used as a good approximation for relating thermodynamic states belonging to this segment. On the rest of this chapter, for all homogeneous pure systems corresponding to a single component we use the same initial pure internal energy $U(V_0,T_0)$ and initial pure entropy $S(V_0,T_0)$.

Remark 4.5. J.P. Joule showed experimentally that for pure component gases of fixed mass subject to low pressures, changes in the internal energy are accounted for changes in the temperature of the gas, and are approximately independent of the volume, see [21]. From this he concluded that at low pressures (or equivalently large volumes) the molar heat capacity is approximately a function of temperature only (consequently we assume that for large volumes the limit $c_{\mathrm{v}}^{\infty}:=\lim_{V^*\to\infty}c_{\mathrm{v}}^*$ exists and is well defined. Using remark 4.4, we conclude that the expressions $u^{0,*}$ and $s^{0,*}$ defined above are approximately functions of temperature only. Addittionally, from the virial expansion of the compressibility factor defined as $Z=PV/RT$, see [78, Pg. 72], we obtain that $P=nRT/V+O(1/V^2)$. We assume the virial expansion is uniformly convergent in V (for large volumes) and its terms are locally continuously differentiable functions of the volume. From these results we conclude that the integrals in Eqs. (4.42), (4.44), (4.45) and (4.46) converge in the limit $V^*\to\infty$.

We can now define

$$nu^0 := U(V_0,T_0) - \int_{V_0}^{\infty} \left(P - T\left(\frac{\partial P}{\partial T}\right)_V \right)(\upsilon,T_0)\, d\upsilon + \int_{T_0}^{T} nc_{\mathrm{v}}^{\infty}\, d\tau, \tag{4.47}$$

$$ns^0 := S(V_0,T_0) - \int_{V_0}^{\infty} \left(\frac{nR}{\upsilon} - \left(\frac{\partial P}{\partial T}\right)_V \right)(\upsilon,T_0)\, d\upsilon + \int_{T_0}^{T} \frac{nc_{\mathrm{v}}^{\infty}}{\tau}\, d\tau + nR\ln\frac{T}{T_0} - nR\ln\frac{V_0}{1[\mathrm{m}^3]}. \tag{4.48}$$

Remark 4.6. From remarks 4.4 and 4.5 we conclude that for a pure component homogeneous system, (4.47) and (4.48) are functions of temperature only. Moreover they are independent of the phase state of the system at the volume V and the temperature T.

We rewrite Eqs. (4.42) and (4.44) using the definitions (4.47), (4.48)

$$U(V,T) = \int_{V}^{\infty} \left(P - T\left(\frac{\partial P}{\partial T}\right)_V \right)(\upsilon,T)\, d\upsilon + nu^0, \tag{4.49}$$

$$S(V,T) = \int_{V}^{\infty} \left(\frac{nR}{\upsilon} - \left(\frac{\partial P}{\partial T}\right)_V \right)(\upsilon,T)\, d\upsilon + nR\ln\frac{V\cdot 1[\mathrm{Pa}]}{nRT} + ns^0. \tag{4.50}$$

These are explicit expressions for the internal energy of a pure component single phase system at the volume V and temperature T.

4.3.2 Homogeneous mixture properties

Consider a homogeneous system of N chemical compounds each with n_i number of moles for $i = 1,\ldots,N$, and let $n_{\mathrm{T}} = \sum_i n_i$ denote the total number of moles in the system. Let U_i^e, S_i^e, $C_{\mathrm{v},i}^{*,e}$, and $c_{\mathrm{v},i}^{*,e}$ denote the *equilibrium* internal energy, entropy, heat capacity and molar heat capacity (at constant volume) of component i in the mixture. For the definition of equilibrium properties see [6]. Beattie [6] showed that at very low pressures under particular equilibrium assumptions for gas mixtures (other important equilibrium assumptions are given by the Gibbs-Dalton law [23] and Lewis and Randall rule [43], see [78]) the following equations are valid:

$$P = \frac{\sum_i n_i RT}{V} \tag{4.51}$$

$$U(V^*,T) = \sum_i U_i^e(V^*,T) \tag{4.52}$$

$$S(V^*,T) = \sum_i S_i^e(V^*,T) \tag{4.53}$$

$$C_{\rm v}^* = \sum_i C_{{\rm v},i}^* = \sum_i n_i c_{{\rm v},i}^* \tag{4.54}$$

where the superscript $(^*)$ stands for evaluation at low pressures (equivalently large volume). For convenience we omit below the superscript e for equilibrium.

Along a reversible transformation at constant composition Eqs. (4.34)-(4.38) are valid for the overall physical properties for homogeneous mixtures. Taking into account Eq. (4.54), the line integral of the total internal energy and total entropy of the system along the reversible transformation (4.39), (4.40) and (4.41) (at constant composition) is given by

$$U(V,T) - U(V_0,T_0) = \int_{V_0}^{V^*} \left(T \left(\frac{\partial P}{\partial T} \right)_{V,\mathbf{n}} - P \right) (\upsilon, T_0)\, d\upsilon + \int_{T_0}^{T} \sum_i n_i c_{{\rm v},i}^*\, d\tau + \int_{V^*}^{V} \left(T \left(\frac{\partial P}{\partial T} \right)_{V,\mathbf{n}} - P \right) (\upsilon, T)\, d\upsilon. \tag{4.55}$$

$$S(V,T) - S(V_0,T_0) = \int_{V_0}^{V^*} \left(\left(\frac{\partial P}{\partial T} \right)_{V,\mathbf{n}} - \frac{\sum_i n_i R}{\upsilon} \right) (\upsilon, T_0)\, d\upsilon + \int_{T_0}^{T} \frac{\sum_i n_i c_{{\rm v},i}^*}{\tau}\, d\tau + \int_{V^*}^{V} \left(\left(\frac{\partial P}{\partial T} \right)_{V,\mathbf{n}} - \frac{\sum_i n_i R}{\upsilon} \right) (\upsilon, T)\, d\upsilon + \sum_i n_i R \ln \frac{V}{V_0}. \tag{4.56}$$

where the subscript $\mathbf{n}$ denotes that the compositions have been fixed. From Eq. (4.55) we have

$$U(V^*,T_0) = \int_{V_0}^{V^*} \left(T \left(\frac{\partial P}{\partial T} \right)_{V,\mathbf{n}} - P \right) (\upsilon, T_0)\, d\upsilon + U(V_0,T_0). \tag{4.57}$$

On the other hand from Eqs. (4.49) and (4.52) we obtain

$$U(V^*,T_0) = \sum_i U_i(V^*,T_0) \tag{4.58}$$

$$= N\int_{V_*}^{\infty}\left(P - T\left(\frac{\partial P}{\partial T}\right)_{V,\mathbf{n}}\right)(\upsilon,T_0)\,d\upsilon + \sum_i n_i u_i^0(V^*,T_0). \tag{4.59}$$

where u_i^0 corresponds to single component systems as given in (4.45). Analogously for the total entropy from Eq. (4.56) we have

$$S(V^*,T_0) = \int_{V_0}^{V^*}\left(\left(\frac{\partial P}{\partial T}\right)_{V,\mathbf{n}} - \frac{\sum_i n_i R}{\upsilon}\right)(\upsilon,T_0)\,d\upsilon + \sum_i n_i R\ln\frac{V^*}{V_0} + S(V_0,T_0), \tag{4.60}$$

and from Eqs. (4.50) and (4.53) we obtain

$$S(V^*,T_0) = \sum_i S_i^e(V^*,T_0) \tag{4.61}$$

$$= \sum_i \int_{V^*}^{\infty}\left(\frac{n_i R}{\upsilon} - \left(\frac{\partial P}{\partial T}\right)_{V,\mathbf{n}}\right)(\upsilon,T)\,d\upsilon + \sum_i n_i R\ln\frac{V^*\cdot 1[\mathrm{Pa}]}{n_i R T_0} \tag{4.62}$$

$$+ \sum_i n_i s_i^0(V^*,T_0).$$

Now from (4.47) and (4.48) we have

$$\sum_i n_i u_i^0 = \int_{T_0}^{T}\sum_i n_i c_{\mathrm{v},i}^{\infty}\,d\tau + \sum_i n_i u_i^0(V^*,T_0), \tag{4.63}$$

$$\sum_i n_i s_i^0 = \int_{T_0}^{T}\frac{\sum_i n_i c_{\mathrm{v},i}^{\infty}}{\tau}\,d\tau + \sum_i n_i s_i^0(V^*,T_0) + \sum_i n_i R\ln\frac{T}{T_0}. \tag{4.64}$$

Therefore combining (4.55), (4.57), (4.59), and (4.63) for the internal energy and (4.56), (4.60), (4.62), and (4.64) for the entropy and using remark 4.5, taking the limit $V^*\to\infty$ we arrive to

$$U(V,T) = \int_{V}^{\infty}\left(P - T\left(\frac{\partial P}{\partial T}\right)_{V,\mathbf{n}}\right)(\upsilon,T)\,d\upsilon + \sum_i n_i u_i^0, \tag{4.65}$$

$$S(V,T) = \int_{V}^{\infty}\left(\frac{\sum_i n_i R}{\upsilon} - \left(\frac{\partial P}{\partial T}\right)_{V,\mathbf{n}}\right)(\upsilon,T)\,d\upsilon - \sum_i n_i R\ln\frac{V\cdot 1[\mathrm{Pa}]}{n_i R T} + \sum_i n_i s_i^0. \tag{4.66}$$

From the expressions above we obtain an expression for the Helmholtz energy

$$A(V,T) = U(V,T) - T \cdot S(V,T) = \int_V^\infty \left(P - \frac{\sum_i n_i RT}{\upsilon} \right) d\upsilon + \sum_i n_i RT \ln \frac{V \cdot 1[\text{Pa}]}{n_i RT} + \sum_i n_i (u_i^0 - T s_i^0). \quad (4.67)$$

The first integral in (4.67) converges uniformly (see remark 4.5). From this assertion we can exchange the derivative and the integration operators to obtain the derivative of A with respect to the amount of moles of component i. We can easily see that

$$\mu_i \equiv \left(\frac{\partial A}{\partial n_i} \right)_{V,T,\mathbf{n}^i}, \quad (4.68)$$

where μ_i is the chemical potential defined in (4.23) (we drop the superscript α as we are only studying a single phase homogeneous system). Eq. (4.68) can be deduced using the thermodynamic relations stated in this chapter. From remark 4.5 the term $u_i^0 - T s_i^0$ is independent of the mixture composition. Therefore from Eqs. (4.67), (4.68) we obtain

$$\mu_i = \int_V^\infty \left(\left(\frac{\partial P}{\partial n_i} \right)_{V,T,\mathbf{n}^i} - \frac{RT}{\upsilon} \right) d\upsilon - RT \ln \frac{V \cdot 1[\text{Pa}]}{n_i RT} + RT + u_i^0 - T s_i^0. \quad (4.69)$$

Notice that V in the equation above represents the total volume of the system. This is the expression for the chemical potential of component i in a homogeneous N-component mixture.

4.4 The equilibrium formulation

As stated in (4.18), if we disregard surface contact energy, the total Gibbs energy of a heterogeneous closed system is given by the sum of its partial Gibbs energies. At fixed pressure and temperature a system in equilibrium can be subject to infinitesimal isobaric and isothermal transformations (for instance molar compositions $\mathbf{n}^\alpha$ of the different phases can change) whenever $dG_{T,P} = 0$. Indeed, as shown in Section 4.1, the Gibbs energy is a minimum for constant pressure and temperature at equilibrium states. Consider a reversible infinitesimal transformation given by the transfer of an infinitesimal amount of mass dm of the i-th component from the α-th phase to the β-th phase at constant pressure and temperature. At its initial and final states, the system is in thermodynamic equilibrium. Notice that $dn_i^\alpha = -dm$, $dn_i^\beta = dm$. From this we obtain

$$dG_{T,P} = dG_{T,P}^\alpha + dG_{T,P}^\beta \quad (4.70)$$

$$= -\left(\frac{\partial G^\alpha}{\partial n_i^\alpha} \right)_{T,P,\mathbf{n}^{\alpha,i}} dm + \left(\frac{\partial G^\beta}{\partial n_i^\beta} \right)_{T,P,\mathbf{n}^{\alpha,i}} dm \quad (4.71)$$

From (4.23) and (4.71) we conclude that a necessary condition for thermodynamic equilibrium is

$$\mu_i^\alpha = \mu_i^\beta . \tag{4.72}$$

This argument can be generalized for a transformation involving more than two phases, for instance see [63, Appendix A]. For a heterogenous closed system with N components and M phases, a necessary and sufficient condition for equilibrium is

$$\mu_i^\alpha = \mu_i^\beta \quad \text{for } i = 1,\dots,N \text{ and } \alpha,\beta \in \{1,\dots,M\}. \tag{4.73}$$

For two-phase, two-component systems, given a (positive) total composition of the different components $\mathbf{n} := (n_1, n_2)^{\mathrm{T}}$, based on (4.32) we can find the equilibrium of the system at fixed temperature and pressure by solving the problem:

$$\begin{aligned} \text{minimize} \quad & \mathbf{G} = \mathbf{G}^{\mathrm{L}} + \mathbf{G}^{\mathrm{V}} \\ & = \langle \mathbf{n}^{\mathrm{L}}, \mu^{\mathrm{L}} \rangle + \langle \mathbf{n}^{\mathrm{V}}, \mu^{\mathrm{V}} \rangle, && (4.74) \\ \text{subject to} \quad & \mathbf{n}_{\mathrm{T}} = \mathbf{n}^{\mathrm{L}} + \mathbf{n}^{\mathrm{V}}, && (4.75) \\ \text{and} \quad & \mathbf{n}^{\mathrm{L}}, \mathbf{n}^{\mathrm{V}} > 0. && (4.76) \end{aligned}$$

where (4.76) represents a component-wise inequality, $\mathbf{n}^{\mathrm{L}} = (n_1^{\mathrm{L}}, n_2^{\mathrm{L}})^{\mathrm{T}}$, and $\mathbf{n}^{\mathrm{V}} = (n_1^{\mathrm{V}}, n_2^{\mathrm{V}})^{\mathrm{T}}$ represent the molar distribution of the different components among the coexisting phases, and the corresponding chemical potentials are given by $\mu^{\mathrm{L}} = (\mu_1^{\mathrm{L}}, \mu_2^{\mathrm{L}})^{\mathrm{T}}$ and $\mu^{\mathrm{V}} = (n_1^{\mathrm{V}}, n_2^{\mathrm{V}})^{\mathrm{T}}$. Phase stability conditions on the Gibbs energy change of mixing are used whenever we substitute either of the inequality constraints (4.76) with an equality, which implies that our system is in fact a single phase, see [4, pg. 269], [63], [78, pg. 575], [88].

The formulation of the problem (4.74)-(4.76) has been written in the notation introduced by Trangenstein [88]. In this work the author illustrates some useful consequences of the Gibbs-Duhem equation (4.33). For instance, for both the liquid and the vapor phase, the 2×2 matrix of partial molar derivatives of the chemical potential given by $\partial \mu^\alpha / \partial \mathbf{n}^\alpha$, where $\alpha = \mathrm{L}, \mathrm{V}$, is symmetric. Indeed, for fixed temperature and pressure the chemical potential is a smooth scalar function of two variables. The Hessian of such a function is symmetric, and from the Gibbs-Duhem equation we obtain

$$\frac{\partial}{\partial \mathbf{n}^\alpha} \left[\frac{\partial \left(\mathbf{n}^{\mathrm{T}} \mu^\alpha \right)}{\partial \mathbf{n}^\alpha} \right]^{\mathrm{T}} = \frac{\partial \mu^\alpha}{\partial \mathbf{n}^\alpha}. \tag{4.77}$$

for $\alpha = \mathrm{L}, \mathrm{V}$, from which we conclude the assertion. Another useful result found in [88] is the description of necessary and sufficient conditions for a minimum of the Gibbs energy: let B denote the 2×4 matrix

$$B = \begin{pmatrix} I \\ -I \end{pmatrix}, \tag{4.78}$$

where I is the identity 2×2 matrix. Based on the formulation (4.74)-(4.76) notice that if $\bar{\mathbf{n}}_0 := \left((\mathbf{n}_0^{\mathrm{L}})^{\mathrm{T}}, (\mathbf{n}_0^{\mathrm{V}})^{\mathrm{T}} \right)^{\mathrm{T}}$ is any solution of (4.75) then the general solution is

$$\bar{\mathbf{n}} := \bar{\mathbf{n}}_0 + B\mathbf{m}, \tag{4.79}$$

where $\mathbf{m} = (m_1, m_2)^{\mathrm{T}}$. Now we can focus on finding the value of $\mathbf{m}$ such that $\bar{\mathbf{n}}$ given by Eq. (4.79) minimizes the Gibbs free energy and simultaneously satisfies the inequality constraints. Notice that this simplification cuts the number of unknowns in half. Moreover observe that $\bar{\mathbf{n}} \geq 0$ if and only if

$$-(n_1^{\mathrm{L}})_0 \leq m_1 \leq (n_1^{\mathrm{V}})_0, \tag{4.80}$$
$$-(n_2^{\mathrm{L}})_0 \leq m_2 \leq (n_2^{\mathrm{V}})_0. \tag{4.81}$$

Using the notation above we obtain the second order Taylor approximation

$$\mathbf{G}(\bar{\mathbf{n}}_0 + B\mathbf{m}) \approx \mathbf{G}(\bar{\mathbf{n}}_0) + [\nabla \mathbf{G}(\bar{\mathbf{n}}_0)]^{\mathrm{T}} B\mathbf{m} + \frac{1}{2} D^2\mathbf{G}(\bar{\mathbf{n}}_0)(B\mathbf{m}, B\mathbf{m}). \tag{4.82}$$

Now notice that $\nabla \mathbf{G}(\bar{\mathbf{n}}_0) = (\nabla G^{\mathrm{L}}(\bar{\mathbf{n}}_0), \nabla G^{\mathrm{V}}(\bar{\mathbf{n}}_0))^{\mathrm{T}}$. Furthermore we have that

$$D^2\mathbf{G} = \begin{pmatrix} \frac{\partial \mu^{\mathrm{L}}}{\partial \mathbf{n}^{\mathrm{L}}} & \mathbf{0} \\ \mathbf{0} & \frac{\partial \mu^{\mathrm{V}}}{\partial \mathbf{n}^{\mathrm{V}}} \end{pmatrix}. \tag{4.83}$$

where $\mathbf{0}$ is the 2×2 matrix of zero entries. Therefore from (4.83) we can rewrite (4.82) as

$$\mathbf{G}(\bar{\mathbf{n}}_0 + B\mathbf{m}) \approx \mathbf{G}(\bar{\mathbf{n}}_0) + [\mathbf{G}^1]^{\mathrm{T}}\mathbf{m} + \frac{1}{2}\mathbf{m}^{\mathrm{T}}\mathbf{G}_2\mathbf{m}, \tag{4.84}$$

where

$$\mathbf{G}_1 = \mathbf{B}^{\mathrm{T}} \begin{pmatrix} \mu^{\mathrm{L}}(\bar{\mathbf{n}}_0) \\ \mu^{\mathrm{V}}(\bar{\mathbf{n}}_0) \end{pmatrix} = \mu^{\mathrm{L}} - \mu^{\mathrm{V}}, \tag{4.85}$$

$$\mathbf{G}_2 = B^{\mathrm{T}} D^2\mathbf{G}(\bar{\mathbf{n}}_0)\mathbf{B} = \frac{\partial \mu^{\mathrm{L}}}{\partial \mathbf{n}^{\mathrm{L}}} + \frac{\partial \mu^{\mathrm{V}}}{\partial \mathbf{n}^{\mathrm{V}}}. \tag{4.86}$$

From (4.84) the Gibbs free energy has a local minimum at $\bar{\mathbf{n}}_0$ if $\mathbf{G}_1 = 0$ and $\mathbf{G}_2$ is a positive definite matrix; if the Gibbs free energy has a local minimum at $\bar{\mathbf{n}}_0$, then $\mathbf{G}_1 = 0$ and $\mathbf{G}_2$ is non-negative. From these observations we obtain again the necessary condition for two-phase two-component equilibrium (4.72).

Before finishing this section, we will show how the Hessian matrix $\mathbf{G}_2$ is calculated. From the Gibbs-Duhem equation (4.33) we find

$$\left(n_1^{\alpha}, n_2^{\alpha}\right) \begin{pmatrix} \frac{\partial \mu_1^{\alpha}}{\partial n_1^{\alpha}} & \frac{\partial \mu_1^{\alpha}}{\partial n_2^{\alpha}} \\ \frac{\partial \mu_2^{\alpha}}{\partial n_1^{\alpha}} & \frac{\partial \mu_2^{\alpha}}{\partial n_2^{\alpha}}, \end{pmatrix} = 0, \tag{4.87}$$

for $\alpha = \mathrm{L}, \mathrm{V}$. As $\partial \mu^{\alpha} / \partial \mathbf{n}^{\alpha}$ is symmetric, from (4.87) we see that

$$\frac{\partial \mu^\alpha}{\partial \mathbf{n}^\alpha} = \frac{n_1^\alpha}{n_2^\alpha}\frac{\partial \mu_1^\alpha}{\partial n_1^\alpha}\begin{pmatrix} \frac{n_2^\alpha}{n_1^\alpha} & -1 \\ -1 & \frac{n_1^\alpha}{n_2^\alpha} \end{pmatrix}. \tag{4.88}$$

Applying (4.88) for both the liquid and vapor phases we obtain the expression for the Hessian

$$\mathbf{G}_2 = \begin{pmatrix} \frac{\partial \mu_1^{\mathrm{L}}}{\partial n_1^{\mathrm{L}}} + \frac{\partial \mu_1^{\mathrm{V}}}{\partial n_1^{\mathrm{V}}} & \hat{\mathbf{G}}_2 \\ \hat{\mathbf{G}}_2 & \left(\frac{n_1^{\mathrm{L}}}{n_2^{\mathrm{L}}}\right)^2 \frac{\partial \mu_1^{\mathrm{L}}}{\partial n_1^{\mathrm{L}}} + \left(\frac{n_1^{\mathrm{V}}}{n_2^{\mathrm{V}}}\right)^2 \frac{\partial \mu_1^{\mathrm{V}}}{\partial n_1^{\mathrm{V}}} \end{pmatrix}, \tag{4.89}$$

where

$$\hat{\mathbf{G}}_2 := -\frac{n_1^{\mathrm{L}}}{n_2^{\mathrm{L}}}\frac{\partial \mu_1^{\mathrm{L}}}{\partial n_1^{\mathrm{L}}} - \frac{n_1^{\mathrm{V}}}{n_2^{\mathrm{V}}}\frac{\partial \mu_1^{\mathrm{V}}}{\partial n_1^{\mathrm{V}}}. \tag{4.90}$$

In practice, we prefer to calculate the partial derivatives relative to molar fractions, rather than relative to the total amount of moles in the system. Therefore performing the change of variables

$$x_1 = \frac{n_1^{\mathrm{L}}}{n_1^{\mathrm{L}} + n_2^{\mathrm{L}}}, \qquad y_2 = \frac{n_2^{\mathrm{V}}}{n_1^{\mathrm{V}} + n_2^{\mathrm{V}}}, \tag{4.91}$$

we obtain

$$\mathbf{G}_2 = \frac{1}{n^{\mathrm{V}}}\begin{pmatrix} \frac{n^{\mathrm{V}}}{n^{\mathrm{L}}}\frac{\partial \mu_1^{\mathrm{L}}}{\partial x_1}(1-x_1) - \frac{\partial \mu_1^{\mathrm{V}}}{\partial y_2} y_2 & \hat{\mathbf{G}}_2 \\ \hat{\mathbf{G}}_2 & \frac{n^{\mathrm{V}}}{n^{\mathrm{L}}}\frac{x_1^2}{1-x_1}\frac{\partial \mu_1^{\mathrm{L}}}{\partial x_1} - \frac{(1-y_2)^2}{y_2}\frac{\partial \mu_1^{\mathrm{V}}}{\partial y_2} \end{pmatrix}, \tag{4.92}$$

where we introduce the notation

$$\hat{\mathbf{G}}_2 = (1-y_2)\frac{\partial \mu_1^{\mathrm{V}}}{\partial y_2} - \frac{n^{\mathrm{V}}}{n^{\mathrm{L}}} x_1 \frac{\partial \mu_1^{\mathrm{L}}}{\partial x_1}, \tag{4.93}$$

and $n^{\mathrm{V}} = n_1^{\mathrm{V}} + n_2^{\mathrm{V}}$ and $n^{\mathrm{L}} = n_1^{\mathrm{L}} + n_2^{\mathrm{L}}$. In practice we can impose the restriction $n^{\mathrm{V}} > 0$ and look for solutions of $\mathbf{G}_1 = 0$ such that the matrix $n^{\mathrm{V}}\mathbf{G}_2$ is positive definite. Such solutions can be found by using sucessive substitution methods commonly called flash calculations, described in many references, see [78, 93]; as an alternative, minimization algorithms as the one introduced in [88] can be applied to solve the constrained minimization problem (4.74)-(4.76).

In Section 4.5 we show that under special conditions there exists a 1-D manifold of equilibrium states in the neighborhood of an equilibrium state satisfying $\mathbf{G}_1 = 0$.

4.4.1 Fugacity

In this section we introduce the *fugacity* as a correction for the partial pressure of a chemical component in a homogeneous mixture of real phases with N components, when cal-

culated from ideal gas principles (this term was first introduced by G.N. Lewis). Below we show the connection of the fugacity (a physical variable) and the chemical potential (a thermodynamic variable). We rephrase the equilibrium condition (4.72) in terms of the fugacity. Finally we introduce the *partial fugacity coefficient* and derive for it an elegant expression based on (4.69). This expression is convenient for numerical computations of equilibrium, as shown in Section 4.5.

Differentiating Eq. (4.51) and using Eq. (4.69) we see that the chemical potential of component i in an ideal gas, which we denote by μ_i^{ig}, is given by

$$\mu_i^{ig} = -RT \ln\left(\frac{V \cdot 1[\text{Pa}]}{n_i RT}\right) + RT + u_i^0 - Ts_i^0. \tag{4.94}$$

In Section 4.3.2 we showed that $\Gamma_i := RT + u_i^0 - Ts_i^0$ is a function of temperature only. Using the ideal gas law for component i we can write

$$\mu_i^{ig} = RT \ln\left(\frac{\xi_i P}{1[\text{Pa}]}\right) + \Gamma_i(T) \tag{4.95}$$

where $\xi_i := n_i/n_{\text{T}}$ is the molar fraction of component i and $\xi_i P$ is its partial pressure in an ideal gas mixture. For the non-ideal case, we define the (partial) *fugacity* of species i as the function $f_i = f_i(V,T,\mathbf{n})$ defined by the equation

$$\mu_i = RT \ln\left(\frac{f_i}{1[\text{Pa}]}\right) + \Gamma_i(T). \tag{4.96}$$

The partial fugacity coefficient is defined as the quotient $\phi_i := f_i/\xi_i P$. From Eqs. (4.69) and (4.94) we conclude that

$$RT \ln \phi_i = \int_V^\infty \left(\left(\frac{\partial P}{\partial n_i}\right)_{V,T,\mathbf{n}^i} - \frac{RT}{\upsilon}\right) d\upsilon - RT \ln Z. \tag{4.97}$$

where $Z = PV/\left(\sum_i n_i RT\right)$ is the compressibility factor of the mixture.

Consider a heterogenous closed system with N components and M phases. Let f_i^α and f_i^β denote the fugacity of component i in phase α and β, respectively, $\alpha,\beta \in \{1,\ldots,M\}$. From (4.96) we can write the pair of equations

$$\mu_i^\alpha = RT \ln\left(\frac{f_i^\alpha}{1[\text{Pa}]}\right) + \Gamma_i^\alpha(T). \tag{4.98}$$

$$\mu_i^\beta = RT \ln\left(\frac{f_i^\beta}{1[\text{Pa}]}\right) + \Gamma_i^\beta(T). \tag{4.99}$$

From remark 4.6 for every component $i \in \{1,\ldots,N\}$ we have $\Gamma_i^\alpha(T) = \Gamma_i^\beta(T)$. Therefore from (4.98) and (4.99) we have that the equilibrium condition (4.73) can be rewritten

as

$$f_i^{\alpha} = f_i^{\beta} \quad \text{for } i = 1,\ldots,N \text{ and } \alpha,\beta \in \{1,\ldots,M\}. \tag{4.100}$$

For instance, using the definition for the fugacity coefficient for a two-phase system at equilibrium we obtain

$$\phi_i^{\mathrm{V}} y_i = \phi_i^{\mathrm{L}} x_i. \tag{4.101}$$

The superscripts indicate the vapor and liquid phases and the subscripts denote the components $i = 1,2$. We write y_i (respectively x_i) for vapor (respectively liquid) phase molar fractions, respectively.

We define the K-value for VLE for a binary system with 2 components distributed in a vapor and liquid phase as

$$K_i = \frac{y_i}{x_i} \tag{4.102}$$

for $i = 1,2$ where y_i (respectively x_i) indicates molar fraction of component i in the vapor (liquid) respectively.

4.5 Flash Calculation (jointly with P. Castañeda)

Consider a two-component system at fixed temperature T, pressure P, and fixed overall composition $\mathbf{z} = (z_i)$, where $z_i = n_i/n_{\mathrm{T}}$, $i = 1,2$. The total number of moles of species i in the system is $n_i = \sum_{\alpha} n_i^{\alpha}$, and n_{T} denotes the total number of moles in the system. The system is in stable vapor-liquid equilibrium whenever

$$P_{\mathrm{dew}}(T) < P < P_{\mathrm{bubble}}(T), \tag{4.103}$$

where P_{dew} is the dew pressure at temperature T (*i.e.*, the pressure at which the last drop of liquid dissapears in an isothermal pressure decrease at temperature T of a vapor-liquid system, see [78, Ch. 10]) and P_{bubble} is the bubble pressure at temperature T (*i.e.*, the pressure at which the first bubble of vapor appears in an isothermal pressure decrease at temperature T).

For a two-component system in vapor-liquid equilibrium, let x_i (respectively y_i) for $i = 1,2$, denote the molar frations in the liquid (resp. vapor) phases. From the equilibrium condition, these molar fractions minimize the Gibbs energy calculated at the temperature and pressure of the system. Let $\mathscr{L}$ denote the molar fraction of the liquid phase, and $\mathscr{V}$ the molar fraction of the vapor phase, see Fig. 4.1. Notice that $\mathscr{L} + \mathscr{V} = 1$. The mass balance equations for species i are given by

$$z_i = x_i(1-\mathscr{V}) + y_i\mathscr{V} \quad \text{for } i = 1,2. \tag{4.104}$$

These equations relate the equilibrium molar fractions and the overall composition with the phase molar fractions. Thus, the vapor and liquid fractions of a binary system in

equilibrium are determined by the temperature, pressure, and the total distribution of the components in the system (*i.e.*, $\mathbf{z}$).

We can solve the nonlinear system of Eqs. (4.101) for fixed temperature T and pressure P in order to find candidates for the minimimum of expression (4.32) that correspond to physical states at thermodynamic equilibrium. The mass balance equations impose restrictions for the system (4.101) as well as for the minimization of the Gibbs energy.

For a fixed pressure P satifying condition (4.103), let x_i^0, y_i^0 for $i = 1,2$ and $\mathscr{L}^0$, $\mathscr{V}^0$ be the equilibrium compositions and equilibrium phase fractions at temperature T^0. As the molar fractions for each component add up to 1, and as the pressure is pre-fixed, we can write the state of equilibria in the compact format $\mathbf{x}^0 := \left(x_1^0, y_2^0, \mathscr{L}^0, \mathscr{V}^0, T^0\right)$. This quintet belongs to the zero set of the mapping $\Pi(\mathbf{x}) = (\Pi_1, \ldots, \Pi_5)(\mathbf{x})$, where we write $\mathbf{x} := (x_1, y_2, \mathscr{L}, \mathscr{V}, T)$. The various components of this mapping are defined by

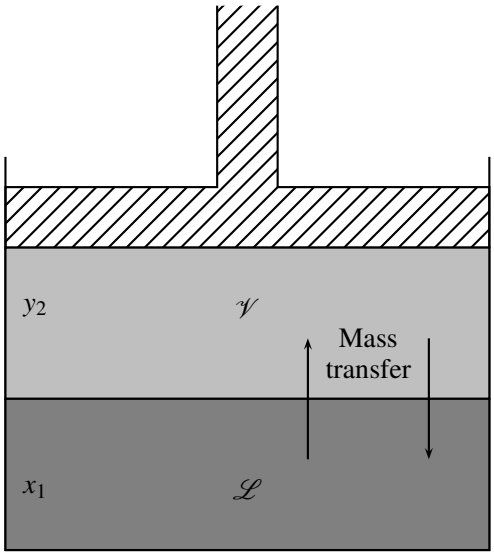

Fig. 4.1 Representation of thermodynamic equilibrium between a liquid and a vapor phase.

$$\Pi_1 := \phi_1^{\mathrm{L}} x_1 - \phi_1^{\mathrm{V}} (1 - y_2), \tag{4.105}$$
$$\Pi_2 := \phi_2^{\mathrm{L}} (1 - x_1) - \phi_2^{\mathrm{V}} y_2, \tag{4.106}$$
$$\Pi_3 := x_1 \mathscr{L} + (1 - y_2) \mathscr{V} - z_1, \tag{4.107}$$
$$\Pi_4 := (1 - x_1) \mathscr{L} + y_2 \mathscr{V} - z_2, \tag{4.108}$$
$$\Pi_5 := \mathscr{L} + \mathscr{V} - 1. \tag{4.109}$$

We assume that the components of Π are twice continuously differentiable. The Jacobian matrix of Π, $D\Pi := d\Pi / d\mathbf{x}$ is given by

$$D\Pi = \begin{pmatrix} x_1\frac{\partial\phi_1^{\mathrm{L}}}{\partial x_1}+\phi_1^{\mathrm{L}} & -(1-y_2)\frac{\partial\phi_1^{\mathrm{V}}}{\partial y_2}+\phi_1^{\mathrm{V}} & 0 & 0 & x_1\frac{\partial\phi_1^{\mathrm{L}}}{\partial T}-(1-y_2)\frac{\partial\phi_1^{\mathrm{V}}}{\partial T} \\ (1-x_1)\frac{\partial\phi_2^{\mathrm{L}}}{\partial x_1}-\phi_2^{\mathrm{L}} & -y_2\frac{\partial\phi_2^{\mathrm{V}}}{\partial y_2}-\phi_2^{\mathrm{V}} & 0 & 0 & (1-x_1)\frac{\partial\phi_2^{\mathrm{L}}}{\partial T}-y_2\frac{\partial\phi_2^{\mathrm{V}}}{\partial T} \\ \mathscr{L} & -\mathscr{V} & x_1 & 1-y_2 & 0 \\ -\mathscr{L} & \mathscr{V} & 1-x_1 & y_2 & 0 \\ 0 & 0 & 1 & 1 & 0 \end{pmatrix}.$$

Let $D\Pi_1, D\Pi_2$ be the submatrices of the matrix $D\Pi$ defined as

$$D\Pi_1 = \begin{pmatrix} x_1\frac{\partial\phi_1^{\mathrm{L}}}{\partial x_1}+\phi_1^{\mathrm{L}} & -(1-y_2)\frac{\partial\phi_1^{\mathrm{V}}}{\partial y_2}+\phi_1^{\mathrm{V}} \\ (1-x_1)\frac{\partial\phi_2^{\mathrm{L}}}{\partial x_1}-\phi_2^{\mathrm{L}} & -y_2\frac{\partial\phi_2^{\mathrm{V}}}{\partial y_2}-\phi_2^{\mathrm{V}} \end{pmatrix}, \tag{4.110}$$

$$D\Pi_2 = \begin{pmatrix} x_1 & 1-y_2 \\ 1-x_1 & y_2 \end{pmatrix}. \tag{4.111}$$

From the implicit function theorem we conclude that there exist a positive real number $T^{0,*}$ and a smooth parametrization

$$E(T) := \big(x_1(T), y_2(T), \mathscr{L}(T), \mathscr{V}(T), T\big), \tag{4.112}$$

with $\Pi(E(T)) = 0$ for each T satisfying $|T - T^0| < T^{0,*}$ whenever $\det D\Pi_1 \times \det D\Pi_2 \neq 0$. At first glance we may ask if quintets belonging to this 1-D manifold are equilibrium states, *i.e.*, if they minimize as well the Gibbs free energy of the system. In Section 4.4 we established criteria for determining whether solutions to $\Pi = 0$ are equilibrium states. Indeed, from the analysis presented in Section 4.4.1, the first two components of Π vanish if and only if $\mathbf{G}_1 = 0$ as given in (4.85). Therefore solutions to $\Pi = 0$ are equilibrium states if $n^{\mathrm{V}}\mathbf{G}_2$ is positive definite. Notice that if the fugacity coefficients are sufficiently smooth then in a neighborhood of an equilibrium state $\mathbf{x}^0$ the matrix $n^{\mathrm{V}}\mathbf{G}_2$ is positive definite, and we can conclude that this 1-D manifold is also a set of equilibrium states in this neighborhood.

In practice it is easier to verify that the matrix $n^{\mathrm{V}}\mathbf{G}_2$ is positive definite by using a convenient representation of the Hessian matrix $\mathbf{G}_2$ solely in terms of the fugacity coefficients and partial molar fractions of the different components. Indeed, as $n^{\mathrm{V}}/n^{\mathrm{L}} = \mathscr{V}/\mathscr{L}$ we can solve the linear system given by the equations (4.107) and (4.108) to find the vapor and liquid fractions in terms of x_1 and y_2. On the other hand from Eq. (4.96) and from the definition of the fugacity coefficient we can see that for a generic component i in phase α we have

$$\frac{\partial\mu_i^\alpha}{\partial\xi_i^\alpha} = \frac{RT}{\phi_i^\alpha}\frac{\partial\phi_i^\alpha}{\partial\xi_i^\alpha} + \frac{RT}{\xi_i^\alpha}. \tag{4.113}$$

Thus, in practice Eq. (4.113) can be used to calculate $\partial\mu_1^{\mathrm{L}}/\partial x_1$ and $\partial\mu_1^{\mathrm{V}}/\partial y_2$ as required by Eq. (4.92).

Remark 4.7. In order to find the wave-pattens of mixed CO_2/water injection in porous media we require up-to second order derivatives of the 1-D smooth parametrizations $x_1(T)$,

and $y_2(T)$, where 1 stands for CO_2 and 2 for water, see Appendix A. Whenever the conditions of the implicit function theorem are valid, we can differentiate the equality $\Pi = 0$ in a neighborhood of the equilibrium state to obtain

$$\frac{d}{dT}\Big(\Pi\big(\mathbf{x}(T)\big)\Big) = D\Pi \cdot \frac{d\mathbf{x}}{dT} = 0. \tag{4.114}$$

Solving Eq. (4.114) we get

$$\begin{pmatrix} \frac{dx_1}{dT} \\ \frac{dy_2}{dT} \end{pmatrix} = -D\Pi_1^{-1} \cdot \begin{pmatrix} x_1 \frac{\partial \phi_1^{\mathrm{L}}}{\partial T} - (1-y_2)\frac{\partial \phi_1^{\mathrm{V}}}{\partial T} \\ (1-x_1)\frac{\partial \phi_2^{\mathrm{L}}}{\partial T} - y_2 \frac{\partial \phi_2^{\mathrm{V}}}{\partial T} \end{pmatrix}. \tag{4.115}$$

The second order derivatives of x_1 and y_2 are found by differentiating Eq. (4.114) again with respect to T to obtain

$$\frac{d}{dT}\left(D\Pi \cdot \frac{d\mathbf{x}}{dT}\right) = D^2\Pi\left(\frac{d\mathbf{x}}{dT}, \frac{d\mathbf{x}}{dT}\right) + D\Pi \cdot \frac{d^2\mathbf{x}}{dT^2} = 0, \tag{4.116}$$

where $D^2\Pi := \frac{d^2\Pi}{d\mathbf{x}^2}$ is the Hessian of Π. Using the block-matrix form of $D\Pi$ and observing that the last component of $\frac{d^2\mathbf{x}}{dT^2}$ is zero we apply Eq. (4.116) to obtain

$$\begin{pmatrix} \frac{d^2x_1}{dT} \\ \frac{d^2y_2}{dT} \end{pmatrix} = -D\Pi_1^{-1} \begin{pmatrix} D^2\Pi\left(\frac{d\mathbf{x}}{dT}, \frac{d\mathbf{x}}{dT}\right)_1 \\ D^2\Pi\left(\frac{d\mathbf{x}}{dT}, \frac{d\mathbf{x}}{dT}\right)_2 \end{pmatrix}. \tag{4.117}$$

The equation above is still valid when we replace second-order derivatives by n-th order derivatives, *i.e.*, when we replace the operators d^2 by d^n, and D^2 by D^n.

In a first attempt for finding equilibrium states numerically, we look for solutions of the system (4.105)-(4.109). We give an initial numerical estimate for the compositions and phase fractions in equilibrium. Next, using an equation of state, we recast the pressure of the system in terms of V^α, T and $\mathbf{n} = (n_i^\alpha)$ and use (4.97) to calculate a symbolic expresssion for the fugacity coefficient of component i in phase α. Initially, the volume of each phase is unknown. Therefore, before evaluating the symbolic expression for the fugacity coefficient, we use again the equation of state to find V^α, for $\alpha = \mathtt{L}, \mathtt{V}$ in terms of T, P and the matrix of compositions $\mathbf{n}$. In the next section we show in an example how this is performed. At this point we check if the expressions in Eqs. (4.105)-(4.109) are close enough to zero (within a numerical tolerance). Otherwise, we make a new estimate for the compositions at equilibrium and repeat the process. When the process converges to a solution of the system, we can proceed to check if the matrix $n^{\mathrm{V}}\mathbf{G}_2$ is positive definite. If the output of this algorithm is a single phase system, we perform a phase stability test, see section (4.4). In future work, we will perform these last two numerical tests in the VLE calculation for the model of mix CO_2-H_2O presented in Chapter 5.

In practice we may apply the following *flash* algorithm as an implementation of the procedure described above:

1. We estimate the equilibrium K-values K_i given by (4.102), for $i = 1,2$, using for instance the well known Wilson equation [98] given by

$$K_i := \frac{y_i}{x_i} \tag{4.118}$$

$$\sim \frac{P_{ci}}{P} \exp\left(5.37(1+\omega_i)\left(1-\frac{T_{ci}}{T}\right)\right) \tag{4.119}$$

   for $i = 1,2$, where ω_i is the accentric factor of pure component i, see [60, 78], and T_{ci} is the critical temperature of component i.
2. For compositions in VLE-equilibrium the mass balance equations (4.104) can be rewritten as

$$x_i = \frac{z_i}{1+\mathscr{V}(K_i-1)}, \qquad y_i = \frac{z_i K_i}{1+\mathscr{V}(K_i-1)} \tag{4.120}$$

   for $i = 1,2$. Using that $\sum_i x_i = 1$ and $\sum_i y_i = 1$ after some calculations we see that at equilibrium the following equation is valid

$$F = \sum_i \frac{z_i(K_i-1)}{1+\mathscr{V}(K_i-1)} = 0. \tag{4.121}$$

   Therefore, in this step, we approximate the value of the vapor fraction $\mathscr{V}$ that satisfies Eq. (4.121) using a single iteration of Newton-Raphson algorithm given by

$$\mathscr{V} = \mathscr{V}_0 - \left(\frac{F}{\frac{dF}{dV}}\right)(\mathscr{V}_0), \tag{4.122}$$

   where the derivative of F is given by

$$\frac{dF}{dV} = -\sum_i \frac{z_i(K_i-1)^2}{[1+\mathscr{V}(K_i-1)]^2}, \tag{4.123}$$

   which is always negative. In this particular case this implies that the Newton-Raphson algorithm is at least quadratically convergent and alternates around the solution during convergence, see [84, Chap. 5]).
3. Using equation (4.120) we recover y_i and x_i whenever the vapor fraction $\mathscr{V}$ satisfies $\mathscr{V} \in (0,1)$. At this point we verify if the errors defined by

$$\varepsilon_1 := 1 - y_1 - y_2, \tag{4.124}$$

$$\varepsilon_2 := 1 - x_1 - x_2, \tag{4.125}$$

$$\varepsilon_3 := \triangle\mathscr{V} := \frac{F}{\frac{dF}{dV}} \tag{4.126}$$

are all less than the predefined tolerance ε. If the answer is positive we stop the iteration process. In the numerical implementation of the algorithm for the example of mixed CO_2-H_2O injection, we observed that the convergence improves when we $\varepsilon_3 := F$ in (4.126).

4. Otherwise, if the answer is negative, as described earlier we use (4.97) to calculate the fugacity coefficient of component i in phase α. Finally we estimate once again the equilibrium K-values K_i for $i = 1,2$ from the equations

$$K_i = \frac{y_i}{x_i} \sim \frac{\phi_i^{\mathrm{L}}}{\phi_i^{\mathrm{V}}}. \tag{4.127}$$

   Using these estimates we restart the cycle from step 2.
5. When $\varepsilon_i < \varepsilon$ for $i = 1,2,3$, the values of the expression given in by Eqs. (4.105)-(4.109) are close to zero, and thus we obtain our candidate for the equilibrium state.

4.6 Example: Partial fugacity coefficient calculation for a CO_2-H_2O system

In this section we illustrate how we find the fugacity coefficients for the particular example of a CO_2-H_2O VLE system.

We want to use expression (4.97) by recasting the pressure P using a suitable EOS that approximates well the P-V-T-$\mathbf{n}$ properties of the different phases of the system. For our interests a good choice is the polar version of the *Soave-Redlich-Kwong* equation [74], known as MSRK (the M stands for modified).

$$P = \frac{RT}{v - b_{\mathrm{mix}}(\xi)} - \frac{a_{\mathrm{mix}}(\xi, T)}{v(v + b_{\mathrm{mix}}(\xi))}, \tag{4.128}$$

where R is the universal gas constant. The intermolecular attraction a_{mix} is a function of the set of compositions ξ and T, and the volume of individual molecules b_{mix} is a function of the temperature only (see Appendix C for details). The variable v represents the partial molar volume of a mixed single phase of the system. It can be used for predicting properties of liquid, gas, and supercritical fluid phases for polar VLE systems.

Integration of expresssion (4.97) using (4.128) yields the expression for the fugacity coefficient of component i (See [63])[1]

[1] We omit the superscript α for visual convenience

$$RT\ln\phi_i = RT\ln\frac{v}{v-b_{mix}} + \frac{RTb_i}{v-b_{mix}} - 2\left(\sum_{k=1}^{2}\frac{\xi_k a_{ki}}{b_{mix}}\right)\ln\frac{v+b_{mix}}{v} + \frac{a_{mix}b_i}{b_{mix}^2}\left(\ln\frac{v-b_{mix}}{v} - \frac{b_{mix}}{v+b_{mix}}\right) - RT\ln Z. \quad (4.129)$$

In practice, the partial molar volume of the different phases is unknown. Therefore in the next step we need to find an expression for the molar volume v of the correspoding phase in terms of P, T, and $\mathbf{n}$. We use the *EOS* (4.128) in the form

$$p(v) \equiv v^3 - \frac{RT}{P}v^2 + \left(\frac{a_{mix}}{P} - b_{mix}^2 - \frac{RT}{P}b_{mix}\right)v - \frac{a_{mix}b_{mix}}{P} = 0. \quad (4.130)$$

We must choose the correct root of this cubic equation; the choice depends on which phase we study. Let

$$a = 1, \qquad c = \left(\frac{a_{mix}}{P} - b_{mix}^2 - \frac{RT}{P}b_{mix}\right),$$
$$b = -\frac{RT}{P}, \qquad d = -\frac{a_{mix}b_{mix}}{P}$$

stand for the coefficients of the cubic p in (4.130). Following the alternative for Cardan's method for solving the cubic as described in [54], we set

$$x_N = -b/3a, \quad y_N = p(x_N), \quad h = \frac{4}{a^4}(b^2 - 3ac).$$

Let's restrict ourselves now to the CO_2-H_2O system at supercritical conditions. The range of temperatures and pressures considered in this work are above the critical point of this system, often called *Upper Critical End Point* or *UCEP*. For calculating the partial molar volume of the supercritical fluid phase, we evaluate a_{mix} and b_{mix} accordingly.

For the CO_2-rich supercritical fluid phase, Eq. (4.130) has only one real root. It is given by

$$v_\sigma = x_N + \sqrt[3]{\frac{1}{2a}\left(-y_N + \sqrt{y_N^2 - h^2}\right)} + \sqrt[3]{\frac{1}{2a}\left(-y_N - \sqrt{y_N^2 - h^2}\right)}. \quad (4.131)$$

On the other hand, for the H_2O-rich aqueous phase, Eq. (4.130) has three real roots. The molar volume of the liquid phase corresponds to the smallest one, given by

$$\nu_a = x_N + 2\delta\cos\Big(\frac{2\pi}{3} - \theta\Big), \tag{4.132}$$

where

$$\cos(3\theta) = -\frac{y_N}{h}, \qquad \delta = \frac{b^2 - 3ac}{9a^2}. \tag{4.133}$$

Chapter 5
Phase equilibria of the CO_2-water system

by A.A. Eftekhari, with H. Wahanik and P. Castañeda

In this chapter we present a sophisticated model for the calculation of vapor-liquid equilibrium (VLE) in the supercritical CO_2-H_2O system performed first by A.A. Eftekhari et al. (2010), which provides the thermodynamic data for the model studied in this work. The equilibrium computation using the model below was performed first in Matlab® with excellent accuracy. P. Castañeda and H. Wahanik improved the convergence speed of the computation using a C++ code; the results were implemented in the RPn package.

This calculation has been used for predicting fluid transport after the injection of a CO_2/water mixture in a geothermal reservoir (Wahanik, Eftekhari, et al. [92]), see also Chapter 6, and it was subsequently improved for finding the vapor-liquid equilibrim of the supercritical CO_2-H_2O-NaCl system (Eftekhari, Bruining, et al. [18]).

We have followed a very general and classic approach in the vapor-liquid equilibrium calculation. Our main contribution is the collection of VLE and density data from the literature and the optimization of the binary interaction parameters for the CO_2-water system. This allowed the usage of the model for a wide range of temperatures and pressures, even outside of the range of experimental data.

Phase equilibrium of the CO_2-water system plays an important role in supercritical fluid extraction and in CO_2 sequestration processes. Therefore, many experimental data of vapor-liquid and liquid-liquid equilibrium (VLE and LLE) of a CO_2 mixture with other components can be found in the literature. The phase equilibrium plays an important role in the separation processes of CO_2 from flue gas. In addition, a lot of effort has been undertaken to find a comprehensive model that can predict accurately the equilibrium composition and density of the different phases for a wide range of temperatures and pressures. In addition to accuracy, these models should have a relatively fast convergence speed to be practical in numerical simulations.

Cubic equations of state inspired in the Van der Waals approach [91], are reasonably fast in numerical multicomponent phase equilibrium calculations (flash). To use an equation of state for the highly nonideal system of CO_2-water, an appropriate mixing rule must be implemented. We compared different mixing rules for four equations of state and finally selected the Peng-Robinson-Stryjek-Vera (PRSV) [62, 86] equation of state with the Modified Huron-Vidal second order (MHV2) mixing rule [15, 29] that uses the Non-

Random Two-Liquid (NRTL) activity coefficient model [69, 70]. The predicted liquid density by the PRSV equation has been adjusted using the volume shift parameter.

5.1 PRSV equation of state with the MHV2 mixing rule

The general form of the PR equation of state (Peng and Robinson, [62]) is

$$P = \frac{RT}{v-b} - \frac{a}{v(v+b)+b(v-b)}, \tag{5.1}$$

where T is the absolute temperature, P is the absolute pressure, and v is the specific (or molar) volume of the mixture; R is the universal gas constant. The effects of the interactions between molecules and the volume of individual molecules are represented by a and b respectively. For each species, the values of a and b are calculated using

$$a_i = 0.457235\frac{R^2T_{c_i}^2}{P_{c_i}}\alpha_i(T), \tag{5.2}$$

and

$$b_i = 0.077796\frac{RT_{c_i}}{P_{c_i}}, \tag{5.3}$$

where T_{ci} is the critical temperature [K] and P_{ci} is the critical pressure [Pa] of component i. The dimensionless parameter $\alpha_i(T)$ is a function of the vapor pressure for component i and is calculated by the following relation suggested by Stryjek and Vera [86]

$$\alpha_i(T) = \left[1+\kappa_i(1-\sqrt{T_{r_i}})\right]^2, \tag{5.4}$$

$$\kappa_i = \kappa_{0_i} + \kappa_{1_i}(1+\sqrt{T_{r_i}})(0.7-T_{r_i}), \tag{5.5}$$

$$\kappa_{0_i} = 0.378893 + 1.4897153\omega_i - 0.17131848\omega_i^2 + 0.0196554\omega_i^3, \tag{5.6}$$

where T_{r_i} is the reduced temperature (T/T_{c_i}) and ω_i is the acentric factor of component i (see Table B.2 in Appendix B for the acentric factors of CO_2 and H_2O). Values of κ_{1_i} are component-specific and are calculated using the vapor pressure data (Orbey and Sandler [58].

The MHV2 (Dahl and Michelsen [15]) is a modification of Huron and Vidal (HV) mixing rule [29]. For parameter b it uses

$$b = \sum_{i=1}^{N_c} \xi_i b_i, \tag{5.7}$$

where N_c denotes the total number of components in the mixture and ξ_i is the mole fraction of species i in the mixture. To find the parameter a for the mixture, the following quadratic equation must be solved for the variable ε and the larger root must be chosen:

$$q_2\varepsilon^2 + q_1\varepsilon + \left(-q_1\sum_{i=1}^{N}\xi_i\varepsilon_i - q_2\sum_{i=1}^{N}\xi_i\varepsilon_i^2 - \frac{g^E}{RT} - \sum_{i=1}^{N}\xi_i\ln\frac{b}{b_i}\right) = 0. \tag{5.8}$$

In the equation above, $\varepsilon_i = a_i/b_iRT$ and the value of g^E [J/mol·K] is a function of T and ξ_i. It is calculated using the NTRL activity coefficient model. For the PRSV equation of state the MHV2 model parameters q_1 and q_2 are -0.4347 and -0.003654, respectively (Huang and Sandler, [28]). Parameter a can be calculated using the definition $\varepsilon = a/bRT$.

To calculate the fugacity coefficient for each component we use Eq. (4.97) to obtain

$$\ln\phi_i = \frac{b_i}{b}(Z-1) - \ln(Z-B) - \frac{1}{2\sqrt{2}}\hat{\varepsilon}_i\ln\frac{Z+(1+\sqrt{2})B}{Z+(1-\sqrt{2})B}, \tag{5.9}$$

$$\hat{\varepsilon}_i = \frac{q_1\varepsilon_1 + q_2(\varepsilon+\varepsilon_i^2+\ln(b/b_i)+(b_i/b)-1)}{q_1+2q_2\varepsilon}, \tag{5.10}$$

and $Z = Pv/(RT)$ is the compressibility factor. It is a root of the following dimensionless form of the equation of state:

$$Z^3 - (1-B)Z^2 + (A-2B-3B^2)Z - B(A-B-B^2) = 0, \tag{5.11}$$

where $A = aP/(RT)^2$ and $B = bp/(RT)$. The smallest positive root of the equation of state represents the liquid phase compressibility factor and the largest one represents the vapor phase compressibility factor.

5.2 NRTL activity coefficient model for a binary mixture

The NRTL model (Renon and Prausnitz [69]) is implemented in the estimation of excess Gibbs free energy of the solution and activity coefficient of individual species:

$$\frac{g^E}{RT} = \xi_1\xi_2\left(\frac{\tau_{21}G_{21}}{\xi_1+\xi_2G_{21}} + \frac{\tau_{12}G_{12}}{\xi_2+\xi_1G_{12}}\right), \tag{5.12}$$

$$\ln\gamma_1 = \xi_2^2\left(\tau_{21}\left(\frac{G_{21}}{\xi_1+\xi_2G_{21}}\right)^2 + \frac{\tau_{12}G_{12}}{(\xi_2+\xi_1G_{12})^2}\right), \tag{5.13}$$

$$\ln\gamma_2 = \xi_1^2\left(\tau_{12}\left(\frac{G_{12}}{\xi_2+\xi_1G_{12}}\right)^2 + \frac{\tau_{21}G_{21}}{(\xi_1+\xi_2G_{21})^2}\right), \tag{5.14}$$

where we have $\tau_{12} = \triangle G_{12}/(RT)$, $\tau_{21} = \triangle G_{21}/(RT)$, $G_{12} = exp(-\alpha_{12}\tau_{12})$ and $G_{21} = exp(-\alpha_{12}\tau_{21})$. For the VLE calculation the value of the nonrandomness parameter α_{12} is set to the constant value 0.3 (Renon and Prausnitz, [70]). The other two parameters of the model $\triangle G_{12}$ and $\triangle G_{21}$ are optimized by fitting the model to the experimental VLE data of the CO_2-H_2O system. In this work we assumed that $\triangle G_{12}$ and $\triangle G_{21}$ are linear functions of the temperature.

5.3 Flash calculation, objective function, and optimization

The vapor liquid phase equilibrium (flash) calculation, descrided in Section 4.5 is performed using the EOS described in Sections 5.1 and 5.2.

The Objective function for the optimization of the NRTL parameters is defined as

$$OF(\triangle G^0_{12}, \triangle G^1_{12}, \triangle G^0_{21}, \triangle G^1_{21}) = \frac{100}{N}\sum_{i=1}^{N}\left(\frac{\left|x^{exp}_{c,i} - x^{calc}_{c,i}\right|}{x^{exp}_{c,i}} + \frac{\left|y^{exp}_{\mathrm{w},i} - y^{calc}_{\mathrm{w},i}\right|}{y^{exp}_{\mathrm{w},i}}\right) \quad (5.15)$$

where $\triangle G_{12} = \triangle G^0_{12} + \triangle G^1_{12}T$, $\triangle G_{21} = \triangle G^0_{21} + \triangle G^1_{21}T$, N is the number of data points, x_c is the mole fraction of CO_2 in the liquid phase and y_{w} is the mole fraction of water in the vapor phase. Superscripts exp and $calc$ denote the experimental and calculated values, respectively. The experimental VLE data of CO_2-water system of references (Wiebe and Gaddy [97]; King, Mubarak et al. [33]; Bamberger, Sieder et al. [5]; Valtz, Chapoy et al. [90]; Koschel, Coxam et al. [35]) were used in this study. The experimental data are within the temperature range of 278.22 [K] and 375.10 [K] and the pressure range is within 4.65 [bar] to 709.28 [bar].

The final result for the NRTL parameter estimation is given in Table 5.1. The model can predict the solubility of gaseous and supercritical CO_2 in water with average relative deviation of 8.34% represented by the first summation term in Eq. (5.15) and the solubility of water in gaseous and supercritical CO_2 with average relative deviation of 9.67% represented by the second summation term in Eq. (5.15).

To make a correction on the liquid density predicted by the equation of state, the volume shift parameters (Peneloux and Rauzy Richard [61]) were used leading to the following equation

$$v^{real}_a = v^{cal}_a + \sum_{i=1}^{N_c} x_i c_i, \quad (5.16)$$

where c_i [m^3/mol] is the volume shift parameter of component i, v^{cal} [m^3/mol] is the specific volume of the mixture calculated by the equation of state, and v^{real} [m^3/mol] is the experimental specific volume. To calculate the volume shift parameters, we used the data published by Hebach et al. [26] who reports the density of liquid water in equilibrium with CO_2 in the temperature range of 283.01-333.02 [K] and the pressure range of 10.9-

Table 5.1 Fitted parameters of the NRTL model. Subscript 1 is for CO_2 and subscript 2 is for H_2O.

Expression	*Value*	*Units*
$\triangle G^0_{12}$	3909.50	[J/mol]
$\triangle G^0_{21}$	1473.60	[J/mol]
$\triangle G^1_{12}$	18.9	[J/(mol· K)]
$\triangle G^1_{21}$	16.98	[J/(mol· K)]
$\frac{100}{N}\sum_{i=1}^{N}\left(\frac{\left\|x_{c,i}^{exp}-x_{c,i}^{calc}\right\|}{x_{c,i}^{exp}}\right)$	8.34	[-]
$\frac{100}{N}\sum_{i=1}^{N}\left(\frac{\left\|y_{\mathrm{w},i}^{exp}-y_{\mathrm{w},i}^{calc}\right\|}{y_{\mathrm{w},i}^{exp}}\right)$	9.67	[-]

306.6 [bar]. As the mole fraction of the aqueous phase is not reported, we first calculate the mole fraction using the optimized thermodynamic model and then we use the liquid phase composition to calculate the liquid compressibility factor at constant temperature and pressure. The specific volume of the liquid phase can be calculated as $v^{cal} = ZRT/P$. The objective function for the optimization of volume shift can be defined as

$$OF(c_c^0, c_c^1, c_{\mathrm{w}}^0, c_{\mathrm{w}}^1) = \frac{100}{N}\sum_{i=1}^{N}\left(\frac{\left|\frac{x_c M_c + x_w M_w}{v^{cal}} - \rho_a^{exp}\right|}{\rho_a^{exp}}\right), \tag{5.17}$$

where c_i is a linear function of the temperature $c_i = c_i^0 + c_i^1 T$, N is the number of data points, M_i is the molecular weight of component i in [kg/mol], x_i is the mole fraction of component i in the aqueous phase, and ρ_a^{exp} is the experimental value of the density in [kg/m^3]. The optimized volume shift values and the objective function value are given in Table 5.2.

Figures 5.1 and 5.2 show the experimental VLE data of the CO_2-H_2O system and the liquid phase density as a function of temperature at 100 [bar].

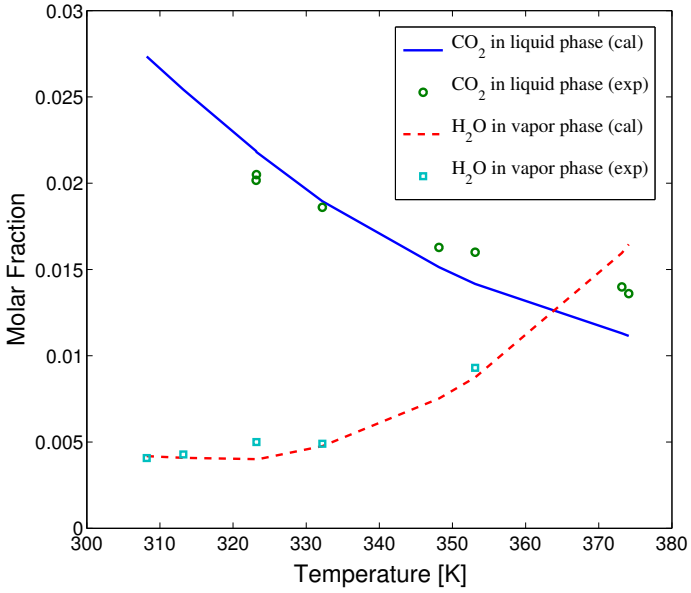

Fig. 5.1 Equilibrium mole fraction of CO_2 in the liquid phase and H_2O in the vapor phase in different temperatures and at 100 [bar]. The experimental values in this figure are given by Wiebe and Gaddy [97], King et. al., Bamberger et al. [5], [33], Valtz et al. [90], and Koschel et al. [35].

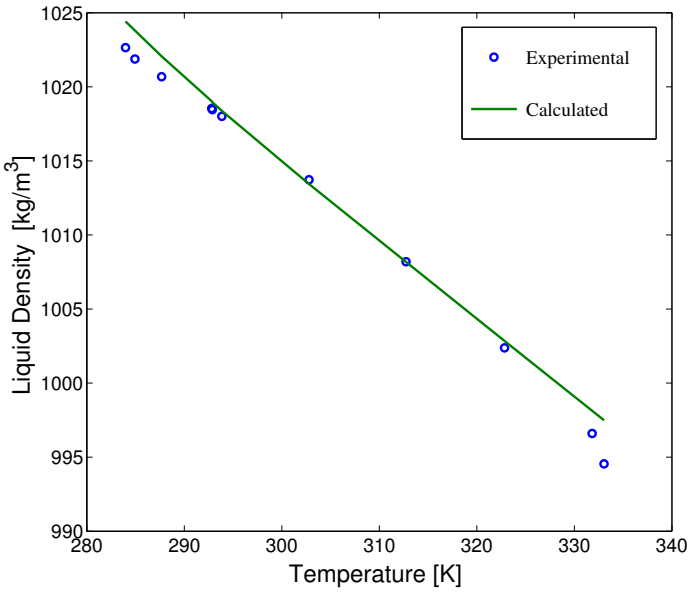

Fig. 5.2 Density of aqueous phase in the equilibrium mixture of CO_2-H_2O at different temperatures and at 100 [bar]. The experimental values in this figure are given by Hebach et al. [26].

Table 5.2 Optimized volume shift values for CO_2 and H_2O for the PRSV-MHV2 equation of state

Expression	*Value*	*Units*
c_c^0	1.496×10^{-6}	[m^3/mol]
c_w^0	-1.072×10^{-7}	[m^3/mol]
c_c^1	4.706×10^{-9}	[m^3/mol· K]
c_w^1	-1.012×10^{-8}	[m^3/mol· K]
Minimized OF value	0.149	[-]

Chapter 6
Explicit solutions for CO_2-water injection in geothermal reservoirs

One way of reducing CO_2 emissions is to replace conventional methods of heating buildings by geothermal energy. Recently it was suggested to co-inject carbon dioxide with cold water for simultaneous geothermal energy production and subsurface carbon dioxide storage. In this chapter we solve a particular injection problem representing a simultaneous CO_2 storage and geothermal energy recovery scenario. Our data correspond to a geothermal energy project proposed for heating the buildings of the Technical University of Delft.

After injection of the water/CO_2 mixture a complex interaction between physical transport and phase redistribution of the components, *i.e.*, water and CO_2, occurs. This redistribution is usually described in terms of local thermodynamic equilibrium. The vapor-liquid equilibrium (VLE) calculations used in this chapter have been described in Chapters 4 and 5, see [92]. There are no published complete Riemann solutions for 1-D problems involving complex thermodynamics that include CO_2 and heat effects in the flow. We take into account the heat effects related to the cold fluid injection and related to the dissolution of CO_2. Due to high pressures and temperatures, CO_2 is in supercritical state.

Due to thermodynamic constraints, the mass balance equations can be written in the compact form

$$\frac{\partial}{\partial t}\mathbf{G}(V) + \frac{\partial}{\partial x}u\mathbf{F}(V) = 0, \tag{6.1}$$

where $\mathbf{G} = (G_1, G_2, G_3)^{\mathbf{T}}$ and $\mathbf{F} = (F_1, F_2, F_3)^{\mathbf{T}}$, where $V = (V_1, V_2)$ indicate the primary variables and the secondary variable is u. We call u secondary because it can be found in terms of the primary variables along wave groups [40, 39].

In this chapter, we follow the methodology introduced in Chapter 3 for understanding the transport of the fluids. First, we study the wave curves and their bifurcations in each configuration of the flow. We study next the discontinuities occurring between different configurations in equilibrium. Finally, we present the Riemann solution for the injection scenario chosen.

6.1 Phase configurations in equilibrium

We focus our study in the regions of equilibrium that appear when cold water/CO_2 supercritical fluid mixtures are injected in porous media saturated with hot carbonated liquid water. The left state L is in the tp configuration. The two-phase configuration consists of a mixture of two phases in thermodynamic equilibrium, one of liquid water with dissolved carbon dioxide, and the other one a CO_2-rich supercritical fluid phase with dissolved H_2O. The right state R is in the spa configuration; in this configuration the pores contain liquid water with dissolved carbon dioxide (see also Chapter 3).

Each thermodynamic configuration appearing in the flow is described by 3 variables, denoted as $W = (V,u)$, where $V = (V_1,V_2)$. We assume ideal mixing rules, i.e., local conservation of volume (see Appendix C.1).

In order to model CO_2, H_2O and horizontal heat transport in porous media, we write two mass conservation equations and a third equation for the conservation of energy. These balance equations are given by (2.7), (2.8) and (2.10) with $g_\beta = 0$. The latter equation is based on the conservation of enthalpy formulation [7, 8]. We neglect longitudinal heat conduction, and neglect heat losses to the surrounding rock. We ignore adiabatic compression and decompression effects.

Throughout this chapter, the unknowns of the system will be a subset of s_σ, T, ψ_{aw} and u.

6.2 Waves in the tp configuration

We concentrate our efforts in finding the waves in the tp configuration. Using Gibbs phase rule for thermodynamic equilibrium $f = c - p + 2$, $c = 2$, $p = 2$, as the pressure is fixed, we obtain $f = 1$: this degree of freedom is the temperature. Therefore the mass concentrations $\rho_{\alpha i}$, where $\alpha = \sigma, a$ and $i = c, w$ are functions of temperature only and can be found from the thermodynamic equilibrium of the components. For instance, they can be found with good qualitative approximations using basic equilibrium principles as given by the Quick thermo calculation, explained in Appendix D. We can obtain accurate quantitative results with sophisticated calculations based on the fugacity approach, see Chapter 4, Chapter 5, and [92].

We conclude that the primary variables in this configuration are (s_σ, T, u), where $(s_\sigma, T) \in \Omega_{\text{tp}}$, where $\Omega_{\text{tp}} := [s_\sigma^{\min}, s_\sigma^{\max}] \times [T^{\min}, T^{\max}]$. In this example we have defined $s_\sigma^{\min} = 0$, $s_\sigma^{\max} = 1$, $T^{\min} = 304.63$ [K], and $T^{\max} = 450$ [K], chosen on the basis of physical conditions, see Section 6.10.

In this configuration the compositions of CO_2 and H_2O in both the supercritical and aqueous phases are secondary variables, which are given by the expressions (3.3.a) and (3.3.b), where ρ_W is the density of pure liquid water taken as the constant 998.2 $[kg/m^3]$. The artificial variable ρ_{aC} is found using the mixing rule for the aqueous phase (D.6.a) as

a function of the remaining variables, and thus of temperature. The remaining secondary variable is u.

For studying the horizontal flow case we set $g_\beta = 0$ in the system of equations given by (2.7), (2.8), and (2.10) found in Chapter 2. After this modification, we rewrite this system in the form (6.1)

$$\frac{\partial}{\partial t}\varphi\left(\rho_{\sigma c}s_\sigma + \rho_{ac}(1-s_\sigma)\right) + \frac{\partial}{\partial x}u\left(\rho_{\sigma c}f_\sigma + \rho_{ac}(1-f_\sigma)\right) = 0, \tag{6.2}$$

$$\frac{\partial}{\partial t}\varphi\left(\rho_{\sigma w}s_\sigma + \rho_{aw}(1-s_\sigma)\right) + \frac{\partial}{\partial x}u\left(\rho_{\sigma w}f_\sigma + \rho_{aw}(1-f_\sigma)\right) = 0, \tag{6.3}$$

$$\frac{\partial}{\partial t}\varphi\left(\hat{H}_r + H_\sigma s_\sigma + H_a(1-s_\sigma)\right) + \frac{\partial}{\partial x}u\left(H_\sigma f_\sigma + H_a(1-f_\sigma)\right) = 0. \tag{6.4}$$

6.3 Rarefaction Waves

We are interested initially in looking for (centered) rarefaction waves, *i.e.*, smooth scale-invariant solutions of (6.1). For systems of the type (6.1) this kind of solutions must satisfy

$$-\frac{\partial}{\partial \xi}\mathbf{G}(V)\xi + \frac{\partial}{\partial \xi}u\mathbf{F}(V) = 0, \tag{6.5}$$

where $V = V(\xi) = (s_\sigma(\xi), T(\xi))$. We introduce the generalized characteristic eigenvalues and (right) eigenvectors for systems of the type (6.1) as solutions to the problem

$$(A - \lambda B)\mathbf{r} = 0, \tag{6.6}$$

where $A = D(u\mathbf{F}(V))$ and $B = D(\mathbf{G}(V))$. Left eigenvectors are defined similarly and will be denoted as $\mathbf{l}$. From Eqs. (6.5) and (6.6) we observe that the values of $(V(\xi), u(\xi))$ must lie on an integral curve of the right generalized eigenvectors $\mathbf{r}$; ξ corresponds to the generalized characteristic speed $\lambda(V(\xi), u(\xi))$. Using the fact that in the tp configuration the main variables are (s_σ, T, u) we have

$$B = \varphi\begin{pmatrix} \rho_1 & \rho_1' s + \rho_{ac}' & 0 \\ \rho_2 & \rho_2' s + \rho_{aw}' & 0 \\ \rho_3 & \rho_3' s + H_a' + \hat{C}_r & 0 \end{pmatrix} \tag{6.7}$$

and

$$A = \begin{pmatrix} u\rho_1\frac{\partial f}{\partial s} & u\left(\rho_1 f' + \rho_1' f + \rho_{ac}'\right) & \rho_1 f + \rho_{ac} \\ u\rho_2\frac{\partial f}{\partial s} & u\left(\rho_2 f' + \rho_2' f + \rho_{aw}'\right) & \rho_2 f + \rho_{aw} \\ u\rho_3\frac{\partial f}{\partial s} & u\left(\rho_3 f' + \rho_3' f + H_a'\right) & \rho_3 f + H_a \end{pmatrix}, \tag{6.8}$$

for the system (6.2)-(6.3), where we used the notation $f \equiv f_\sigma$, and $s \equiv s_\sigma$ and

$$\rho_1 = \rho_{\sigma c} - \rho_{ac}, \tag{6.9}$$
$$\rho_2 = \rho_{\sigma w} - \rho_{aw}, \tag{6.10}$$
$$\rho_3 = H_\sigma - H_a. \tag{6.11}$$

These notation conventions will be used throughout this chapter. As we are interested in finding solutions for the generalized eigenvector/eigenvalue problem for this system, we study $(A - \lambda B)$ given by the expression

$$A - \lambda B = \begin{pmatrix} \gamma_1(\lambda)\rho_1 & \rho_1'\gamma_2(\lambda) + \rho_{ac}'(u - \lambda\varphi) + uf'\rho_1 & \rho_1 f + \rho_{ac} \\ \gamma_1(\lambda)\rho_2 & \rho_2'\gamma_2(\lambda) + \rho_{aw}'(u - \lambda\varphi) + uf'\rho_2 & \rho_2 f + \rho_{aw} \\ \gamma_1(\lambda)\rho_3 & \rho_3'\gamma_2(\lambda) + H_a'(u - \lambda\varphi) + uf'\rho_3 - \lambda\varphi\hat{C}_r & \rho_3 f + H_a \end{pmatrix}. \tag{6.12}$$

In the matrices (6.7)-(6.12) the terms γ_j, $j = 1, 2$ are defined as follows:

$$\gamma_1(\lambda) = u\frac{\partial f}{\partial s} - \lambda\varphi, \tag{6.13}$$
$$\gamma_2(\lambda) = uf - \lambda\varphi s. \tag{6.14}$$

We notice inmediately that the characteristic polynomial of the generalized problem, *i.e.*, $\det(A - \lambda B)$ has degree 2. For our model A is invertible. Therefore generalized finite eigenvalues can be found by solving the problem

$$A^{-1}B\mathbf{r} = (1/\lambda)\mathbf{r}. \tag{6.15}$$

Note that $(0,0,1)^{\mathbf{T}}$ is an eigenvector of the problem (6.15) with $1/\lambda = 0$ as an eigenvalue. Therefore, the system (6.1) has an infinite speed of propagation associated with u.

From (6.15) we also conclude that the geometric multiplicity of finite eigenvalues is less than or equal to their algebraic multiplicity. Therefore the generalized eigenvector/eigenvalue problem has at most two different eigenvectors and eigenvalues associated with finite speeds of propagation.

From expression (6.12) we see that when $\gamma_1 = 0$, the characteristic polynomial vanishes. Therefore, an eigenvector/eigenvalue pair is given by

$$\lambda_s = u\tilde{\lambda}_s := \frac{u}{\varphi}\frac{\partial f}{\partial s}, \qquad \mathbf{r}_s = (1,0,0)^{\mathbf{T}}. \tag{6.16}$$

Rarefaction waves associated to this family can be constructed by solving the ordinary differential equation initial value problem (see Furtado (1989) [22])

$$s_\eta = 1, \tag{6.17}$$
$$s(\eta_0) = s_0. \tag{6.18}$$

We obtain the solution $s(\eta) = \eta$, $s_0 = \eta_0$ for fixed T, u. Whenever $d^2f/ds^2 > 0$, we can invert the relation $\lambda_s(s, T, u) = x/t$ to obtain $s = s(x/t)$. Thus, the rarefaction wave

is given by $(s,T,u) = (s(\xi),T,u)$, with $\xi = x/t$. Rarefaction waves associated to this family are represented by straight lines in the (s,T,u)-space and their stopping site is the Buckley-Leverett inflection locus, see Fig. 6.1.

6.3.1 Evaporation rarefaction waves

In this section we show the details of the procedure applied for finding the remaining eigenvalue/eigenfield for the model of mixed CO_2/water injection.

Let $r_i,\ i = 1,2,3$ denote the rows of matrix $A - \lambda B$ in (6.12). In our physical setting we have observed that inside of the physical boundary of the tp configuration ρ_1 is different from zero. Therefore, we can apply the following Gaussian reduction to $A - \lambda B$:

$$\begin{aligned} r_2 &\to \rho_1 r_2 - \rho_2 r_1, \\ r_3 &\to \rho_1 r_3 - \rho_3 r_1, \\ r_3 &\to r_3 - \Lambda r_2, \end{aligned}$$

where Λ is given by

$$\Lambda = \frac{(\rho_3'\rho_1 - \rho_3\rho_1')\gamma_2(\lambda) + (\rho_1 H_a' - \rho_3\rho_{ac}')\,(u - \lambda\varphi) - \lambda\varphi\rho_1\hat{C}_r}{(\rho_2'\rho_1 - \rho_2\rho_1')\gamma_2(\lambda) + (\rho_1\rho_{aw}' - \rho_2\rho_{ac}')\,(u - \lambda\varphi)}, \tag{6.19}$$

where $\hat{C}_r$ is given in Section 2.1.

The notation $r_i \to (\cdot)$, means: row i is substituted by $(\cdot)$. The resulting reduced matrix denoted as $(A - \lambda B)_r$, is given by

$$\begin{pmatrix} \gamma_1(\lambda)\rho_1 & \rho_1'\gamma_2(\lambda) + \rho_{ac}'(u - \lambda\varphi) + uf'\rho_1 & \rho_1 f + \rho_{ac} \\ 0 & (\rho_2'\rho_1 - \rho_2\rho_1')\gamma_2(\lambda) + (\rho_1\rho_{aw}' - \rho_2\rho_{ac}')\,(u - \lambda\varphi) & \rho_1\rho_{aw} - \rho_2\rho_{ac} \\ 0 & 0 & \Delta \end{pmatrix}, \tag{6.20}$$

where

$$\Delta = (\rho_1 H_a - \rho_3\rho_{ac}) - \Lambda\,(\rho_1\rho_{aw} - \rho_2\rho_{ac})\,. \tag{6.21}$$

When Δ vanishes we have $\det(A - \lambda B) = \det\big((A - \lambda B)_r\big) = 0$, therefore solving $\Delta = 0$ from (6.21) we find the eigenvalue

$$\lambda_e = u\tilde{\lambda}_e := \frac{u}{\varphi}\frac{fM + N_1}{sM + N_2}, \tag{6.22}$$

where M, N_1 and N_2 are functions of the temperature only, given by

$$M = (\rho_3'\rho_1 - \rho_3\rho_1')(\rho_1\rho_{aw} - \rho_2\rho_{ac}) - (\rho_2'\rho_1 - \rho_2\rho_1')(\rho_1 H_a - \rho_3\rho_{ac}), \tag{6.23}$$

$$N_1 = (H_a'\rho_1 - \rho_3\rho_{ac}')(\rho_1\rho_{aw} - \rho_2\rho_{ac}) - (\rho_1\rho_{aw}' - \rho_2\rho_{ac}')(\rho_1 H_a - \rho_3\rho_{ac}), \tag{6.24}$$

$$N_2 = N_1 + \hat{C}_r\rho_1(\rho_1\rho_{aw} - \rho_2\rho_{ac}). \tag{6.25}$$

We can verify numerically that for all physically relevant values of T, $sM + N_2 \neq 0$. Therefore expression (6.22) is well defined. For the values of T for which $M \neq 0$, expression (6.22) can be simplified to

$$\tilde{\lambda}_e := \frac{1}{\varphi}\frac{f - f_e}{s - s_e}, \tag{6.26}$$

where $f_e = -N_1/M$, and $s_e = -N_2/M$. Notice that for a fixed temperature, expression (6.26) is proportional to the slope of the secant from the point (s_e, f_e) to the graph of the fractional flow function f.

In order to find the eigenvector $\mathbf{r}_e = (r_e^1, r_e^2, r_e^3)$ associated to the characteristic speed λ_e, we set

$$r_e^2 = \gamma_1(\lambda_e)/u = \varphi\left(\tilde{\lambda}_s - \tilde{\lambda}_e\right) \tag{6.27}$$

and use the reduced form of $A - \lambda B$, *i.e.*, $(A - \lambda B)_r$ given by (6.20); the other components of $\mathbf{r}_e$ are yet to be found. Notice that from (6.16) and (6.26), expression (6.27) vanishes over the coincidence locus (of the characteristic speeds). With this choice for the second component of r_e^2, after a lenghthy calculation we obtain the other components of $\mathbf{r}$:

$$r_e^1 = -\frac{1}{\rho_1}\Big((f\rho_1' + \rho_{ac}') - \tilde{\lambda}_e\varphi(s\rho_1' + \rho_{ac}')\Big) - \frac{r_e^3}{\gamma_1(\lambda_e)\rho_1}(\rho_1 f + \rho_{ac}) - \frac{\partial f}{\partial T}, \tag{6.28}$$

$$r_e^2 = \varphi\left(\tilde{\lambda}_s - \tilde{\lambda}_e\right), \tag{6.29}$$

$$r_e^3 = \gamma_1(\lambda_e)\frac{\Big((f(e_2 - e_1) + e_1) - \tilde{\lambda}_e\varphi\left(s(e_2 - e_1) + e_1\right)\Big)}{\rho_2\rho_{ac} - \rho_1\rho_{aw}}, \tag{6.30}$$

where

$$e_1 = \rho_1\rho_{aw}' - \rho_2\rho_{ac}', \tag{6.31}$$

$$e_2 = \rho_1\rho_{\sigma w}' - \rho_2\rho_{\sigma c}'. \tag{6.32}$$

In the expressions (6.28), (6.29), and (6.30) above, f, $\partial f/\partial T$, $\partial f/\partial s$, λ_e, and $\gamma_1(\lambda_e)$ depend both in s and T. The remaining functions depend on temperature only.

Notice that all eigenvectors/eigenvalues have the following form:

$$\lambda(V,u) = u\tilde{\lambda}(V) := u\vartheta(V), \tag{6.33}$$

$$\mathbf{r}(V,u) = (g^1(V), g^2(V), ug^3(V))^{\mathbf{T}}, \tag{6.34}$$

$$\mathbf{l}(V,u) = (l^1(V), l^2(V), l^3(V)). \tag{6.35}$$

This form was established by Lambert et al (2009) [39] for systems of the type (6.1). On several occasions we have used the notation $\tilde{\lambda} := \vartheta(V)$ (Eqs. (6.26) and (6.33)). Rarefaction waves corresponding to this type of systems can be constructed by solving the ODE initial value problem

$$(V,u)_\xi = \mathbf{r}(V,u) = \left(g^1(V), g^2(V), ug^3(V)\right)^{\mathbf{T}}, \tag{6.36}$$

$$(V,u)(\xi_0) = (V_0,u_0), \tag{6.37}$$

where $\mathbf{r}$ is properly oriented for obtaining a vector field, which can be done in the parameter region of our interest. In practice we solve (using a standard ODE solver) the modified system

$$\frac{d(V,u)}{d\eta} = \frac{\mathbf{r}(V,u)}{|\mathbf{r}(V,u)|}, \tag{6.38}$$

$$(V,u)(\eta_0) = (V_0,u_0), \tag{6.39}$$

providing solutions for this ODE which also solve (6.36) and (6.37), except that they are parametrized by arc length. The choice of the sign of $\mathbf{r}$ is made to satisfy

$$\frac{d}{d\eta}\lambda((V,u)(\eta)) = \nabla\lambda \cdot \mathbf{r}((V,u)(\eta)) > 0, \tag{6.40}$$

at least near η_0. In this neighborhood one can invert the relation

$$\lambda\left((V,u)(\eta)\right) = x/t, \tag{6.41}$$

to obtain the arc length η as a function of x/t, *i.e.*, $\eta = \eta(x/t)$. Thus in such neighborhood, the rarefaction wave is given by $(V,u)(\xi) := (V,u)(\eta(\xi))$ where $\xi = x/t$.

In order to find rarefaction waves for this kind of systems of conservation laws, it is essentially enough to find the projected rarefaction wave in the space of primary variables V. This result is given by the following proposition proved in [39].

Proposition 6.1. *Assume that near $W_0 = (V_0,u_0)$ the eigenvector $\mathbf{r}$ associated to a certain family forms a vector field. Then the calculation of any rarefaction curves can be performed in two steps. In the first step, we calculate the projection of the rarefaction curve in the space of primary variables (using the first two ODEs of the system (6.36)). In the second step, the calculation is completed using the formulae:*

$$u(\xi) = u_0 exp(\gamma(\xi)), \tag{6.42}$$

with

$$\gamma(\xi) = \int_{\xi_0}^{\xi} g^3(V(\eta))d\eta. \tag{6.43}$$

The rarefaction solutions $V(\xi)$ can be found by inverting the equation $exp(\gamma(\xi))\vartheta(\xi) = x/(u_0 t)$. For the tp configuration corresponding to the CO_2-H_2O system, we found the (projected) (s,T)-rarefaction waves for both families λ_s and λ_e as shown in Fig. 6.1. Inflection loci, *i.e.*, where $\nabla\lambda \cdot \mathbf{r} = 0$, are rarefaction-stopping sites.

An important bifurcation locus for Riemann problems is the coincidence curve, defined as

$$\mathbb{C}_{s,e} = \{(s,T,u) \text{ such that } \lambda_s = \lambda_e\}. \tag{6.44}$$

From Eqs. (6.28)-(6.30) we obtain the following results:

Lemma 6.1. *Let $\mathbb{I}_e$ denote the inflection locus for the Evaporation family (or e-family). Then $\frac{\partial\lambda_e}{\partial s} = 0$ and $\mathbf{r}_e$ is parallel to $\mathbf{r}_s$ on $\mathbb{C}_{s,e}$. Moreover $\mathbb{C}_{s,e} \subset \mathbb{I}_e$.*

Proof. The terms M, N_1 and N_2 given by Eqs. (6.23), (6.24) and (6.25) are functions of T only. Therefore we have,

$$\frac{\partial\lambda_e}{\partial s} = \frac{u}{\varphi}\frac{\frac{\partial f}{\partial s}M(sM+N_2) - M(fM+N_1)}{(sM+N_2)^2}, \tag{6.45}$$

$$= \frac{M}{sM+N_2}u\Big(\tilde{\lambda}_s - \tilde{\lambda}_e\Big), \tag{6.46}$$

implying $\frac{\partial\lambda_e}{\partial s} = 0$ on the coincidence curve. From Eqs. (6.28), (6.29) and (6.30) we see that the components r_e^2 and r_e^3 vanish on $\mathbb{C}_{s,e}$. This implies that $\mathbf{r}_e$ is parallel to $\mathbf{r}_s$. We can verify immediately that on the coincidence locus $\mathbb{C}_{s,e}$ we have

$$\nabla\lambda_e \cdot \mathbf{r}_e = \frac{\partial\lambda_e}{\partial s}r_e^1 + \frac{\partial\lambda_e}{\partial T}r_e^2 + \frac{\partial\lambda_e}{\partial u}r_e^3 = 0. \tag{6.47}$$

Therefore part of the inflection locus is given by the coincidence locus $\mathbb{C}_{s,e}$. The projection of the coincidence locus, $C_{s,e}$ was found as the 0-level set of $\tilde{\lambda}_s - \tilde{\lambda}_e$, found using Matlab® `contour` algorithm and it was found too using the 2-D `Contour` algorithm of the RPn package, see Fig. 6.1.

For a deeper understanding of the inflection locus $\mathbb{I}_e$ we calculate the expression $\nabla\lambda_e \cdot \mathbf{r}_e$ explicitly. The partial derivatives of λ_e are:

$$\frac{\partial\lambda_e}{\partial s} = \frac{M}{sM+N_2}u\Big(\tilde{\lambda}_s - \tilde{\lambda}_e\Big), \tag{6.48}$$

$$\frac{\partial\lambda_e}{\partial T} = \frac{u}{\varphi}\left(\frac{\frac{\partial f}{\partial T}M + fM' + N_1' - \tilde{\lambda}_e\varphi(sM'+N_2')}{sM+N_2}\right), \tag{6.49}$$

$$\frac{\partial\lambda_e}{\partial u} = \tilde{\lambda}_e. \tag{6.50}$$

Using the partial derivatives above and the components of $\mathbf{r}_e$ given by equations (6.28), (6.29) and (6.30), and using Eq. (6.22), after some rearrangements we obtain

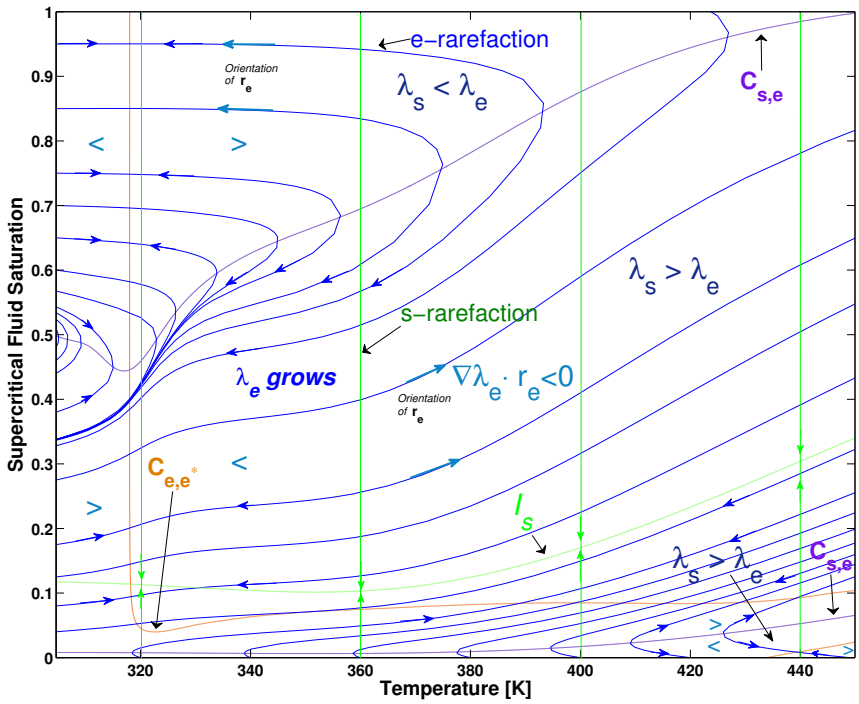

Fig. 6.1 Projected rarefactions and inflection loci for the s and e families. The orientation of the vector field $\mathbf{r}_e$ used for finding the rarefactions is given by expressions (6.28), (6.29), and (6.30).

$$\nabla\lambda_e \cdot \mathbf{r}_e = \frac{\gamma(\lambda_e)}{\varphi} \frac{\left(f\widetilde{M}+\widetilde{N}_1\right) - \tilde{\lambda}_e\varphi\left(s\widetilde{M}+\widetilde{N}_2\right)}{(sM+N_2)\rho_1 e_3}, \tag{6.51}$$

where $e_3 = \rho_{\sigma w}\rho_{ac} - \rho_{\sigma c}\rho_{aw}$ and

$$\widetilde{M} = (e_2-e_1)(N_1\rho_1 - \rho_{ac}M) + e_3(M'\rho_1 - M\rho_1'), \tag{6.52}$$

$$\widetilde{N}_1 = e_1(N_1\rho_1 - \rho_{ac}M) + e_3(N_1'\rho_1 - M\rho_{ac}'), \tag{6.53}$$

$$\widetilde{N}_2 = e_1(N_1\rho_1 - \rho_{ac}M) + e_3(N_2'\rho_1 - M\rho_{ac}'). \tag{6.54}$$

From this we conclude that the projected inflection locus for e-rarefactions I_e is given by the union of $C_{s,e}$ with the set C_{e,e^*} given by the pairs $(s,T) \in \Omega_{\text{tp}}$ such that $\left(f\widetilde{M}+\widetilde{N}_1\right) - \tilde{\lambda}_e\varphi\left(s\widetilde{M}+\widetilde{N}_2\right) = 0$. Whenever $s\widetilde{M}+\widetilde{N}_2 \neq 0$ and $\widetilde{M} \neq 0$ the set C_{e,e^*} represents the coincidence of the e-eigenvalue with the slope of the secant from the point (s_e^*, f_e^*) to the fractional flow function f, where $s_e^* := \widetilde{N}_2/\widetilde{M}$ and $f_e^* := \widetilde{N}_1/\widetilde{M}$. In fact, C_{e,e^*} is given by the set of pairs $(s,T) \in \Omega_{\text{tp}}$ such that

$$\frac{f-f_e}{s-s_e}=\frac{f-f_e^*}{s-s_e^*}. \tag{6.55}$$

where the left side of Eq. (6.55) corresponds to $\tilde{\lambda}_e$. The set C_{e,e^*} is shown in Fig. 6.1. This figure is actually a projection of integral curves which "contain" the rarefaction wave curves for both families; vertical lines represent s-integral curves which contain s-rarefactions with inflection loci $\mathbb{I}_s$. We represent e-integral curves (crossing the vertical s-integral curves) containing e-rarefactions together with the pair of subsets $\mathbb{C}_{s,e}$ and $\mathbb{C}_{e,e^*}$ of the inflection locus.

We also show the regions where either $\lambda_s > \lambda_e$ or $\lambda_s < \lambda_e$. As explained above, the eigenfield given by equations (6.28), (6.29), and (6.30) has been chosen for finding Evaporation integral curves (or e-integral curves) and thus finding e-rarefactions. We show in detail the orientation of this field as well as the sign of $\nabla\lambda_e \cdot \mathbf{r}_e$.

6.4 Shock Waves

In this section we show the details of the procedure applied for finding the Rankine-Hugoniot Locus, and admissible shock waves. Shock waves are self-similar discontinuities appearing in the solutions of (6.1) for piecewise initial value problems, e.g. Riemann problems, given by the triplets (W_0, W, υ) where $W = (V, u)$ is in the zero-set of the function $\mathbb{H}_{W_0}(W, \upsilon)$ defined by

$$\mathbb{H}_{W_0}(W, \upsilon) := \upsilon(\mathbf{G} - \mathbf{G}_0) - u\mathbf{F} + u_0\mathbf{F}_0, \tag{6.56}$$

where $W_0 = (V_0, u_0)$ is the *reference point*, $\mathbf{G}_0 = \mathbf{G}(V_0)$, $\mathbf{F}_0 = \mathbf{F}(V_0)$, $\mathbf{G} = \mathbf{G}(V)$ and $\mathbf{F} = \mathbf{F}(V)$. In (6.56), $\upsilon = \upsilon(W, W_0)$ is the propagation speed of the shock wave. We say that W is contained in the Rankine-Hugoniot Locus of the point W_0 $\big($ which is written as $W \in RH(W_0)$ $\big)$.

The total differential of $\mathbb{H}_{W_0}$ is given by

$$d\mathbb{H}_{W_0}(V, u, \upsilon) = \big(\upsilon D\mathbf{G} - D(u\mathbf{F})\big)dW + (\mathbf{G} - \mathbf{G}_0)d\upsilon, \tag{6.57}$$

$$= \big(\upsilon D\mathbf{G} - uD\mathbf{F}\big)dV - \mathbf{F}du + (\mathbf{G} - \mathbf{G}_0)d\upsilon. \tag{6.58}$$

Let $W^* = \big((V^*, u^*), \upsilon^*\big)$ be a point in the zero set of $\mathbb{H}_{W_0}(W, \upsilon)$. The implicit function theorem garantees that this zero-set is a smooth 1-D manifold in a neighborhood of (W^*, υ^*) provided the Jacobian matrix $\mathbb{H}'_{W_0}$ has rank 3. From (6.58) this is satisfied except when

$$\upsilon^* = \lambda_i(W^*) \qquad \text{and} \qquad \mathbf{l}_i(W^*) \cdot (G(V^*) - G(V_0)) = 0, \tag{6.59}$$

where $\mathbf{l}_i$ is the left eigenvector associated to the i-th family, see [37]. If there exists a point W^*, different from W_0 and contained in $RH(W_0)$ such that (6.59) is satisfied, we say that

W_0 belongs to the secondary bifurcation manifold [73]. Notice that W_0 satisfies condition (6.59). Points different from W_0, satisfying (6.59) and stable under perturbations are self-intersection points.

Now observe that for a reference state (V_0, u_0) in the tp configuration (6.56) can be written as

$$\Pi(V)\begin{pmatrix} \upsilon \\ u \\ u_0 \end{pmatrix} := \begin{pmatrix} [G_1]\ (-F_1)\ (F_1)_0 \\ [G_2]\ (-F_2)\ (F_2)_0 \\ [G_3]\ (-F_3)\ (F_3)_0 \end{pmatrix}\begin{pmatrix} \upsilon \\ u \\ u_0 \end{pmatrix} = 0. \tag{6.60}$$

This is a linear system in (υ, u, u_0). We use the notation $[G_i] := (G_i) - (G_i)_0$, for $i = 1,2,3$. Let $W_0 = (V_0, u_0)$ with $u_0 \neq 0$. We can find the RH Locus first in the variables V by looking for the points such that $\det(\Pi)$ vanishes and use expression (6.60) to find υ and u in terms of $V = (V_1, V_2)$ and W_0, provided

$$\mathbf{F} \times (\mathbf{G} - \mathbf{G}_0) \neq 0 \tag{6.61}$$

is satisfied, see Appendix A for details of the proof corresponding to the n-dimensional case, see Lemma A.2 in Appendix A.

We introduce the following notation for the determinants (up to a sign) of the 2×2 sub-matrices of Π appearing in the system (6.60):

$$Y_{kj} = (F_k)(F_j)_0 - (F_j)(F_k)_0, \tag{6.62}$$

$$\chi_{kj} = (F_k)\left[G_j\right] - (F_j)\left[G_k\right], \tag{6.63}$$

$$(\chi_{kj})_0 = (F_k)_0\left[G_j\right] - (F_j)_0\left[G_k\right], \tag{6.64}$$

for $\{k, j\} \in \mathbb{K} = \{\{1,2\},\{1,3\},\{2,3\}\}$. This yields another form of the *RH* Locus $RH(W_0)$ defined as the set of pairs $V = (V_1, V_2)$ for which

$$H_V := [G_1]\, Y_{32} + [G_2]\, Y_{13} + [G_3]\, Y_{21} \tag{6.65}$$

vanishes and (6.61) is valid. Let $RH(V_0)$ be the set of states in the space of primary variables such that $H_V = 0$. Notice that $RH(V_0)$ is a 1-D manifold in a neighborhood of one of its points $V \neq V_0$ provided the gradient $\partial H_V / \partial V$ does not vanish at V.

After fixing a left state $W_0 = (V_0, u_0)$ and finding a right state $V \in RH(V_0)$, we can find the remaining unknowns u and υ (for the complete determination of a state $W \in RH(W_0)$) from the following equations obtained from the system (6.60):

$$u = u_0 \frac{(\chi_{kj})_0}{\chi_{kj}}, \tag{6.66}$$

$$\upsilon = u_0 \frac{Y_{jk}}{\chi_{kj}}, \tag{6.67}$$

for all pairs $\{k, j\}$. This suggests the definition of *reduced* quantities related to Eqs. (6.66) and (6.67): $\tilde{\upsilon}^0 := \frac{\upsilon}{u_0}$, $\tilde{\upsilon} := \frac{\upsilon}{u}$, and $\mathscr{Z} := \frac{u}{u_0}$ as introduced in [37].

We can use alternative expressions for (6.66) and (6.67), appropriate for numerical calculations

$$u = u_0 \frac{\sum_{\{p,q\}\in\mathbb{K}}(\chi_{pq})0(\chi_{pq})}{\sum_{\{p,q\}\in\mathbb{K}}(\chi_{pq})^2}, \qquad \upsilon = u_0 \frac{\sum_{\{p,q\}\in\mathbb{K}}(Y_{pq})(\chi_{pq})}{\sum_{\{p,q\}\in\mathbb{K}}(\chi_{pq})^2}, \tag{6.68}$$

as given in [39].

Notice that the equations above are well defined unless $\chi_{kj} = 0$ for all $\{k, j\} \in \mathbb{K}$. This is the case when condition (6.61) is not satisfied, and therefore either u or υ cannot be found simultaneously from the remaining variables V, V_0 and u_0. Fortunately for these exemptions we can apply the following proposition relating υ, u and u_0:

Proposition 6.2. *When* $\mathbf{F} \neq 0$, $\mathbf{G} - \mathbf{G}_0 \neq 0$ *and* $\mathbf{F} \times (\mathbf{G} - \mathbf{G}_0) = 0$, *there exist constants* π_1, π_2 *such that*

$$\upsilon = \frac{u - u_0\pi_2}{\pi_1}. \tag{6.69}$$

Proof. See Lambert et al [38], Appendix B.

Generically, condition (6.61) is satisfied. Therefore we can find the set $RH(W_0)$ by looking first for the Rankine-Hugoniot Locus in the primary variables $RH(V_0)$ and then using the formulae $(6.68.a)$ and $(6.68.b)$ for finding the remaining unknowns.

In the tp configuration, we write explicitly the Rankine-Hugoniot shock condition in matrix form (6.60)

$$\Pi_{\text{tp}} := \begin{pmatrix} \varphi\left[\rho_1 s + \rho_{ac}\right]) & -(\rho_1 f + \rho_{ac}) & (\rho_1 f + \rho_{ac})_0 \\ \varphi\left[\rho_2 s + \rho_{aw}\right]) & -(\rho_2 f + \rho_{aw}) & (\rho_1 f + \rho_{ac})_0 \\ \varphi\left[\rho_3 s + \hat{H}_r + H_a\right] & -(\rho_3 f + H_a) & (\rho_1 f + \rho_{ac})_0 \end{pmatrix}, \tag{6.70}$$

where Π_{tp} stands for the matrix Π. In the tp configuration the system (6.1) is strictly hyperbolic except on a 1-D manifold contained in the space of primary variables (s_σ, T) where eigenvalues coincide. For V_0 outside of this locus, the set $RH(V_0)$ has two branches passing through V_0 (the proof of this assertion follows the lines of Th. 17.1 Chapter 17 [79], and Th. A.1). We conclude that the set $RH(W_0)$ has two different branches passing through the original reference point W_0. One of these branches is the straight line where T is constant. Indeed, curves parametrizing shock curves coincide with curves parametrizing rarefactions, when such curves are straight lines or when they parametrize contact discontinuities [87]. Putting $T = T_0$ in (6.70) and from the fact that the partial densities and enthalpies are functions of temperature only (see Chapter 2), after a simple Gaussian reduction we obtain a non-trivial solution to the system (6.60) given by

$$\upsilon = \frac{u}{\varphi} \frac{f(s,T) - f(s_0,T)}{s - s_0}, \tag{6.71}$$

with $u = u_0$. This equation represents the secant from the point $(s_0, u/\varphi f(s_0,T))$ to a point $(s, u/\varphi f(s,T))$, where both points are over the graph of the Buckley-Leverett flow

function. Therefore shocks and rarefactions corresponding to the the s-family, coincide with those found from the fractional flow waves with constant Darcy velocity u_0.

The non-isothermal branch of the set $RH(W_0)$ can be found by looking for the zero level set of the equation

$$det(\Pi_{tp}(s,T)) = 0, \tag{6.72}$$

corresponding to $RH(V_0)$. In a first stage, this was done numerically by solving for each fixed T (in Matlab®) a third order polynomial equation in s given by (6.72). A 2-D `Contour` algorithm was developed for finding this zero-set in the RPn package.

We consider both connected and disconnected branches of the RH Locus. Therefore we combine Liu E-condition and Lax shock condition for finding admissible shock waves (see [14]). The Lax shock admissibility criterion guarantees existence and uniqueness for the solution of Riemann problems defined in sufficiently small domains for hyperbolic non-degenerate systems of the type (6.1). The proof of this assertion follows the lines of Lax Theorem as initially presented by Lax 1957 [42]. The latter can be found in [14] and [79].

In order to establish the admissible subsets of the RH Locus, we must understand how the characteristics impinge on the shock wave. For this reason we compare the shock speed with the slow and fast characteristic speeds. The different subsets of the RH Locus can be classified according to the shock type: e.g. classical (Slow and Fast Lax). For example, the left-hand slow and fast characteristic lines collide with the shock (*i.e.*, their speed is faster than the shock speed), the slow right-hand characteristic lines collide (*i.e.*, their speed is slower than the shock speed) and the fast right-hand characteristic speed is faster than the 1-Lax shock speed. The Lax shock admissibility criteria for systems of the type (6.1) are better stated as follows.

Definition 6.1. Let W_0 be a fixed (left) state in state space. We say that a pair (W,W_0) with $W \in RH(W_0)$ satisfies the 1-Lax shock condition when the following inequalities are satisfied:

$$\lambda_{slow}(W) < \upsilon < \lambda_{slow}(W_0), \tag{6.73}$$

$$\upsilon < \lambda_{fast}(W). \tag{6.74}$$

On the other hand, we say that the pair (W,W_0) satisfies 2-Lax shock condition whenever the following inequalities hold:

$$\lambda_{slow}(W_0) < \upsilon, \tag{6.75}$$

$$\lambda_{fast}(W) < \upsilon < \lambda_{fast}(W_0). \tag{6.76}$$

In (6.73) and (6.75) $\upsilon = \upsilon(W_0,W)$ and $\lambda_{slow}(\cdot)$, $\lambda_{fast}(\cdot) \in C^1(\Omega,\mathbb{R})$ are the value of the slowest and fastest velocities of the characteristics calculated at each requested point. The domain Ω corresponds to the domain of the state variables; in the tp configuration $\Omega \equiv \Omega_{tp}$. Inequality (6.73) implies that $\upsilon < \lambda_{fast}(W_0)$. Analogously, inequality (6.75)

implies $\lambda_{slow}(W_0) < \upsilon$. Slow shocks (Fast shocks) are discontinuity waves in the PDE satisfying the 1-Lax (respectively 2-Lax) shock admissibility condition.

Liu E-condition requires the construction of shock curves where the shock speed υ decreases from the left state to the right state along connected branches. For the mathematical definition of Liu E-condition see Appendix A and [14].

In order to check Liu E-condition, we look for stationary points of the shock speed, characterized by the Bethe-Wendroff Theorem, see Appendix A Th. A.2. Instead of stationary points we search for points at which $\lambda_k = \upsilon$ is satisfied, see (A.38) in Appendix A.

A k-shock, $k = 1,2$ of moderate strength satisfies the viscous shock admissibility criterion if and only if it satisfies the Liu E-condition. Indeed, under certain restrictive hypotheses on the generalized system (6.1), (see Chapter 8 in [14]), Liu E-condition implies Lax E-condition. Additionally if the k-family is genuinely nonlinear, for weak shocks the reciprocal is true. In practice, Riemann solutions with moderate shocks satisfying the viscous shock admissibility criterion can be found by using a more "flexible" Lax-type shock admissibility criterion, the Lax E-condition [14].

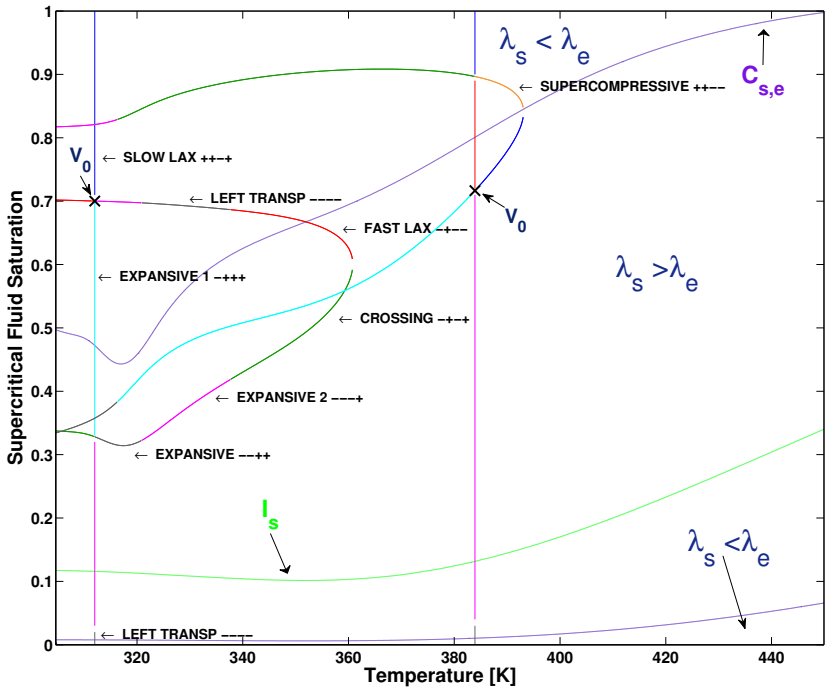

Fig. 6.2 Example: Two "projected" RH Locus, for different left states V_0. The classification follows the notation of Table 6.1. In this problem Slow Lax and Fast Lax curves may represent admissible right states.

A convenient notation for the classification of discontinuities given by the pairs (W_0, W) satisfying the Rankine-Hugoniot shock condition for hyperbolic systems of the kind (6.1), can be built in the following manner. Consider the 4-tuple (α_1^0, α_2^0, α_1, α_2) of "characters", where α_k^0, $\alpha_k =$ "+"or "-". We put $\alpha_k^0 =$ " $+$ " ("-") when $\lambda_k(W_0) - \upsilon > 0$ (< 0, respectively) and $\alpha_k =$ " $+$ " ("-") when $\lambda_k(W) - \upsilon > 0$ (< 0, respectively) for $k = 1, 2$, where 1 (2) stands for the slow (fast) family respectively, and $\upsilon \equiv \upsilon(W_0, W)$.

Remark 6.1. On different sides of the coincidence locus, the slow and fast family are either the *e*-family, or the *s*-family. This has been depicted in Figures 6.1 and 6.2.

In the Table 6.1 we give the classification of discontinuity waves for problems of type (6.1). For instance the inequalities correponding to 1-Lax shocks are:

$$\lambda_1(W_0) - \upsilon > 0, \tag{6.77}$$
$$\lambda_2(W_0) - \upsilon > 0, \tag{6.78}$$
$$\lambda_1(W) - \upsilon < 0, \tag{6.79}$$
$$\lambda_2(W) - \upsilon > 0, \tag{6.80}$$

where $\upsilon \equiv \upsilon(W_0, W)$ and therefore we associate with this type of shocks the 4-tuple given by $+ + - +$.

Table 6.1 Notation for discontinuities.

Type	*4-tuple*
1-Lax	$+ + - +$
2-Lax	$- + - -$
Overcompressive	$+ + - -$
Crossing	$- + - +$
Expansive 1	$- + + +$
Expansive 2	$- - - +$
Right Transport	$+ + + +$
Left Transport	$- - - -$
Central Transport	$- - + +$

In the literature Lax shocks are called compressive shocks, because a family of characteristics "compresses" the shock; in contrast across crossing discontinuities neither fam-

ilies of characteristic lines are compressive. Crossing or "undercompressive" discontinuities that satisfy the viscous shock admissibility criterion are called transitional shocks, see [30]. The remaining discontinuities are not physical, but provide essential information for understanding bifurcation loci for wave curves. In Fig. 6.2 we can observe two example RH Locus for states in the tp configuration whose branches were classified using the convention above.

Remark 6.2. In practice, for comparing the characteristic speeds at the left and right of the shock (*i.e.*, $\lambda(W_0)$, $\lambda(W)$) and the shock speed $\upsilon(W_0,W)$ we compare instead the quantities $\tilde{\lambda}(V_0) \equiv \vartheta(V_0)$, $\lambda(V)/u_0 = \frac{u}{u_0}\tilde{\lambda}(V)$ and $\tilde{\upsilon}^0 := \upsilon(W,W_0)/u_0 \equiv \frac{u}{u_0}\tilde{\upsilon}(V,V_0)$. Indeed, we can calculate explicit expressions for $\vartheta(V)$. Moreover the quotient u/u_0, and the reduced shock speed $\tilde{\upsilon}$ can be easily calculated using (6.68.a) and (6.68.b). This is a simple observation, which is applied for finding bifurcation locus with three variables through the projection of the locus on the two dimensional space of primary variables V.

6.5 Bifurcation Curves

Bifurcation curves are loci where the solutions change topology, such as: secondary bifurcation, coincidence, inflection, hysteresis, and interior boundary contact.

Coincidence curves are locus where the eigenvalues coincide. In Section 6.3.1 we calculated explicit expressions for the eigenvalues of the system. We were then able to use the packaged Matlab® `contour` algorithm and the 2-D `Contour` code of the RPn package for finding the (projected) coincidence curve in the tp configuration, see Fig. 6.1.

An important bifurcation locus for Riemann problems is the double contact locus (see [39]). The (i,j) double contact locus $DC^{i,j}$ is given by the pairs (W^l,W^r) with $W^r \in RH(W^l)$ where

$$\upsilon(W^l,W^r) = \lambda_i(W^l), \tag{6.81}$$

$$\upsilon(W^l,W^r) = \lambda_j(W^r), \tag{6.82}$$

with $i,j \in \{1,2\}$, where 1 (2) is the slow (fast) family. Double contact locus for the k-th family satisfy $i = j \equiv k$ in (6.81)-(6.82). On the contrary, when $i \neq j$ the double contact is of *mixed* type. From (6.68.a), (6.68.b),(6.72), and Remark 6.2 we can find the double contact locus by looking for the solutions (V_1,V_2) of the reduced system

$$\begin{aligned} det(\Pi_{\text{tp}}(V^l,V^r)) &= 0,\\ \frac{u^r}{u^l}\tilde{\upsilon}(V^l,V^r) &= \vartheta_i(V^l),\\ \tilde{\upsilon}(V^l,V^r) &= \vartheta_j(V^r), \end{aligned} \tag{6.83}$$

where the expressions for the reduced shock speed $\tilde{\upsilon}$ are given in (6.68); we have found symbolic expressions for ϑ for the two families appearing in the tp configuration, see equations (6.16) and (6.26). The numerical calculation of the double contact locus was performed by the 4-D `Contour` code implemented in the RPn package.

Another set of important bifurcation locus is given by the *extension* curves. Let $C^l := \{W^l\} \subset \Omega$ denote a curve in phase space: its right k-extension $E_k^r(C^l)$ is given by the set of states $\{W^r\}$ for which there exists a state W^l such that $W^r \in RH(W^l)$ and $\lambda_k(W^r) = \upsilon(W^l, W^r)$. We define the left k-extension similarly but we impose the condition $\lambda_k(W^l) = \upsilon(W^l, W^r)$. Notice that from this definition we have $C^l \subset E_k^r(C^l)$ for both the left and right k-extensions. We can also impose the restriction $W^r \neq W^l$ for the elements of $E_k^r(C^l)$ which evidently implies that the intersection set $C^l \cap E_k^r(C^l)$ is empty.

Important extension curves are the extension of the boundary and the extension of the inflection locus (or *hysteresis*).

Calculation of the extension curves is also done in the space of primary variables. They are calculated using the `Extension curve` code developed for the RPn package.

6.6 Waves in the single phase aqueous configuration

In this section we look for the wave curves in the spa configuration. Using Gibbs phase rule for thermodynamic equilibrium $f = c - p + 2$ with $c = 2$ and $p = 1$, as the pressure is fixed, we obtain $f = 2$. The degrees of freedom are the composition of H_2O in the aqueous phase ψ_{aw} and the temperature T, being also the primary variables.

The composition ψ_{aw} was introduced in Chapter 3 (see Remark 3.1). The aqueous carbon composition ψ_{ac} was also introduced in that chapter, as well as the density of pure CO_2 in the aqueous phase, denoted as ρ_{aC}. The latter is a function of temperature only, and accounts for the volume increase of carbonated water when found in the tp configuration. See Appendix C.

In the spa configuration, the value of ψ_{aw} satisfies the inequality

$$\psi_{aw}^{tp}(T) \leq \psi_{aw} \leq 1, \tag{6.84}$$

where $\psi_{aw}^{tp}(T)$ denotes the composition of H_2O in the aqueous phase in the tp configuration calculated at the temperature T. Indeed, at a fixed temperture T, the liquid phase becomes carbon dioxide saturated at the composition $\psi_{ac}^{tp}(T)$. The physical domain of the spa configuration, denoted as Ω_{spa}, is given by the pairs (ψ_{aw}, T) such that ψ_{aw} satisfies (6.84) and $T \in [T^{\min}, T^{\max}]$ (see Fig. 6.3).

We conclude that the balance laws (6.2), (6.3) and (6.4) are expressed in terms of ψ_{aw}, T, and u. We write $V = (\psi_{aw}, T)$ (notice that in this configuration $s_\sigma = 0$). As in the tp configuration, in the spa configuration the corresponding system of balance laws can be written in the form (6.1). It is important to highlight that the accumulation and flux terms are different in the tp and spa configurations.

In this configuration we rewrite the system of equations (6.2)-(6.4) in the form

$$\frac{\partial}{\partial t}\varphi\rho_{aC}\psi_{ac}+\frac{\partial}{\partial x}u\rho_{aC}\psi_{ac}=0, \tag{6.85}$$

$$\frac{\partial}{\partial t}\varphi\psi_{aw}+\frac{\partial}{\partial x}u\psi_{aw}=0, \tag{6.86}$$

$$\frac{\partial}{\partial t}\varphi\left(\hat{H}_r+\rho_W h_W\psi_{aw}\right)+\frac{\partial}{\partial x}u\rho_W h_W\psi_{aw}=0. \tag{6.87}$$

6.7 Wave analysis

We look for rarefaction waves in the spa configuration analogously as it was performed in Section 6.3 for the tp configuration. As observed above, we can write the system (6.85), (6.86) and (6.87), in the form $\partial_t\mathbf{G}(V)+\partial_x u\mathbf{F}(V)=0$. We are interested in finding solutions for the characteristic problem for this system. Therefore, we study $A-\lambda B$ given by the expression

$$A-\lambda B=\begin{pmatrix}\gamma_3(\lambda)(-\rho_{aC}) & \gamma_3\rho'_{aC}\psi_{ac} & \rho_{aC}\psi_{ac}\\ \gamma_3(\lambda) & 0 & \psi_{aw}\\ \gamma_3(\lambda)H_W & \gamma_3 H'_W\psi_{aw}-\lambda\varphi\hat{C}_r & H_W\psi_{aw}\end{pmatrix}, \tag{6.88}$$

where $A=\frac{\partial(u\mathbf{F}(V))}{\partial(V,u)}$, $B=\frac{\partial(\mathbf{G}(V))}{\partial(V,u)}$, $\gamma_3(\lambda):=u-\lambda\varphi$ and $H_W=\rho_W h_W$.

We can perform the following Gaussian reduction on the matrix (6.88):

$$\begin{aligned}r_1&\to r_1+\rho_{aC}r_2,\\ r_3&\to r_3-H_W r_2.\end{aligned}$$

The resulting reduced matrix is given by making $\gamma_3=0$ as

$$\begin{pmatrix}0 & \gamma_3(\lambda)\rho'_{aC}\psi_{ac} & \rho_{aC}\\ \gamma_3(\lambda) & 0 & \rho_{aw}\\ 0 & \gamma_3(\lambda)H'_W\psi_{aw}-\lambda\varphi\hat{C}_r & 0\end{pmatrix}. \tag{6.89}$$

We can see immediately that one solution for the associated generalized eigenvalue/eigenvector problem is given by

$$\lambda_\psi=\frac{u}{\varphi},\qquad\qquad \mathbf{r}_\psi=(1,0,0)^{\mathbf{T}}, \tag{6.90}$$

which generates straight line rarefaction curves with constant speed. Notice that the H_2O-composition remains constant along waves associated with the ψ-family.

From (6.89) we obtain also the second root for the (generalized) characteristic polynomial

$$\lambda_T = \frac{u}{\varphi}\frac{H'_W \psi_{aw}}{H'_W \psi_{aw} + \hat{C}_r}. \tag{6.91}$$

In order to find the eigenvector $\mathbf{r}_T = (r_T^1, r_T^2, r_T^3)$ associated to the characteristic speed λ_T, we set

$$r_T^3 = u\hat{C}_r(1-\psi_{aw}), \tag{6.92}$$

and use the reduced form of $A-\lambda B$ given by (6.89) and denoted as $(A-\lambda B)_r$ to obtain

$$r_T^1 = -\psi_{aw}(1-\psi_{aw})(H'_W \psi_{aw} + \hat{C}_r), \tag{6.93}$$

$$r_T^2 = -\frac{\rho_{aC}}{\rho'_{aC}}(H'_W \psi_{aw} + \hat{C}_r), \tag{6.94}$$

$$r_T^3 = u\hat{C}_r(1-\psi_{aw}). \tag{6.95}$$

With a straightforward calculation we can see that both families of eigenvalues and eigenvectors satisfy the equality $\nabla\lambda \cdot \mathbf{r} = 0$ so integral curves parametrize *contact discontinuities*. The latter are particular degenerate discontinuities; they are abrupt changes in weak solutions $W(x,t)$ of (6.1) that travel with characteristic speed. They are represented in the space of variables (V,u) by solutions to (6.38) and (6.39) along which the eigenvalue remains constant, *i.e.*, where

$$\big(\nabla\lambda \cdot \mathbf{r}\big)(V(\eta),u(\eta)) = 0. \tag{6.96}$$

Moreover these discontinuities satisfy the RH shock condition. Contact discontinuity curves parametrize simultaneously rarefactions and shock waves [87]. We note that in the tp configuration we do not observe this kind of waves.

As the system is strictly hyperbolic in the ψ_{aw} and T coordinates, the two branches of the RH Locus coincide with the integral curves that parametrize contact discontinuity waves. From (6.90) and (6.91) we see that T-contacts are slower than ψ-contacts, for all states in the spa configuration. Therefore when building Riemann solutions using waves in the spa configuration, we must start the construction with a slow T-contact wave and continue with a fast ψ-contact wave.

In order to find the T-contacts in the spa configuration it is enough to find integral curves for the ODE initial value problem[1]

[1] The artificial partial density ρ_{aC} is a function of temperature only. For numerical computations we perform a fit with smoothing 1D Reinsch splines (see [68]) over a sampling of discrete values found using the VLE Flash given in Chapter 5 and the expression $\rho_{aC} = \frac{\rho_W \rho_{ac}}{\rho_W - \rho_{aw}}$ derived from an ideal mixing rule for the aqueous phase.

$$\frac{d\psi_{aw}}{d\eta} = -\psi_{aw}(1-\psi_{aw})\mathbb{A}, \tag{6.97}$$

$$\frac{dT}{d\eta} = -\frac{\rho_{aC}}{\rho'_{aC}}\mathbb{A}, \tag{6.98}$$

$$\frac{du}{d\eta} = u\hat{C}_r\left(1-\psi_{aw}\right), \tag{6.99}$$

where $\mathbb{A} := H'_W\psi_{aw} + \hat{C}_r$. The initial value is $\big(\psi_{aw}(\eta_0), T(\eta_0), u(\eta_0)\big) = \big((\psi_{aw})_0, T_0, u_0\big)$.

Integral curves for systems of the type (6.1) can be found by calculating their projection in the primary variables V by solving (6.97), (6.98) and subsequently recovering the result for finding their parametrization in the secondary variable u, by solving (6.99). We will perform this procedure explicitly.

Eqs. (6.97) and (6.98) yield the new ODE initial value problem

$$\frac{d\psi_{aw}}{dT} = \frac{\rho'_{aC}}{\rho_{aC}}\psi_{aw}(1-\psi_{aw}), \tag{6.100}$$

with $\psi_{aw}(T_0) = \big(\psi_{aw}\big)_0$. The solution to (6.100) with the prescribed initial conditions $\big(\psi_{aw}\big)_0$ and T_0 is given by

$$\psi_{aw} = \frac{b_0\rho_{aC}}{1+b_0\rho_{aC}}, \qquad \text{where} \qquad b_0 = \frac{(\psi_{aw})_0}{\rho_{aC}\big(T_0\big)\big(1-(\psi_{aw})_0\big)}. \tag{6.101}$$

Combining Eq. (6.98) in Eq. (6.99) we obtain the ODE initial value problem

$$\frac{du}{dT} = -\frac{u\hat{C}_r(1-\psi_{aw})}{\big(H'_W\psi_{aw}+\hat{C}_r\big)}\frac{\rho'_{aC}}{\rho_{aC}}, \tag{6.102}$$

with $u(T_0) = u_0$. The solution is given by

$$u = u_0\frac{q(T)}{q(T_0)}, \qquad \text{where} \qquad q(T) = \frac{c_0\rho_{aC}+1}{\rho_{aC}}, \tag{6.103}$$

and $c_0 = \mathbb{A}(T_0)\left(1+\dfrac{H'_W}{\hat{C}_r}\right)$.

In Fig. 6.3 we show the spa configuration together with the tp boundary ψ^{tp}_{aw}. We also show both families of contacts: the fast T-contacts with characteristic speed λ_T, and the slow ψ-contacts with characteristic speed λ_ψ. We also show the tp boundary and the initial reservoir state for the Riemann problem treated in the section that follows.

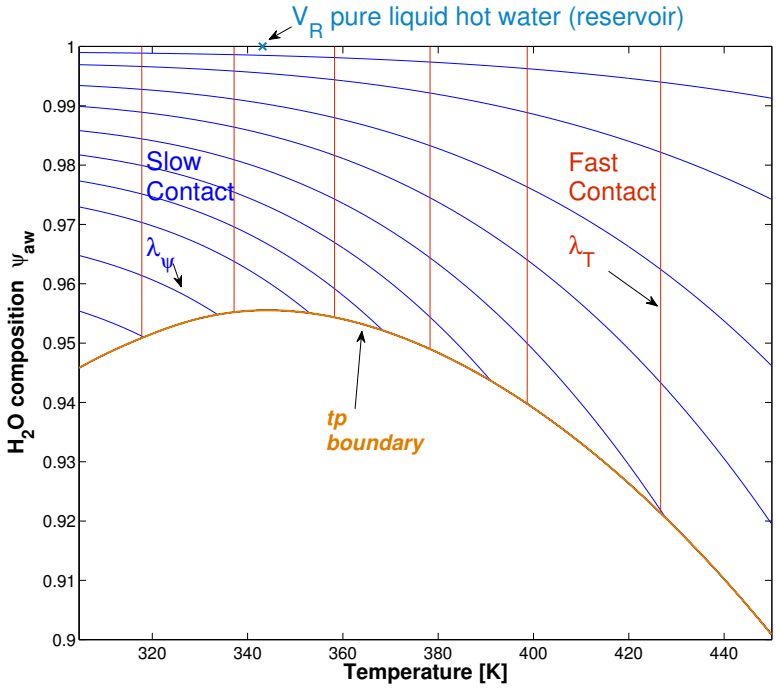

Fig. 6.3 Waves in the single phase aqueous configuration. The system of balance laws is given by Eqs. (6.85), (6.86), and (6.87).

6.8 Waves in Riemann Solutions for thermal flow

The mathematical modelling of compositional transport ocurrying after fluid injection in a horizontal porous rock cylinder can be formulated by a specific type of Riemann Problem for systems of the type (6.1), e.g., for the system (6.2)-(6.3). Indeed, as the speeds of the waves are positive, instead of a Riemann problem we prescribe the Riemann-Goursat problem

$$\begin{cases} W^{\mathrm{L}} \equiv (V_1^{\mathrm{L}}, V_2^{\mathrm{L}}, u^{\mathrm{L}}) \text{ if } x = 0,\ t > 0, \\ W^{\mathrm{R}} \equiv (V_1^{\mathrm{R}}, V_2^{\mathrm{R}}, \cdot) \quad \text{if } x > 0,\ t = 0. \end{cases} \tag{6.104}$$

In this case, V_1 stands for either s_σ or ψ_{aw} and V_2 stands for T. The velocity u^{L} represents the volumetric flow rate of injection. The downstream velocity u^{R} is not specified at the right.

6.9 Shocks Waves between configurations

Discontinuities can also occur between configurations in distinct thermodynamic equilibrium. Let $W_0^\alpha = (V_0^\alpha, u_0^\alpha)$ denote a reference point in configuration α. The corresponding

domain for its primary variables $V_0^\alpha = (V_{0,1}^\alpha, V_{0,2}^\alpha)$ is Ω_α. For states in a configuration in equilibrium, fluid transport is described by a system of balance laws of the type (6.1) with accumulation $\mathbf{G}^\alpha$ and flux $\mathbf{F}^\alpha$. Let γ denote another configuration in equilibrium with associated domain for its primary variables Ω_γ, and corresponding accumulation $\mathbf{G}^\gamma$ and flux $\mathbf{F}^\gamma$.

Remark 6.3. We impose the following condition: there exists a 1-D manifold of states $\Lambda_{\gamma,\alpha}$ contained in the boundary of the domains of primary variables Ω_γ and Ω_α. (e.g., the boundary of the spa and tp configurations).

Discontinuity waves between different configurations are given by the triplets $(W_0^\alpha, W^\gamma, \upsilon)$, where $W^\gamma := (V^\gamma, u^\gamma)$ is in the zero-set of the function $\mathbb{H}_{W_0^\alpha}^{\gamma,\alpha}$ defined by

$$\mathbb{H}_{W_0^\alpha}^{\gamma,\alpha}(W^\gamma, \upsilon) := \upsilon(\mathbf{G}^\gamma - \mathbf{G}_0^\alpha) - u^\gamma \mathbf{F}^\gamma + u_0^\alpha \mathbf{F}_0^\alpha, \tag{6.105}$$

where $\mathbf{G}_0^\alpha = \mathbf{G}^\alpha(V_0^\alpha)$, $\mathbf{F}_0^\alpha = \mathbf{F}^\alpha(V_0^\alpha)$, $\mathbf{G}^\gamma = \mathbf{G}^\gamma(V^\gamma)$ and $\mathbf{F}^\gamma = \mathbf{F}^\gamma(V^\gamma)$. In (6.105), $\upsilon = \upsilon(W, W_0)$ is the propagation speed of the shock wave. We say that the point W^γ is contained in the (γ, α)-RH Locus of the reference point W_0^α $\big($which can be written as $W^\gamma \in RH^{\gamma,\alpha}(W_0^\alpha)\big)$.

Let $(W^{\gamma,*}, \upsilon^*)$ be a point belonging to the zero-set of $\mathbb{H}_{W_0^\alpha}^{\gamma,\alpha}$, and where $W^{\gamma,*} = (V^{\gamma,*}, \upsilon^*)$, and $V^{\gamma,*}$ is in the interior of Ω_α. This zero-set is a smooth 1-D manifold in a neighborhood of a point $(W^{\gamma,*}, \upsilon^*)$, provided the Jacobian $\partial \mathbb{H}_{W_0^\alpha}^{\gamma,\alpha} / \partial(W^\gamma, \upsilon)$ has rank 3. From the expression of the total differential of $\mathbb{H}_{W_0^\alpha}^{\gamma,\alpha}$ (derived analogously as expression (6.58)) this is satisfied except when

$$\upsilon^* = \lambda_i^\gamma(W^{\gamma,*}) \qquad \text{and} \qquad \mathbf{l}_i^\gamma(W^{\gamma,*}) \cdot (G^\gamma(V^{\gamma,*}) - G^\alpha(V_0^\alpha)) = 0, \tag{6.106}$$

where λ_i^γ, $\mathbf{l}_i^\gamma$ is the i-th family eigenvalue and left eigenvector respectively, associated to the system of conservation laws describing the fluid transport for states in the γ configuration.

Analogously as in (6.60), (6.105) can be written as

$$\Pi^{\gamma,\alpha}(V^\gamma) \begin{pmatrix} \upsilon \\ u^\gamma \\ u_0^\alpha \end{pmatrix} := \begin{pmatrix} [G_1]^{\gamma,\alpha} & (-F_1^\gamma) & (F_1^\alpha)_0 \\ [G_2]^{\gamma,\alpha} & (-F_2^\gamma) & (F_2^\alpha)_0 \\ [G_3]^{\gamma,\alpha} & (-F_3^\gamma) & (F_3^\alpha)_0 \end{pmatrix} \begin{pmatrix} \upsilon \\ u^\gamma \\ u_0^\alpha \end{pmatrix} = 0. \tag{6.107}$$

This is a linear system in $(\upsilon, u^\gamma, u_0^\alpha,)$. We use the notation $[G_i]^{\gamma,\alpha} := (G_i^\gamma) - (G_i^\alpha)_0$, for $i = 1, 2, 3$. Let $W_0^\alpha = (V_0^\alpha, u_0^\alpha)$ with $u_0^\alpha \neq 0$ be the reference point in the configuration α. As in Section 6.4 we can find the (γ, α)-RH Locus first in the variables V^γ by looking for the points such that $\det(\Pi^{\gamma,\alpha})$ vanishes and use expression (6.107) to find υ and u^γ in terms of $V^\gamma = (V_1^\gamma, V_2^\gamma)$ and W_0^α, provided

$$\mathbf{F}^\gamma \times (\mathbf{G}^\gamma - \mathbf{G}_0^\alpha) \neq 0 \tag{6.108}$$

is satisfied.

The set $RH^{\gamma,\alpha}(V_0^\alpha)$ is the set of states V^γ in the γ configuration such that $\det(\Pi^{\gamma,\alpha})$ vanishes, i.e. $H_{V^\gamma}^{\gamma,\alpha} = 0$, where the set $H_{V^\gamma}^{\gamma,\alpha}$ is defined similarly as the set H_V was defined in Section 6.4. The set $RH^{\gamma,\alpha}(V_0^\alpha)$ is a 1-D manifold of states in a neighborhood of one of its points $V^\gamma \neq V_0^\alpha$ provided the gradient $\partial H_{V^\gamma}^{\gamma,\alpha}/\partial V^\gamma$ does not vanish at V^γ.

In the case where V^γ is contained in $\Lambda_{\gamma,\alpha}$, using continuation arguments for the domain Ω_γ and for the accumulation and flux terms, $\mathbf{G}^\gamma$ and $\mathbf{F}^\gamma$, the implicit function theorem gives a local parametrization $W^\gamma(\xi) = (V^\gamma(\xi), u^\gamma(\xi))$ of an "extended" branch passing through W^γ, provided condition (6.106) is satisfied. We may choose a reparametrization for obtaining the "physically admissible" section of the projected branch given by the parametrization $V^\gamma(\xi)$, *i.e.*, the section contained in Ω_γ. Notice that in this case, V^γ also belongs to the projected locus $RH^{\gamma,\alpha}(V_0^\alpha)$. Therefore, from this construction we conclude that if a branch of the projected RH Locus $RH(V_0)$ (contained in configuration α) intersects a boundary adjacent to configuration γ, this branch can be continuously extended in the γ configuration. In other words, projected branches of the Rankine-Hugoniot locus "cross" projected domains. This has been illustrated in Fig. 6.4 for the (tp, spa)-RH Locus.

The secondary bifurcation manifold, self-intersection points, etc., can be defined following the same reasoning in Section 6.4.

We calculate the (tp,spa)-RH Locus using (6.107) with γ=tp, α =spa for the variables V^{tp} by looking first for the points such that

$$\det(\Pi^{\text{tp,spa}}) = 0, \tag{6.109}$$

and next we find υ and u^{tp} in terms of $V^{\text{tp}} = (V_1^{\text{tp}}, V_2^{\text{tp}})$ and W_0^{spa}.

Equations (6.66), (6.67), (6.68), and Proposition (6.2) can be re-stated analogously for shocks between configurations.

Numerical experiments performed with Matlab® `contour` function showed that the lines $(s_\sigma, T) \in [0,1] \times T_0^{\text{spa}}$ are good approximations for projected branches of the (tp,spa)-RH Locus with reference point $W_0^{\text{spa}} = ((\psi_{aw}^{\text{spa}})_0, T_0^{\text{spa}}, u_0^{\text{spa}})$, *i.e.*, the equality $T^{\text{tp}} = T_0^{\text{spa}}$ implies $\det(\Pi^{\text{tp,spa}}) \sim 0$. The projection of the (tp, spa) non-isothermal branch was found by solving for each fixed T^{tp} (in Matlab®) a third order polynomial equation in s obtained after writing (6.109) explicitly.

The classification of discontinuities between different configurations in equilibrium is performed analogously as the classification in Section 6.4, taking into account that eigenvalues calculated at the reference state and at states in the (γ,α)-RH Locus belong to different configurations in equilibrium.

Bifurcation locus between configurations can be defined similarly as in Section 6.5. For instance, we define the (γ, α) double contact locus for the k-th family using the definition of the shock speed between different configurations and calculating left and right families accordingly.

The extension curves between configurations are defined in the same fashion. Indeed, the right k-extension between configurations of a curve $C_\alpha^l := \{W_\alpha^l\}$ contained in the

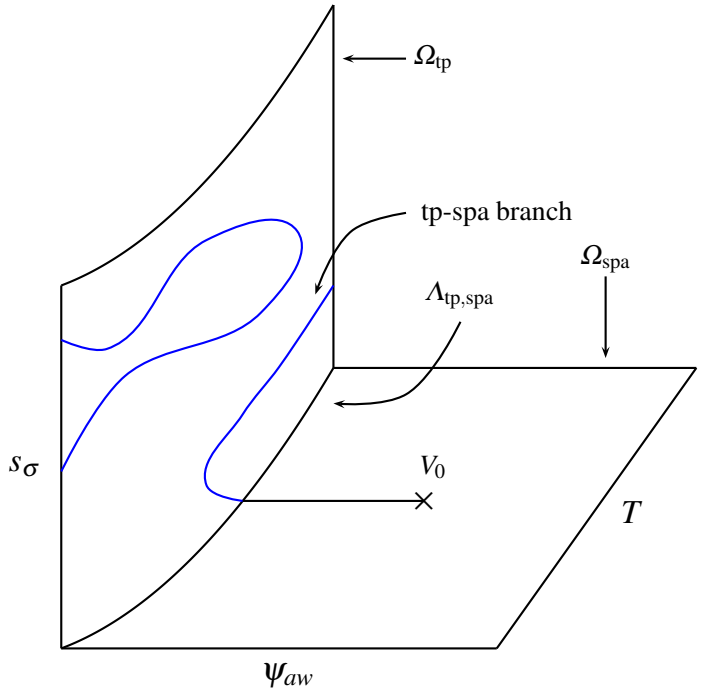

Fig. 6.4 Illustration of the projected (tp,spa)-RH Locus between the tp and spa configurations.

domain of the α configuration is defined as the set of states $\{W_\gamma^r\}$ for which there exists a state W_α^l on C_α^l such that $W_\gamma^r \in RH(W_\alpha^l)$ and $\lambda_k^\gamma(W_\gamma^r) = \upsilon(W_\alpha^l, W_\gamma^r)$, where λ_k^γ is the k-th eigenvalue in configuration γ. The k-extension curve is denoted as $E_k^{r,\gamma\text{-}\alpha}(C_\alpha^l)$.

Extension curves between configuration are calculated in the space of primary variables. For instance, we have calculated extension curves between the tp and spa configurations by interpolating discrete numerical values obtained with our Matlab® package.

6.10 The Riemann Solution for a CO_2-enhanced geothermal system

In this section we show the Riemann solution for an specific scenario: we inject a two-phase CO_2/water mixture with 50% weight of carbon dioxide at a temperature of 305.15 [K], with injection rate $4.22 \times 10^{-3}[m^3/m^2 \cdot s]$ in porous rock with pure liquid hot water at 343.15 [K]. For the physical conditions of the reservoir see Table B.2. In order to build the wave curve for the solution we must carefully study the compatibility between the speed of the rarefaction fans, shock waves and contact discontinuities (always starting

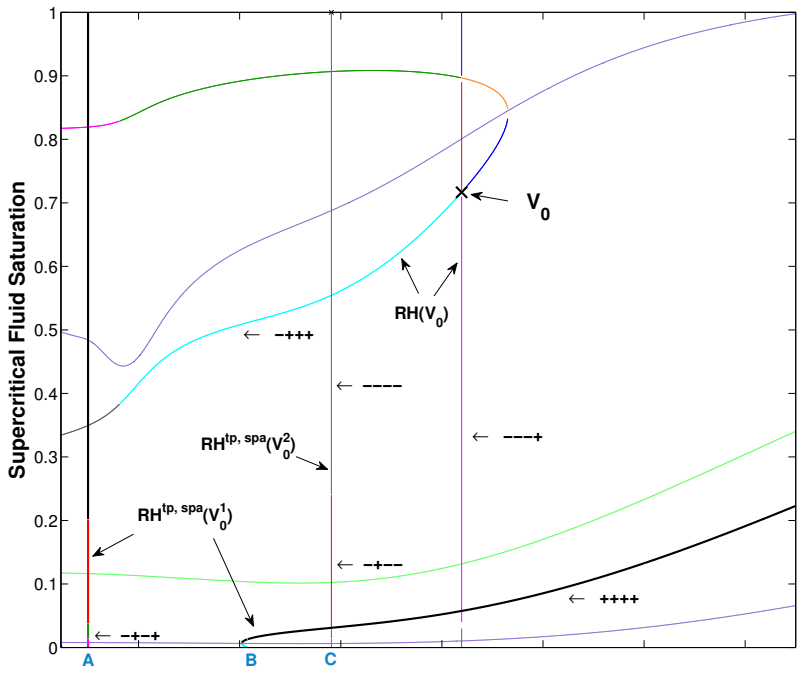

Fig. 6.5 Two examples of projected (tp,spa)-RH Loci, together with their classification. The reference states V_0^1 and V_0^2 are in the spa configuration, and are shown in Fig. 6.6.

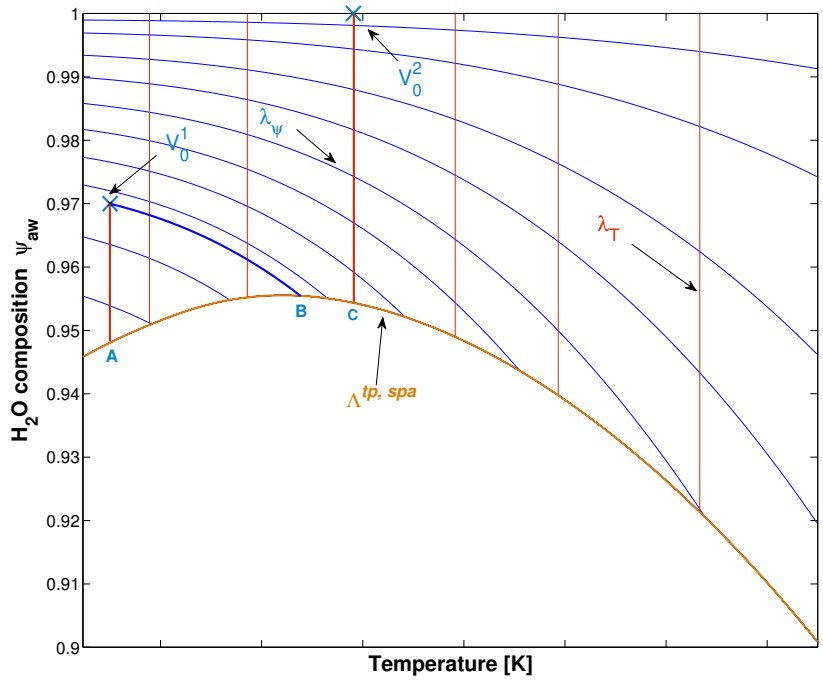

Fig. 6.6 Reference states V_0^1 and V_0^2 are in the spa configuration. Notice that two branches emanate from V_0^1, and eventually they "cross" the boundary between configurations at the points A, B and C. Compare with Fig. 6.5.

with slow waves followed by faster waves) from upstream to downstream and determine the admissibility of the shock waves to be considered. Wave groups can contain shocks between different configurations, as explained in Section 6.9.

The regions studied (tp and spa) have a boundary in common, given by the curve $(s_\sigma = 0, T, \psi_{aw}(T))$ where $T \in [T_{\min}, T_{\max}]$; see Section 6.2 for the definition of this interval[2].

After a mass balance calculation we find that the injection value for the supercritical fluid saturation is $s_\sigma = 0.5713$. The left state (injection) $(x = 0, t > 0)$ is denoted by V_L,

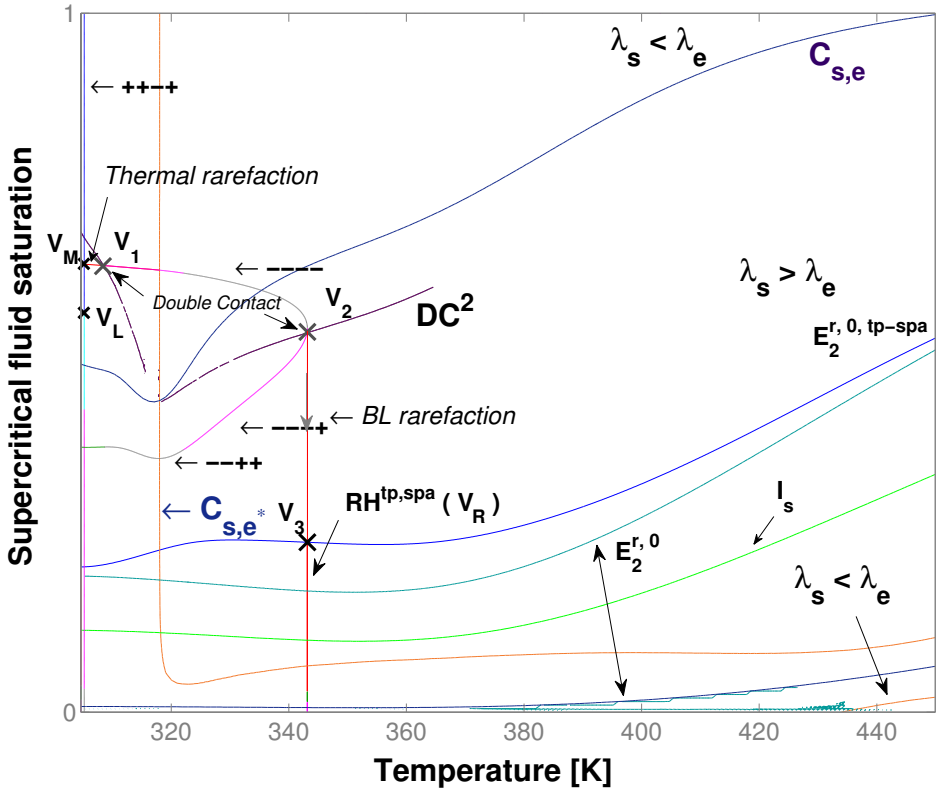

Fig. 6.7 Wave curves and bifurcations used for finding the Riemann solution. We use the BL-branch (vertical) of the RH Locus passing through V_L, the thermal rarefaction curve (or e-rarefaction curve) passing through V_M, the (fast) double contact from V_1 to V_2, the BL-rarefaction curve through V_2, and the tp-a RH Locus with left state V_3 and right state V_R which is in the spa configuration, see Figures 6.3 and 6.9. $E_2^{r,0}$ is the extension of the zero saturation boundary, and $E_2^{r,0,\text{tp-spa}}$ stands for the (tp,a)-extension of the pure water boundary in the tp configuration. The projection of the double contact locus of the fast family is denoted as DC^2.

[2] An extended temperature interval can be given by $T_{\text{UCEP}} \leq T \leq T_{dew}$, where T_{UCEP} is the upper critical temperature and 551 [K] is the dew point of the CO_2/water mixture at constant pressure found with a standard dew point calculation (Walas [93]).

see Fig. 6.7 and Fig. 6.8. The right state (reservoir) ($x > 0$) is denoted by V_R, see Figures 6.3 and 6.9. In Figures 6.7-6.8 we show the wave curves used in the construction of the Riemann solution.

In Figures 6.10-6.12 we present the profile of the solution for the injection problem at a fixed positive time. The slowest wave is a Buckley-Leverett saturation shock. At the time of this snapshot, the shock is located at p_M. Upstream of p_M there is a region containing the injected CO_2/H_2O mixture. As it can be seen in the remaining figures, only the saturation varies throughout this shock. At p_1 we can observe a saturation-temperature rarefaction wave (thermal rarefaction) up to p_2, where the seepage speed varies too. There is a slightly faster evaporation shock, which is located at p_2, where we observe an abrupt change in saturation, temperature and in the seepage speed of the flow. While the temperature changes along these waves, the compositions of CO_2 and H_2O in the supercritical and aqueous phase change too as dictated by local thermodynamic equilibrium between phases. Downstream of the shock located at p_2, there is a Buckley-Leverett rarefaction wave up to p_3, along which only saturation varies. At p_3 there is a shock wave separating a two-phase mixture upstream, from pure water downstream. All quantities vary along this shock, which is the fastest wave. Downstream of this shock there is a region containing the pure hot water initially present in the reservoir.

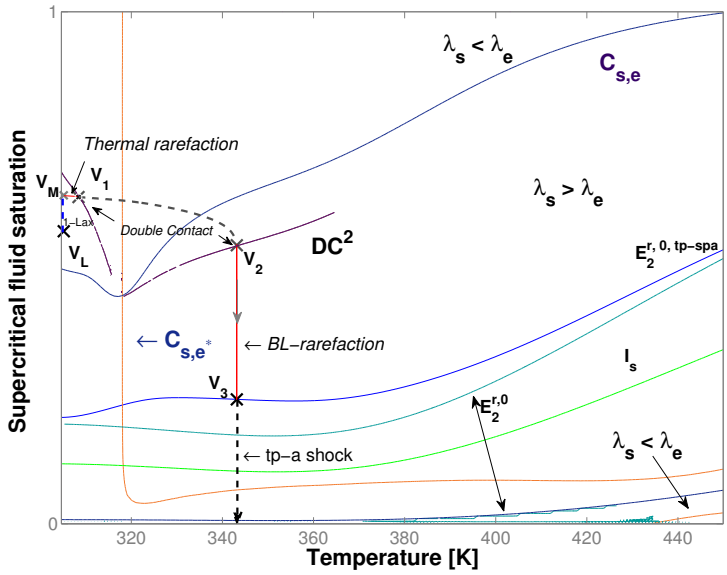

Fig. 6.8 The wave sequence for the CO_2-EGS example. There exists a slow Lax BL shock wave between V_L and the intermediate state V_M, and a fast thermal rarefaction wave between V_M and V_1. The state V_1 is connected to V_2 by a double contact discontinuity wave. A BL rarefaction wave connects V_2 and V_3. Finally there exist a tp-a shock wave between V_3 and the right state V_R (see Fig. 6.9), travelling with speed proportional to the derivative of the fractional flow function calculated at V_3.

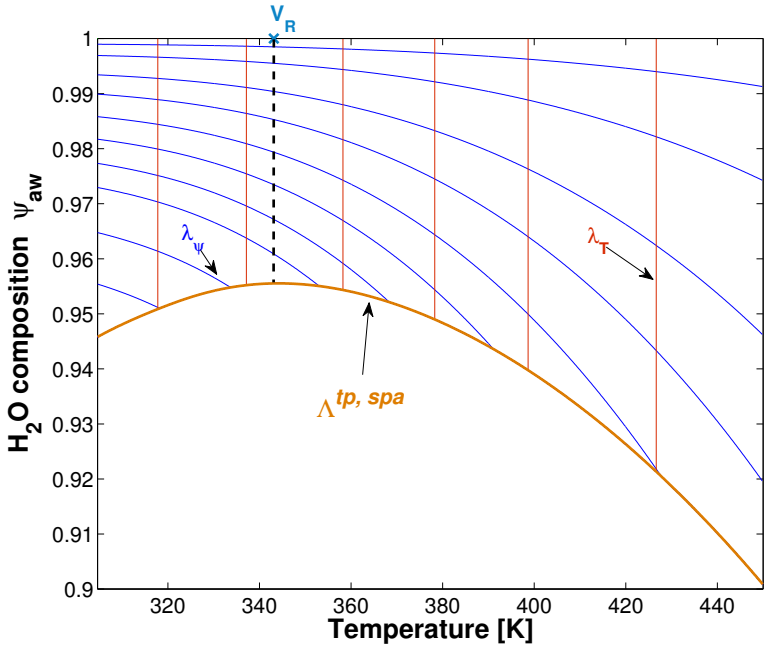

Fig. 6.9 Illustration of the tp-a shock up to V_R in the spa configuration.

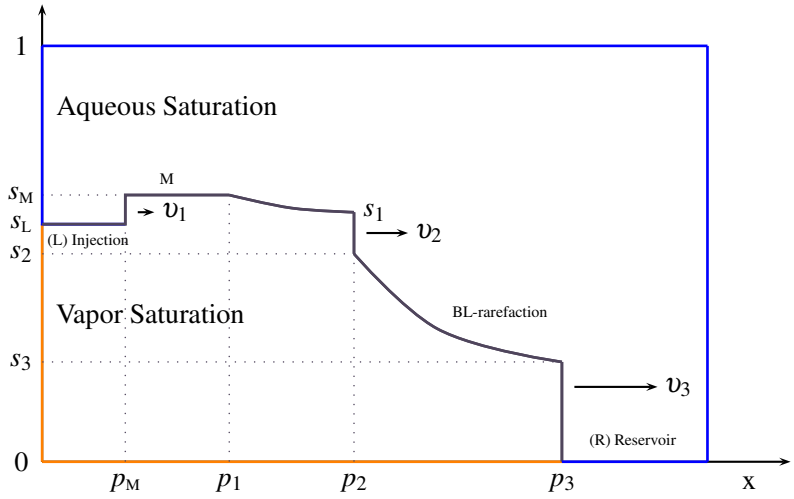

Fig. 6.10 Saturation of the fluids at a fixed time. The fraction represented by the lower part of the front corresponds to the saturation of the supercritical fluid. The upper fraction up to 1 stands for the saturation of the liquid.

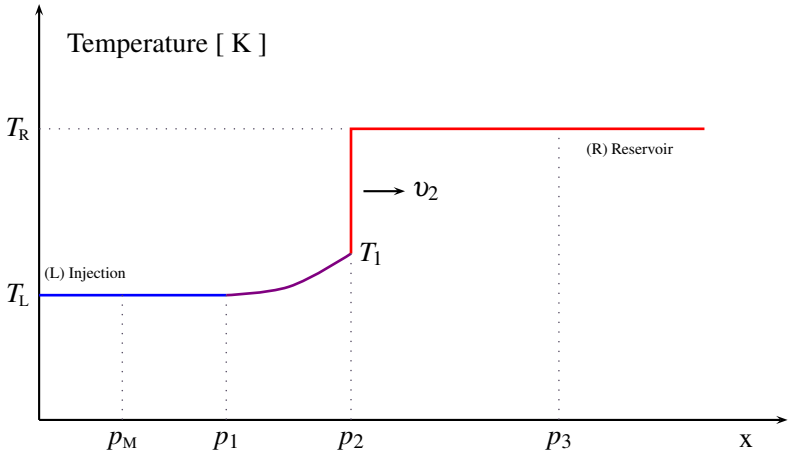

Fig. 6.11 Temperature profile.

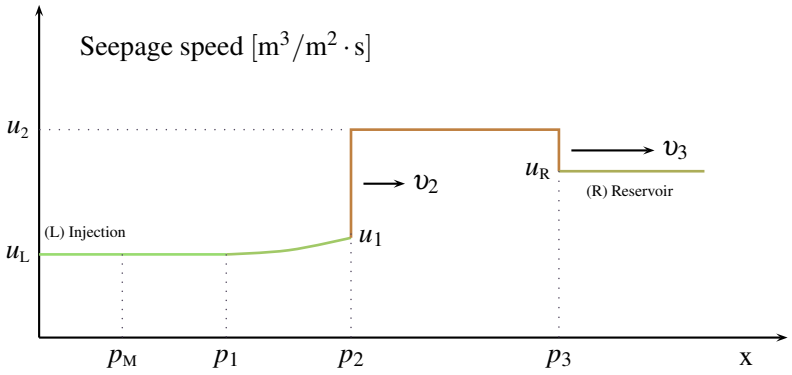

Fig. 6.12 Seepage speed profile.

6.11 Conclusions

- We describe a 1-D model of CO_2 injection in aquifers. This model was illustrated with two examples, one for slanted isothermal flow after CO_2 injection in a water reservoir. As a second example, the application of the model was geothermal energy recovery and simultaneous sequestration of carbon dioxide in a horizontal water reservoir.
- The example for isothermal flow has been solved using fractional flow theory with additional considerations for non-constant total velocity. Indeed, the total velocity changes across shocks between different regions of equilibrium. The thermodynamic model applied here uses the modified (polar) version of the Soave-Redlich-Kwong equations of state, and the classic Van der Waals mixing rules for calculation of the effects of

the interactions between molecules as well as the effects of the volume of individual molecules.

- We were able to explain in a concise manner all thermodynamic concepts required for the calculation of phase equilibria in a language accessible both to mathematicians and engineers. From basic principles, we developed an alternative more mathematically oriented version of the derivations by Beattie. The classic VLE substitution or flash algorithm was derived; we showed how equilibrium states parametrize a 1-D manifold of states. One of our contributions in this thesis consists of obtaining the partial derivatives of the compositions in the different phases up to any order.
- We applied for the CO_2-H_2O mixture, the Peng-Robinson-Stryjek-Vera equation of state with the Modified Huron-Vidal second order (MHV2) mixing rule that uses the Non-Random Two-Liquid (NRTL) activity coefficient model. The predicted liquid density by the PRSV equation has been adjusted using the volume shift parameter. Optimal coefficients were obtained by fitting with experimental data in the literature. The results have good agreement with data for CO_2-H_2O mixtures at 100 [bar].
- We solved the second example concerning the injection of CO_2-H_2O mixtures. It is shown that it is not possible to use the fractional flow theory to solve this problems due to the existence of a temperature-saturation rarefaction wave appearing in the solution. Therefore, we use the wave-curve method for finding a sequence of rarefactions, shock waves and contact discontinuities.
- Numerical methods were developed for the calculation of the wave curves. They are described in Appendix A. These methods were implemented in the n-dimensional Riemann Problem package (RPn), developed at the Fluid Dynamics Laboratory at IMPA for the creation of a state-of-the-art software in the style of a Computer-Aided-Design (CAD) package for wave curves.

Appendix A
Numerical methods for the computation of fundamental waves

In this chapter we study numerical methods designed for calculating fundamental waves for generalized system of conservation laws of the type

$$\frac{\partial}{\partial t}\mathbf{G}(V)+\frac{\partial}{\partial x}\mathbf{Q}(V,u)=0, \tag{A.1}$$

with $\mathbf{G}\in C^2(\mathbb{R}^{n-1},\mathbb{R}^n)$ and $\mathbf{Q}\in C^2(\mathbb{R}^{n-1}\times\mathbb{R},\mathbb{R}^n)$, where $u\in\mathbb{R}$. We use the notation $W=(V,u)$, where $W\in\mathbb{R}^n$. We observe that the majority of the results of this chapter apply equally well to the case where $G=G(W)$ in (A.1).

Notice that this formulation is general enough to include the model for the isothermal migration of CO_2 injected in porous rock containing water as described in Chapter 3, and the model for mixed CO_2-water injection in geothermal reservoirs, where gravity segregation does not have an important role; see Chapter 6. In practice, absence of gravity segregation can occur in thin layers with a low vertical to horizontal permeability ratio. These are among the models of multiphase longitudinal transport in porous media that can be described by systems of balance laws of the type (A.2)

$$\frac{\partial}{\partial t}G_i+\frac{\partial}{\partial x}uF_i \quad \text{where} \quad i=1,\ldots,n. \tag{A.2}$$

The model taking into account both heat effects in the flow and vertical carbon dioxide migration due to buoyancy effects belongs also to problems of type (A.1). It is described by Eqs. (2.18), (2.19) and Eq. (2.20), of Chapter 6. It can be written in the general form

$$\frac{\partial}{\partial t}G_i+\frac{\partial}{\partial x}(uF_i+K_i) \quad \text{where} \quad i=1,2,3, \tag{A.3}$$

which is also a system of the type (A.1).

A.1 Rarefaction Waves

We are interested in finding numerically rarefaction curves that parametrize (centered) rarefaction waves, *i.e.*, smooth scale-invariant solutions of (A.1); for systems of this type this solutions must satisfy

$$-\xi \frac{d}{d\xi}\mathbf{G} + \frac{d}{d\xi}\mathbf{Q} = 0, \tag{A.4}$$

where $\xi = x/t$. By the chain rule, Eq. (A.4) can be written as

$$\left(-\xi \frac{d\mathbf{G}}{dW} + \frac{d\mathbf{Q}}{dW}\right)\frac{dW}{d\xi} = 0. \tag{A.5}$$

Therefore, rarefaction curves are solutions $W = W(\xi)$ to (A.5). To find them we look for the eigenvalues and (right) eigenvectors of the equation

$$(A - \lambda B)\mathbf{r} = 0, \tag{A.6}$$

with

$$A = \frac{\partial \mathbf{Q}}{\partial W} \qquad \text{and} \qquad B = \frac{\partial \mathbf{G}}{\partial W}. \tag{A.7}$$

For systems of the kind (A.2), generalized eigenvalues and eigenvectors have special properties. Indeed, the eigenvalues can be written in the form $\lambda(V,u) = u\vartheta(V)$. The right eigenvectors $\mathbf{r} = (r^i)_{i=1,\dots,n}$, have the special form $r^i = g^i(V)$, for $i < n$ and $r^n = ug^n(V)$. Left eigenvectors $\mathbf{l} = (l^i)_{i=1,\dots,n}$ can be written as $l^i = l^i(V)$, see the case $n = 3$ for our model in Chapter 6 or the general case in [39].

Solutions of (A.5) arise from setting for the k-th eigenvalue and eigenvector

$$\lambda_k(W(\xi)) = \xi \qquad \text{and} \qquad \mathbf{r}_k = \frac{dW}{d\xi}, \tag{A.8}$$

Generalized eigenvalues and generalized (right) eigenvectors are defined as solutions for the equation (A.6) for real $n \times n$ matrices A and B. Left eigenvectors are defined similarly and will be denoted as $\mathbf{l}$.

We can find each one of the $n-1$ rarefaction curves by solving the ODE initial value problem

$$\frac{d}{d\xi}W_k(\xi) = \mathbf{r}_k(V,u), \tag{A.9}$$

$$W_k(\xi_0) = (V_0, u_0)\,. \tag{A.10}$$

for $k = 1,\dots,n-1$. Notice that the eigenvector on the right-hand side of (A.9) is defined only up to sign and amplitude, i.e, $\mathbf{r}_k$ forms a line field; we will choose the sign of $\mathbf{r}_k$ so that this line field becomes a vector field. The amplitude of the eigenvector field is also arbitrary, thus we solve numerically (using a standard ODE solver) the modified system

$$\frac{dW_k}{d\eta} = \frac{\mathbf{r}_k(V,u)}{|\mathbf{r}_k(V,u)|}, \tag{A.11}$$

$$W_k(\eta_0) = (V_0, u_0)\,. \tag{A.12}$$

Notice that the solution curves for this ODE are the same as for (A.9) and (A.10), except that they are parametrized by arc length. The choice of the sign of $\mathbf{r}_k$ is made to satisfy

$$\frac{d}{d\eta}\lambda_k(W_k(\eta)) = \nabla\lambda_k \cdot \mathbf{r}_k(W_k(\eta)) > 0, \tag{A.13}$$

In this case we can invert the relation

$$\lambda_k\big(W_k(\eta)\big) = x/t, \tag{A.14}$$

to obtain the arc length η as a function of x/t, *i.e.*, $\eta = \eta(x/t)$. The rarefaction wave is thus given by $W_k(\xi) := W_k(\eta(\xi))$ where $\xi = x/t$. Notice that with this construction we satisfy (A.8). From (A.13) we see that in order to perform the initialization of the rarefaction curve, we must choose a parametrization direction where (A.13) is satisfied, *i.e.*, along which λ_k grows over the rarefaction curve. Let W_0 be the initial point over the rarefaction curve. For the next point over the rarefaction curve we choose one of the two points, for ε_0 small

$$W_k^+ \equiv W_k^+(\varepsilon_0) := W_0 + \varepsilon_0 \mathbf{r}_k(W_0), \tag{A.15}$$

$$W_k^- \equiv W_k^-(\varepsilon_0) := W_0 - \varepsilon_0 \mathbf{r}_k(W_0); \tag{A.16}$$

The choice is dictated by the requirements that $\lambda_k(W_k^{\pm}) > \lambda_k(W_k(\eta_0))$.

The inflection locus is defined as the set

$$W_k \in \mathbb{R}^n \quad \text{such that} \quad \nabla\lambda_k(W)\cdot\mathbf{r}_k(W) = 0, \tag{A.17}$$

i.e., where (A.13) fails irrespectively of the sign of $\mathbf{r}_k$. From (A.13) we see that the rarefaction curve construction must stop at the inflection locus.

In order to find rarefaction waves for systems of conservation laws of the type (A.2) it is enough to find the projected rarefaction wave in the space of primary variables $V \in \mathbb{R}^{n-1}$, see [39] and Proposition 6.1, Chapter 6. In this particular case, rarefactions can be found by inverting the equation $exp(\gamma(\xi))\vartheta(\xi) = x/(u_0\, t)$.

For systems of the kind (A.1) we find the inflection loci by using the following result, which generalizes Lemma 17.10 of Smoller [79] giving an explicit expression for $\nabla\lambda_k \cdot \mathbf{r}_k$ in terms of the accumulation and flux terms of equation (A.1) whenever $\mathbf{l}_k \cdot B\mathbf{r}_k \neq 0$.

Lemma A.1. *Let $\mathbf{l}_k$ and $\mathbf{r}_k$ denote the left and right generalized eigenvectors corresponding to the generalized eigenvalue λ_k corresponding to the system (A.1). Then*

$$(\nabla\lambda_k \cdot \mathbf{r}_k)(\mathbf{l}_k \cdot B\mathbf{r}_k) = \mathbf{l}_k \cdot \left(\frac{d^2\mathbf{Q}}{dW^2}(\mathbf{r}_k,\mathbf{r}_k) - \lambda_k \frac{d^2\mathbf{G}}{dW^2}(\mathbf{r}_k,\mathbf{r}_k)\right) \tag{A.18}$$

where $A := \frac{d\mathbf{Q}}{dW}, B = \frac{d\mathbf{G}}{dW}$ *as in (A.7) and* $\frac{d^2\mathbf{Q}}{dW^2}$ *and* $\frac{d^2\mathbf{G}}{dW^2}$ *are the Hessians of* $\mathbf{Q}$ *and* $\mathbf{G}$.

Proof. We differentiate the equation $A\mathbf{r}_k = \lambda_k B\mathbf{r}_k$ in the direction $\mathbf{r}_k$ to obtain

$$\begin{aligned}\frac{d}{dW}A(\mathbf{r}_k)\mathbf{r}_k + A\frac{d}{dW}\mathbf{r}_k(\mathbf{r}_k)\\ = \frac{d}{dW}\lambda_k(\mathbf{r}_k)B\mathbf{r}_k + \lambda_k\left(\frac{d}{dW}B(\mathbf{r}_k)\mathbf{r}_k + B\frac{d}{dW}\mathbf{r}_k(\mathbf{r}_k)\right).\end{aligned} \tag{A.19}$$

Multiplying by $\mathbf{l}_k$ on the left we get

$$\begin{aligned}\mathbf{l}_k\frac{d}{dW}A(\mathbf{r}_k)\mathbf{r}_k + \mathbf{l}_k A\frac{d}{dW}\mathbf{r}_k(\mathbf{r}_k)\\ = \frac{d}{dW}\lambda_k(\mathbf{r}_k)\mathbf{l}_k\cdot B\mathbf{r}_k + \lambda_k\left(\mathbf{l}_k\frac{d}{dW}B(\mathbf{r}_k)\mathbf{r}_k + \mathbf{l}_k B\frac{d}{dW}\mathbf{r}_k(\mathbf{r}_k)\right).\end{aligned} \tag{A.20}$$

From the definition of left generalized eigenvector we have

$$\mathbf{l}_k A\frac{d}{dW}\mathbf{r}_k(\mathbf{r}_k) = \lambda_k\mathbf{l}_k B\frac{d}{dW}\mathbf{r}_k(\mathbf{r}_k). \tag{A.21}$$

Subtracting Eq. (A.21) from Eq. (A.20) we obtain

$$\mathbf{l}_k\cdot\left(\frac{d}{dW}A(\mathbf{r}_k) - \lambda_k\frac{d}{dW}B(\mathbf{r}_k)\right)\mathbf{r}_k = \mathbf{l}_k B\mathbf{r}_k\frac{d}{dW}\lambda_k(\mathbf{r}_k), \tag{A.22}$$

which has the alternative form

$$\mathbf{l}_k\cdot\left(\frac{d^2\mathbf{Q}}{dW^2}(\mathbf{r}_k,\mathbf{r}_k) - \lambda_k\frac{d^2\mathbf{G}}{dW^2}(\mathbf{r}_k,\mathbf{r}_k)\right) = (\nabla\lambda_k\cdot\mathbf{r}_k)(\mathbf{l}_k\cdot B\mathbf{r}_k). \tag{A.23}$$

In the particular case when the Jacobian of the accumulation term B is the identity, (A.23) reduces to the result [79].

A.2 Shock Waves

Shock waves are discontinuous self-similar weak solutions of the system (A.1). They are given by triplets (W_0, W, υ), where $W = (V,u) = (V^1,\ldots,V^{n-1},u)$ and $W_0 = (V_0,u_0) = (V_0^1,\ldots,V_0^{n-1},u_0)$ where W is in the zero-set of the mapping $\mathbb{H}_{W_0}(W,\upsilon)$ defined by

$$\mathbb{H}_{W_0}(W,\upsilon) := \upsilon(\mathbf{G}-\mathbf{G}_0) - \mathbf{Q} + \mathbf{Q}_0, \tag{A.24}$$

where $W_0 = (V_0, u_0)$ is the *reference point*, $\mathbf{G}_0 = \mathbf{G}(V_0)$, $\mathbf{Q}_0 = \mathbf{Q}(V_0)$, $W = (V, u)$, $\mathbf{G} = \mathbf{G}(V)$ and $\mathbf{F} = \mathbf{F}(V)$. In (6.56), $\upsilon = \upsilon(W, W_0)$ is the propagation speed of the shock wave. We say that W is contained in the Rankine-Hugoniot Loci of W_0 , (which is written as $W \in RH(W_0)$). Alternatively the set $RH(W_0)$ is given by the solutions of

$$\upsilon[G_i] = [Q_i], \qquad \text{where} \qquad i = 1, \ldots, n, \tag{A.25}$$

which represents the system of equations

$$\upsilon(G_i(V) - G_i(V_0)) = Q_i(V, u) - Q_i(V_0, u_0), \tag{A.26}$$

for $i = 1, \ldots, n$.

Multiplying the i-th equation in (A.26) by $[Q_{i+1}]$, the (i)-th by $[Q_{i+1}]$ and subtracting the second from the first one, we are able to write the system (A.26) in the equivalent form

$$\upsilon\big([Q_{i+1}][G_i] - [Q_i][G_{i+1}]\big) = 0, \qquad \text{where} \qquad i = 1, \ldots, n-1. \tag{A.27}$$

This approach can be generalized further. We introduce the list of indices $[\alpha^1, \alpha^2, \ldots \alpha^n]$, which is a permutation of the list of indices $[1, 2, \ldots, n]$. For each permutation the system (A.26) can be written in the alternative way

$$\upsilon\big([Q_{\alpha^{i+1}}][G_{\alpha^i}] - [Q_{\alpha^i}][G_{\alpha^{i+1}}]\big) = 0, \qquad \text{where} \qquad i = 1, \ldots, n-1. \tag{A.28}$$

We leave the details to the reader. Generically, $\upsilon \neq 0$, therefore the Rankine-Hugoniot Locus for a point (u_0, V_0) is given by the zero set of the mapping $\Gamma(V_0, u_0, V, u) \in C^2(\mathbb{R}^n, \mathbb{R}^{n-1})$ defined component-wise by

$$\Gamma_i(V_0, u_0, V, u) = \Gamma_i\big(W_0, W\big) = [Q_{\alpha^{i+1}}][G_{\alpha^i}] - [Q_{\alpha^i}][G_{\alpha^{i+1}}], \qquad \text{where} \qquad i = 1, \ldots, n-1. \tag{A.29}$$

Whenever we fix the reference state $W_0 = (V_0, u_0)$, we use the notation

$$\Gamma\big(W\big) = \Gamma(V, u) := \Gamma\big(V_0, u_0, V, u\big). \tag{A.30}$$

Remark A.1. Following the formulation (A.29), we observe that the k-shock curve with reference state $(V_0, u_0) \in \mathbb{R}^{n-1} \times \mathbb{R}$ is given by a subset of the intersection of the $n-1$ surfaces given implicitly by the components of the mapping $\Gamma(V_0, u_0, V, u)$.

We can simplify this approach further whenever we deal with systems of conservation laws of the type (A.2). In fact, under the hypotheses of Lemma A.2 shown next, in this case the Rankine-Hugoniot relationship (A.2) can be written as

$$\Pi(V) \begin{pmatrix} \upsilon \\ u \\ u_0 \end{pmatrix} := \begin{pmatrix} [G_1] & -(F_1) & (F_1)_0 \\ [G_2] & -(F_2) & (F_2)_0 \\ \vdots & \vdots & \vdots \\ [G_n] & -(F_n) & (F_n)_0 \end{pmatrix} \begin{pmatrix} \upsilon \\ u \\ u_0 \end{pmatrix} = 0. \tag{A.31}$$

This factorization was introduced by Lambert and Marchesin (2009) [39]. The entries of the matrix Π are contained in the space $C^2(\mathbb{R}^{n-1})$, *i.e.*, they are twice-continuous differentiable functions of $n-1$ variables, provided $\mathbf{G}$, $\mathbf{F}$ are C^2.

Lemma A.2. *Let $(V_0, u_0) \in \mathbb{R}^n$, with $u_0 \neq 0$, (V,u) be the left and right states of a shock wave for a system of the kind (A.2). Then the pair of states (V_0, u_0) and (V,u) satisfy Eq. (A.31) in a generic way, (i.e., given V, two of the variables υ, u, u_0 are recovered from the previous 2) whenever the following two conditions are valid:*

1. *$Rank(\Pi) = 2$*
2. *$\mathbf{F}$ and $[\mathbf{G}]$ are linearly independent, where $\mathbf{F}$ and $[\mathbf{G}]$ are the column vectors of Π in (A.31) with $(\mathbf{F})_i := F_i$, $[\mathbf{G}]_i = G_i$.*

Shock waves satisfying this conditions will be called *non-degenerate* shocks.

Proof. Indeed, condition 1 comes from basic linear algebra: the kernel of the matrix must have non-trivial dimension; otherwise the system (A.31) would only possess the zero solution, which is impossible because $u_0 \neq 0$.

The case when $Rank(\Pi) < 2$ should be discarded because at least one of the variables υ or u would be able to take arbitrary values in which case the solution is not generic. Condition 2 together with 1 guarantee that the third column of Π, (*i.e.*, the column vector $\mathbf{F}_0$) belongs to the subspace generated by $[\mathbf{G}]$ and $\mathbf{F}$.

Condition 1 alone is not enough to ensure the existence of generic solutions. Indeed, let us assume that the first condition is true but not the second one: a Gaussian reduction of the matrix Π will produce one of the two following outcomes for the system (A.31)

$$\begin{pmatrix} 1 & \cdot & 0 \\ 0 & 0 & 0 \\ 0 & \cdot & 1 \\ 0 & 0 & 0 \\ \vdots & \vdots & \vdots \\ 0 & 0 & 0 \end{pmatrix} \begin{pmatrix} \upsilon \\ u \\ u_0 \end{pmatrix} = 0, \qquad \begin{pmatrix} 0 & 0 & 0 \\ \cdot & 1 & 0 \\ \cdot & 0 & 1 \\ 0 & 0 & 0 \\ \vdots & \vdots & \vdots \\ 0 & 0 & 0 \end{pmatrix} \begin{pmatrix} \upsilon \\ u \\ u_0 \end{pmatrix} = 0. \tag{A.32}$$

Both cases contradict the hypothesis $u_0 \neq 0$.

In the case $n = 3$, we need to check that $det(\Pi) = 0$ and $\mathbf{F} \times (\mathbf{G} - \mathbf{G}_0) \neq 0$. We can find the set of points satisfying the first condition using the `Contour` routine of the RPn package. The second condition is valid generically for the model of mixed CO_2-water injection in geothermal reservoirs.

Consider the conservation law (A.1). Let us assume that the system (A.1) has $n-1$ different characteristic eigenvalues. We state a result that can be written in the same lines of Theorem 17.1 Chapter 17 of the classical work by Smoller (1983) [79].

Theorem A.1. *Let the system (A.1) be hyperbolic with $n-1$ different charateristic speeds in a neighborhood N of W_0. Then there exist $n-1$ smooth one-parameter family of states*

$W = W_k(\xi)$, $k = 1,2,\ldots,n-1$ defined for small ξ, where $W_k(0) = W_0$, all of which satisfy the Rankine-Hugoniot shock condition given by Eq. (A.25). If the k-th characteristic field is genuinely nonlinear, we can choose a parametrization of $W_k(\xi)$ such that for an appropriate choice of the orientation of the k-eigenvector we have

$$\upsilon(0) = \lambda_k(W_0), \qquad \frac{dW_k}{d\xi}(0) = \mathbf{r}_k(W_0), \tag{A.33}$$

$$\frac{d\upsilon}{d\xi}(0) = \frac{1}{2}, \qquad \frac{d^2W_k}{d\xi^2}(0) = \frac{d\mathbf{r}_k}{d\xi}(W_0). \tag{A.34}$$

Proof. We leave it to the reader.

The k-shock curve is defined as the section of the k-th one-parameter family $W_k(\xi)$ given by Th. A.1 where Liu E-condition is satisfied, see [14], *i.e.*, where the shock speed decreases monotonically. Notice that when the k-field is genuinely nonlinear in a neighborhood of W_0, (A.34) asserts there actually exists a direction where this happens, namely the one given by negative values of ξ.

The differential of $\mathbb{H}_{W_0}$ in (A.24) is given by

$$d\mathbb{H}_{W_0}(V,u,\upsilon) = \big(\upsilon D\mathbf{G} - D\mathbf{Q}\big)dW + (\mathbf{G} - \mathbf{G}_0)d\upsilon \tag{A.35}$$

From definition (A.24)and (A.35) the implicit function theorem guarantees that we can construct the k-shock curve given by Th. A.1 for a point $W^* := W(\xi^*) = (V(\xi^*), u(\xi^*))$ and $\upsilon^* := \upsilon(W_0, W^*)$ unless

$$\upsilon^* = \lambda_k(W^*) \qquad \text{and} \qquad \mathbf{l}_k(W^*)\cdot(\mathbf{G}(V^*) - \mathbf{G}(V_0)) = 0 \tag{A.36}$$

where $\mathbf{l}_k$ is the k-th left eigenvector of the system. For instance, condition (A.36) is valid at the reference point $W_0 = (V_0, u_0)$ of the RH Locus. If there exists a point W^*, different from W_0 and contained in $RH(W_0)$ such that (A.36) is satisfied, we say that W_0 belongs to the secondary bifurcation manifold, see Section 6.4 and [73]. Points different from W_0 satisfying (6.59) and stable under perturbations are self-intersection points. If $RH(W_0)$ has no self-intersection points, it is reasonable to look for continuation methods for finding connected branches of the RH Locus.

We define below the initialization process to construct the k-shock curve. By an ODE algorithm we define a integration process for building it. We will describe in Section A.5 a continuation method as an alternative for this integration process. The latter method was originally built and tested succesfully for use in the RPn software. In Section A.5.2 we provide the details for the stopping criteria for the integration process independent of the method used. Stopping criteria for the shock curve construction are essential to ensure that Liu E-condition and Oleinik E-condition are satisfied, see [14] and [48]. At this point we want to highlight that the most important stopping criteria used requires the precise calculation of the stationary points of the shock speed, *i.e.*, where $d\upsilon/d\xi = 0$ is valid. In practice we find them using the following important result.

Theorem A.2 (Bethe-Wendroff). *Consider the Hugoniot locus through a state W_0. Let W be a point on the k-branch and assume that (A.36) does not hold at W. Then the following are equivalent:*

$$\frac{d\upsilon}{d\xi}(\xi^W) = 0, \tag{A.37}$$

$$\lambda_k(W) = \upsilon(\xi^W), \tag{A.38}$$

for some k, and $W = W_k(\xi^W)$, where $W = W(\xi)$ is a parametrization of the k-shock. In this case, $\lambda_k(W) - \upsilon(W, W_0)$ and $\frac{d\upsilon}{d\xi}(W)$ vanish to the same order. Also the characteristic vector of the k-family is tangent with the same order to the Hugoniot locus.

This result has been generalized for systems of the type (A.2), see [39], and was first introduced in the work by Furtado (1989) [22]. In Section A.4.1 we give a summary of the routines for the implementation of both the shock curve integration algorithm and the shock curve continuation algorithm.

A.3 Shock Curve Initialization

From Eq. (A.33) we obtain the tangent to the k-branch of the RH Locus at W_0. Therefore, we may start our numerical calculation of the k-branch of shock curve at either one of the points

$$W_0^{+\varepsilon_0} := W_0 + \varepsilon_0 \mathbf{r}_k(W_0) \tag{A.39}$$

$$W_0^{-\varepsilon_0} := W_0 - \varepsilon_0 \mathbf{r}_k(W_0) \tag{A.40}$$

for a small ε_0, which will be called the *size parameter*. As the k-branch of the shock curve is smooth, for small values of ε_0, one of the points $W_0^{\beta\varepsilon_0}$, where β stands for either the symbol $+$ or $-$, are close enough to the k-branch in the sense that $\Gamma(W_0^{\beta\varepsilon_0}) \sim 0$, with Γ given in Eq. (A.29). When building the k-branch we are interested in finding the section of the k-shock curve where the shock speed υ decreases monotonically, *i.e.*, such that it satisfies Liu E-condition: this is the criterion we use to determine the direction of integration until the monotonicity is violated, at a point given by Th. A.2. Unless the left state W_0 belongs to the inflection loci, one of the following inequalities is true

$$\upsilon(W^-, W_0) < \lambda_k(W_0) < \upsilon(W^+, W_0), \tag{A.41}$$

$$\upsilon(W^-, W_0) > \lambda_k(W_0) > \upsilon(W^+, W_0). \tag{A.42}$$

Indeed, outside of the inflection locus the system (A.1) is genuinely nonlinear. Therefore from Eq. (A.33.a) the shock speed coincides with λ_k at the reference state and from Eq. (A.34.a) it decreases in one of the parametrization directions. (On the inflection lo-

cus the shock speed can decrease or increase on both sides of the reference state W_0, and therefore we would have either two possible directions of integration or none).

According to inequalities (A.41) and (A.42), we choose W_1 as the starting point for the k-branch integration in the decreasing direction of the shock speed. For a small value of ε_0, W_1 is close to the k-branch of the RH locus.

A.4 Shock Curve Integration

As stated in Eq. (A.29), the RH Locus with reference point W_0 is given by the intersection of the $n-1$ hypersurfaces given by

$$\Gamma_i(V,u) := \left([Q_{\alpha^{i+1}}][G_{\alpha^i}] - [Q_{\alpha^i}][G_{\alpha^{i+1}}]\right) = 0 \qquad \text{where} \qquad i = 1,\ldots,n-1. \quad \text{(A.43)}$$

Let W^* be a point contained in the RH Locus of a reference state W_0, where $W^* \neq W_0$ is not a point where the RH Locus self-intersects, more precisely the hypotheses of the implicit function theorem hold. The tangent line to the locus is the intersection of the $n-1$ hyperplanes tangent to each hypersurface. Therefore this line is normal to the $n-1$ normals to the hypersurfaces.

The implicit function theorem provides a local parametrization $W(\xi) = (V(\xi), u(\xi))$ of the RH-branch passing through W^*: in our numerical implementation, an ODE can be solved because we are able to find a smooth normalized vector field $X(W) \propto (V', u')$ tangent to the shock curve, and coherently oriented, *i.e.*, whenever W_1 and W_2 are close, we must have that $X(W_1) \cdot X(W_2) > 0$.

The normal vectors to the hypersurfaces at the point $W^* = (V^*, u^*)$ are given by the gradients $\nabla\Gamma_i$, where $i = 1,\ldots,n-1$. The first $n-1$ components of the gradients are

$$\begin{aligned}\left(\nabla\Gamma_i\right)_j = \frac{\partial Q_{\alpha^{i+1}}}{\partial V_j}(u^*,V^*)[G_{\alpha^i}] + [Q_{\alpha^{i+1}}]\frac{\partial G_{\alpha^i}}{\partial V_j}(V^*) \\ - \frac{\partial Q_{\alpha^i}}{\partial V_j}(u^*,V^*)[G_{\alpha^{i+1}}] - [Q_{\alpha^i}]\frac{\partial G_{\alpha^{i+1}}}{\partial V_j}(V^*) \quad \text{(A.44)}\end{aligned}$$

for $j = 1,\ldots,n-1$, and the last component (*i.e.*, $j = n$) is given by

$$\left(\nabla\Gamma_i\right)_n = \frac{\partial Q_{\alpha^{i+1}}}{\partial u}(u^*,V^*)[G_{\alpha^i}] - \frac{\partial Q_{\alpha^i}}{\partial u}(u^*,V^*)[G_{\alpha^{i+1}}] \quad \text{(A.45)}$$

Let

$$E(\Gamma) := \langle \nabla\Gamma_1, \nabla\Gamma_2, \ldots, \nabla\Gamma_{n-1} \rangle \quad \text{(A.46)}$$

denote the affine space spanned by the normal vectors to the hypersurfaces at the point W^*. We are assuming that its dimension is $n-1$. Therefore the line tangent to the shock curve at the point W^* is given by the vector orthogonal to this space. This vector, denoted by $X(W^*)$ is found using the modified (or numerically stable) Gram-Schidmt orthonor-

malization process (for instance see Trefethen (1997) [89]). From the line field found in this manner we obtain a vector field as explained before. Notice that from the hypothesis $\mathbf{Q}, \mathbf{G} \in C^2(\mathbb{R}^n)$, the resulting vector field is smooth.

A packaged ODE solver can then be used for finding the local parametrization of the shock curve around W^*; whenever the implicit function theorem is violated, we stop the integration process.

Notice that in the integration process we are able to calculate simultaneously the shock speed υ; indeed, if we multiply every component of Eq. (A.25) by the term $[G_i]$, adding all equations and solving for υ we obtain

$$\upsilon = \frac{\sum_i [Q_i][G_i]}{\sum_j [G_j]^2} \tag{A.47}$$

where υ is the shock speed between W^* and and the reference state W_0. Evidently, Eq. (A.47) is valid when there exist i such that $[G_i]^2 \neq 0$. Lambert et al. [39] found an alternative expression for υ based on the factorization (A.31) for systems of the type (A.2) and n=3, see Chapter 6. In the next section we show how perform the integration process in practice.

A.4.1 Integration Algorithm

We start the integration process for the k-shock curve using the "first" point W^1 as given in Section A.3 in the direction of decreasing shock speed, whenever the reference state W_0 does not belong to the inflection locus of the k-family.

Let us assume that W^1 does not belong to the set of self-intersection points of the RH-Locus. As seen in Section A.4 we can find approximations $X(W^{*,1})$ for the tangent of the k-branch at points $W^{*,1}$ contained in a neighborhood of W_1, which are correct up to sign. The orientations of $X(W^{*,1})$ are chosen consistently with the integration direction, *i.e.*, given the direction reference vector $\mathbf{r}^{\mathrm{D},1} := W_1 - W_0$ we check if $X(W^{*,1}) \cdot \mathbf{r}^{\mathrm{D},1} > 0$; otherwise we replace $X(W^{*,1})$ by its opposite.

We can now start our continuation process using a packaged ODE integrator for finding the next point over the k-branch, *i.e.*, W_2. Next we store the new reference vector $\mathbf{r}^{\mathrm{D},2} := W^2 - W^1$.

At the end of step n of the integration process we have the point W_n and the reference vector $\mathbf{r}^{\mathrm{D},n} := W_n - W_{n-1}$. If the implicit function theorem is still valid, in the $n+1$-th step we can find the approximations for the tangent near W_n, given by $X(W^{*,n})$. We orient this approximations consistently with $\mathbf{r}^{\mathrm{D},n}$. We use the packaged ODE integrator to find the next approximated point contained in the k-branch, W_{n+1}. The process will continue until we arrive at a stopping point as explained in Section A.5.2.

This integration method may fail to converge in our class of problems. It certainly fails at self-intersection points which are a common feature of the RH-Locus. Experience

shows that if may fail to converge at other points. This is the motivation for developing the method that follows.

A.5 Alternative Shock-Curve Continuation Algorithm

The method below differs from the integration algorithm described in Section A.4.1 in two aspects. The first is that it does not accumulate integration errors from solving an ODE. The second is that experience shows that it is more robust. An example of the weakness of the integration algorithm is the initialization process described in Section A.3. Indeed, it provides a point $W_0^{\beta\varepsilon_0}$, where $\beta = +$ or $-$, that may be too far away from the k-branch of the shock curve. Therefore it is reasonable to find a method for correcting this deviation, and to keep repeating this correction procedure at every time step.

A.5.1 Mathematical description

We consider here the particular case where $n = 3$ in the system (A.26), and where we have two different eigenvalues and linearly independent eigenvectors. Without loss of generality we study the problem described in Chapter 6. The k-family will represent the e-family with eigenvector $\mathbf{r}_e$; the other eigenvector is $\mathbf{r}_s$. The two eigenvectors are linearly independent as we assume that we are not near the coincidence locus C_e where the eigenvectors are parallel.

By (A.33), the tangent to the connected k-branch of the RH Locus at the point W_0 is given by $\mathbf{r}_k(W_0)$. In order to initialize the continuation algorithm we find the points $W_0^{\beta\varepsilon_0}$, $\beta = +, -$ given in (A.39) and (A.40). As mentioned before one of these points is close to the k-branch for a sufficiently small value of the parameter ε_0. We are interested in finding a new point W^1 over the k-branch within a specified accuracy.

In order to perform the correction for $W_0^{\beta\varepsilon_0}$, we find numerically the intersection of a plane through $W_0^{\beta\varepsilon_0}$ with the k-shock curve. We denote this plane $P_1^{\beta\varepsilon_0}$ which is built in such a way that its intersection with the k-shock curve is close to $W_0^{\beta\varepsilon_0}$. In this case we use the plane $P_1^{\beta\varepsilon_0}$ through $W_0^{\beta\varepsilon_0}$ spanned by the normalized vectors

$$\mathbf{r}_1^1 := \mathbf{r}_e \times \mathbf{r}_s / \left\|\mathbf{r}_e \times \mathbf{r}_s\right\|_2 \tag{A.48}$$

$$\mathbf{r}_2^1 := \mathbf{r}_s / \left\|\mathbf{r}_s\right\|_2. \tag{A.49}$$

evaluated at W_0. We apply a Newton method as described in section A.5.1.1 for a fixed tolerance δ^p, for finding a candidate for the intersection of $P_1^{\beta\varepsilon_0}$ with the k-shock curve. If found, this candidate is denoted by $W_1^{\beta\varepsilon_0}$.

We repeat the process dividing ε_0 by 2 and use $W_0^{\beta\frac{\varepsilon_0}{2}}$ (and the plane $P_1^{\beta\frac{\varepsilon_0}{2}}$) instead of the point $W_0^{\beta\varepsilon_0}$ (and $P_0^{\beta\varepsilon_0}$), and so on until a candidate $W_1^{\beta\frac{\varepsilon_0}{2^m}}$, $m\in\mathbb{Z}$ is found such that

$$\left\| W_1^{\beta\frac{\varepsilon_0}{2^m}} - W_0^{\beta\frac{\varepsilon_0}{2^m}} \right\|_2 < \delta \tag{A.50}$$

is valid. Here $W_1^{\beta\frac{\varepsilon_0}{2^m}}$ is the intersection of the plane $P_1^{\beta\frac{\varepsilon_0}{2^m}}$ (based on $W_0^{\beta\frac{\varepsilon_0}{2^m}}$) with the shock curve.

This process is performed on $W_0^{+\varepsilon_0}$ and $W_0^{-\varepsilon_0}$; we calculate the speed of the shocks between W_0 and the states found in both directions, and motivated by Lie E-condition choose the direction corresponding to decreasing shock speed, . The result of this procedure is denoted by W_1, which will be assumed to lie on the k-branch of the shock curve. The corresponding size parameter used for finding W_1 will be denoted as ε_1. P_1 will denote the plane given by the point W_1 and spanned by the vectors $\mathbf{r}_1^1$ and $\mathbf{r}_2^1$. A reference vector $\mathbf{r}^{\mathrm{D},1} := W_1 - W_0$ is also stored for later use. See Fig. A.1 for a graphical representation of the continuation algorithm.

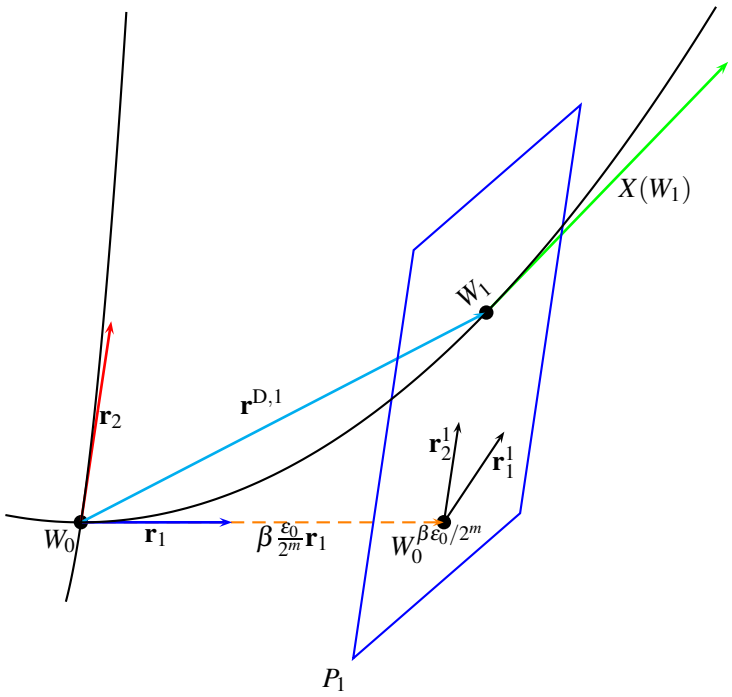

Fig. A.1 Geometrical representation of the first step of the construction of the alternative shock-curve continuation algorithm

The inductive step of the continuation algorithm is described next. Let W_n be the point over the shock curve found during the n-th step of the process, P_n, ε_n, and $\mathbf{r}^{\mathrm{D},n}$ the corresponding plane, size parameter, and reference vector respectively. If W_n is not a self-intersection point, we can find a tangent $X_n := X(W_n)$ of length 1 to the k-branch at W_n (see section A.4) consistently oriented with the reference vector $\mathbf{r}^{\mathrm{D},n}$ (their inner product is positive).

Under the assumption that X_n is not parallel to the plane P_n, we define $P_{n+1}^{\varepsilon_n}$ as the plane through the point $W_n^{\varepsilon_n} := W_n + \varepsilon_n X_n$ spanned by the pair of vectors $\mathbf{r}_1^{n+1}$ and $\mathbf{r}_2^{n+1}$ given by

$$\mathbf{r}_1^{n+1} := \frac{X_n \times \mathbf{r}_1^n}{\left\| X_n \times \mathbf{r}_1^n \right\|_2} \tag{A.51}$$

$$\mathbf{r}_2^{n+1} := \frac{X_n \times \mathbf{r}_1^{n+1}}{\left\| X_n \times \mathbf{r}_1^{n+1} \right\|_2} \tag{A.52}$$

The vectors $\mathbf{r}_1^{n+1}$ and $\mathbf{r}_2^{n+1}$ are orthogonal, and X_n is normal to $P_{n+1}^{\varepsilon_n}$ (see Fig. A.1). Using Newton's method we find the candidate for the intersection $W_{n+1}^{\varepsilon_n}$, of this plane with the shock curve. Analogously as for the first step of the continuation algorithm we repeat the process above using the new point $W_n^{\frac{\varepsilon_n}{2}}$ $\left(\text{ based on } P_{n+1}^{\frac{\varepsilon_n}{2}}\right)$ and so on until for some $m \in \mathbb{N}$

$$\left\| W_n^{\frac{\varepsilon_n}{2^m}} - W_n^{\frac{\varepsilon_n}{2^m}} \right\|_2 < \delta \tag{A.53}$$

The new point over the k-branch is denoted by W_{n+1}. The corresponding size parameter used for finding W_{n+1} will be denoted as ε_{n+1}. P_{n+1} will denote the plane through the point W_{n+1} spanned by the vectors $\mathbf{r}_1^{n+1}$ and $\mathbf{r}_2^{n+1}$. A reference vector $\mathbf{r}^{\mathrm{D},n+1} := W_{n+1} - W_n$ is also stored for later use.

The process continues until a stopping criterion is satisfied. The most important such criterion is Bethe-Wendroff, see Section A.5.2.

A.5.1.1 Restricted Newton method

The following method is used for finding the intersection of the shock curve with a plane, in $\mathbb{R}^3$. The idea is to restrict the equations for the shock curve to the plane so that the problem reduces to finding the zero of a mapping from $\mathbb{R}^2$ to $\mathbb{R}^2$.

Let P be the plane through W spanned by the vectors $\mathbf{r}_1$ and $\mathbf{r}_2$. The following condition is satisfied for points in P:

$$(x_1, x_2, x_3) \in P \Longleftrightarrow (x_1, x_2, x_3) = W + a_1\mathbf{r}_1 + a_2\mathbf{r}_2. \tag{A.54}$$

where a_1 and a_2 are the *plane coordinates* of the point W.

The shock curve is given by the zero set of the mapping Γ given by (A.29) with $n = 3$. Therefore, we are interested in finding the point W^* contained in the plane P (*i.e.*, of the form (A.54)) that satisfies $\Gamma_i = 0$ where $i = 1, 2$, as explained in Section A.2. Using (A.54), the plane coordinate of W^* given by $\mathbf{a}^* = (a_1^*, a_2^*)$ must then satisfy $N(a_1^*, a_2^*) = \mathbf{0}$ where

$$N(a_1, a_2) := \Gamma(W) = \Gamma\big(W + a_1\mathbf{r}_1 + a_2\mathbf{r}_2\big) \tag{A.55}$$

Therefore we apply a 2-D Newton-Raphson algorithm for finding a good approximation for (a_1^*, a_2^*). As initial estimates we use the plane coordinates of W, which are zero.

The l-th iteration of the Newton-Raphson method [84] is given by

$$\mathbf{a}^{l+1} = \mathbf{a}^l - \left(\frac{\partial N}{\partial \mathbf{a}}(\mathbf{a}^l)\right)^{-1} N(\mathbf{a}^l), \tag{A.56}$$

with $\mathbf{a}^0 = \mathbf{0}$, and the jacobian of N is given by

$$\frac{\partial N_i}{\partial a_j} = \sum_{m=1}^{3} \frac{\partial \Gamma_i}{\partial x_m}\frac{\partial x_m}{\partial a_j} = \nabla\Gamma_i \cdot \mathbf{r}_j, \quad \text{for } \; i, j = 1, 2 \tag{A.57}$$

The jacobian of N can also be written as the product of the 2×2 matrices

$$\frac{\partial N}{\partial \mathbf{a}} = \begin{pmatrix} \nabla\Gamma_1 \\ \nabla\Gamma_2 \end{pmatrix} \begin{pmatrix} \mathbf{r}_1 \; \mathbf{r}_2 \end{pmatrix} \tag{A.58}$$

Unless $\partial N/\partial \mathbf{a}(\mathbf{a}^k)$ fails to be invertible, the Newton method converges whenever the initial iteration point $\mathbf{a}^0$ is chosen close enough to the desired solution $\mathbf{a}^*$ (see Theorem 5.2 [84]). From Eq. (A.58), as the vectors $\mathbf{r}_i$ for $i = 1, 2$ are linearly independent, we see that DN is invertible whenever the gradients $\nabla\Gamma_i$ are linearly independent, *i.e.*, under the hypotheses of the implicit function theorem applied to Γ. Therefore N is nearly singular in a neighborhood of the self-intersection points of the RH-Locus or secondary bifurcations. Near these points, the Newton method may fail to converge. Repeated failure of convergence may be a stopping criterion.

A.5.2 Stopping criteria

We have seen above that local parametrizations can be found except at the left state W_0 of the shock curve and at the secondary bifurcation loci or at self-intersections. A stopping criterion must be devised such that the construction stops when the shock curve ceases to represent admissible shocks. For local shock curves we can use Liu E-condition, and for non-local branches we can use Lax shock admissibility criterion. When these two fail we can apply the viscous shock admissibility criteria (for the definition of this conditions see [14]). Details will appear in future work.

For checking Liu E-condition we use the Bethe-Wendroff Theorem, [96]; for instance for problems of the type (A.2), we can use the generalized version of Bethe-Wendroff, proved by Lambert (2009) [39].

Liu E-condition requires the construction of shock curves where the shock speed υ decreases from the left state. It was introduced by Liu (1976) [48] and can be stated as follows (see [14]):

Definition A.1. Given a state W_0, and a k-branch of its corresponding RH Locus parametrized as $W_k(\xi)$, a k-shock wave between $W = W_k(\xi^{\mathrm{w}})$ and W_0 is said to satisfy the Liu E-condition if

$$\upsilon(\xi^{\mathrm{w}}, W_0) \leq \upsilon(\xi, W_0), \quad \text{for all } \xi \text{ between } 0 \text{ and } \xi^{\mathrm{w}}, \tag{A.59}$$

where $\upsilon(\xi, W_0)$ stands for the shock speed parametrized by ξ between states $W(\xi)$ and W_0 both contained in the k-branch of $RH(W_0)$.

In order to check Liu E-condition, we look for stationary points of the shock speed, *i.e.*, where $\frac{d\upsilon}{d\xi} = 0$. To do so, we use the Bethe-Wendroff Theorem, see Th. A.2, and instead of stationary points we search for points in the continuation algorithm at which $\lambda_k = \upsilon$ is satisfied, see (A.38).

In practice we proceed as follows. Let us consider the difference between the shock and characteristic speeds along the k-branch, *i.e.*, $\upsilon(W(\xi), W_0) - \lambda_k(W(\xi))$. Let $W_n = W(\xi_n)$ and $W_{n+1} = W(\xi_{n+1})$ be consecutive steps of the shock curve continuation algorithms as described in Sections A.4, A.5, such that the difference reverses sign.

The difference is continuous as the coefficients of the PDEs are smooth. From the intermediate value theorem there exists ξ_n^{BW} such that the difference vanishes, so that we have to stop the construction of the k-branch. This is true provided W_n and W_{n+1} are extremely close to the actual k-branch, *i.e.*, if the Newton-Raphson continuation algorithm is employed.

Let us find the stopping point. A first guess, denoted by W_n^0 is obtained by linear interpolation of the difference fuction on the segment between W_n and W_{n+1}. We can improve it by applying Newton-Raphson algorithm [84] for finding the zeros of the system of n equations

$$\Gamma_i = \left([Q_{\alpha^{i+1}}][G_{\alpha^i}] - [Q_{\alpha^i}][G_{\alpha^{i+1}}]\right) = 0 \qquad \text{where} \qquad i = 1, \ldots, n-1. \tag{A.60}$$

$$\upsilon - \lambda_k = 0 \tag{A.61}$$

for an appropriate choice of indices $[\alpha_1, \alpha_2, \ldots, \alpha_n]$. The iterations are given by

$$W_n^{l+1} = W_n^l - \left(DM(W_n^l)\right)^{-1} M(W^l) \tag{A.62}$$

where M is the $n \times n$ jacobian matrix of the system (A.60) and (A.61), given by

$$DM = \begin{pmatrix} \nabla \Gamma_1 \\ \nabla \Gamma_2 \\ \vdots \\ \nabla \Gamma_{n-1} \\ \nabla \upsilon - \nabla \lambda_k \end{pmatrix} \tag{A.63}$$

We calculate $\nabla \Gamma_i$ using expressions (A.44) and (A.45). In order to calculate $\nabla \upsilon$, we use Eq. (A.47).

For the case $n = 3$ we prefer expression (6.68) of Chapter 6 for calculating the partial derivatives of the shock speed. For this case we know the explicit expression for the gradients of the eigenvalues λ_s and λ_e. Indeed, the first one is easily calculated by using the partial derivatives of the fractional flow function $f_\sigma(s_\sigma, T)$. The second one is given by Eqs. (6.48), (6.49), and (6.50) of Chapter 6.

In general, we do not have an explicit formula for λ_k. In order to calculate $\nabla \lambda_k$ we can alternatively calculate $\nabla \lambda_k \cdot \mathbf{x}_i$ for n linearly independent vetors $\mathbf{x}_1, \mathbf{x}_2, \ldots, \mathbf{x}_n$ in $\mathbb{R}^n$, in particular we can use the canonical base $\mathbf{e}_i$ for $i = 1, \ldots, n$. In practice this can be done using a slight variation of Lemma A.1: under the same hypotheses we obtain the formulae

$$(\nabla \lambda_k \cdot \mathbf{e}_i)(\mathbf{l}_k \cdot B\mathbf{r}_k) = \mathbf{l}_k \cdot \left(\frac{d^2\mathbf{Q}}{dW^2}(\mathbf{e}_i, \mathbf{r}_k) - \lambda_k \frac{d^2\mathbf{G}}{dW^2}(\mathbf{e}_i, \mathbf{r}_k) \right), \tag{A.64}$$

for $i = 1, \ldots, n$.

Remark A.2. In Chapter 6 we show how it is possible to calculate a set of non-degenerate shock waves with reference state W_0 for systems of conservation laws of the type (A.2) and $n = 3$ using the 2-D `Contour` algorithm.

Remark A.3. Contact Discontinuities are particular degenerate shocks; they are abrupt changes in weak solutions $W(x,t)$ of (A.1) that travel with characteristic speed. They are represented in the space of variables (V,u) by solutions to (A.11) and (A.12) where the eigenvalue remains constant, *i.e.*, where

$$\big(\nabla \lambda \cdot \mathbf{r}\big)(V(\eta), u(\eta)) = 0 \tag{A.65}$$

Moreover these discontinuities satisfy the RH shock condition. In the tp configuration for the particular model of mix CO_2/water injection in geothermal reservoirs, we do not observe this kind of waves. They exist in single phase conditions, e.g., in the single phase aqueous configuration; see Section 6.6 in Chapter 6 and [92] for its complete analysis (they have been found analytically by integration of a system of ODEs).

A.6 Bifurcation Curves

Bifurcation curves are loci where the solutions change topology, such as: secondary bifurcation, coincidence, inflection, hysteresis and interior boundary contact. We restrict its numerical computation for the systems of conservation laws of the type (A.2) with two families of characteristic speeds, as the ones studied in Chapter 6.

Coincidence curves are locus where the eigenvalues coincide. In Chapter 6 we calculate explicit expressions for the eigenvalues of the system. We are then able to use a packaged Matlab® `contour` algorithm for finding the coincidence curve in the tp configuration. For the complete implementation of the RPn package, a 2-D `Contour` algorithm was developed, providing equivalent results to the ones depicted in Fig. 6.1. The results can be seen throughout Chapter 6.

An important bifurcation locus for Riemann problems is the double contact locus. The (i,j) double contact locus, denoted as $DC^{i,j}$ is given by the pairs (W^l, W^r) with $W^r \in RH(W^l)$ where

$$\upsilon(W^l, W^r) = \lambda_i(W^l), \tag{A.66}$$

$$\upsilon(W^l, W^r) = \lambda_j(W^r), \tag{A.67}$$

with $i, j \in \{1,2\}$, where 1 (2) is the slow (fast) family. Double contact locus for the k-th family satisfy $i = j \equiv k$ in (6.81)-(6.82). On the contrary, when $i \neq j$ the double contact is of *mixed* type. The numerical calculation of the double contact locus was performed using the 4-D `Contour` code; this calculation was applied for finding these bifurcation curves in the tp configuration for the CO_2-H_2O flow model, see Chapter 6 for the results.

Another set of important bifurcation locus is given by the extension curves. Let $C^l := \{W^l\} \subset \Omega$ denote a curve in phase space: its k-extension $E_k^r(C^l)$ is given by the set of states $\{W^r\}$ such that for all $W^r \in E_k^r(C^l)$ there exists a W^l such that $W^r \in RH(W^l)$ and $\lambda_k(W^r) = \upsilon(W^l, W^r)$. We define the left k-extension similarly but we impose the condition $\lambda_k(W^l) = \upsilon(W^l, W^r)$. Notice that from this definition we have $C^l \subset E_k^r(C^l)$.

Important extension curves are the extension of the boundary (or interior boundary contact) and the extension of the inflection locus (or *hysteresis*).

These have been calculated too using the `Extension` curve code. For the numerical results on the tp configuration, see Chapter 6.

Remark A.4. In Figure 6.7 we can see several examples of wave curves and bifurcation loci calculated using the numerical methods presented here and implemented in the RPn package. For instance, the coincidence loci $C_{s,e}$ and C_{s,e^*} were calculated with the `Contour` algorithm. The shock curves were calculated with the Alternative Shock-Curve Continuation Algorithm. The (fast) double contact DC^2 was calculated with the 4-D `Contour` code. The extension of the boundary $E_2^{r,0}$ was calculated with the `Extension` curve code. The Buckley-Leverett rarefaction and the thermal rarefaction curves were calculated using the rarefaction curve algorithm.

Appendix B
Physical Data

B.1 Physical quantities

As the amount of H_2O solute in the supercritical CO_2-rich fluid phase is low, i.e., $y_w \ll 1$, we can approximate the viscosity of the supercritical fluid phase by the viscosity of pure supercritical carbon dioxide at the reservoir temperature, using the experimental values given by Fenghour et al. [20]. In an initial fitting approach we can interpolate values for the viscosity depending on pressure and temperature: this can be done numerically using Matlab® princomp routine for performing an orthogonal regression using principal components analysis.

On the other hand we can fit a polynomial in T, using different values for the viscosity at the constant reservoir pressure. This is done with the Matlab® polyfit function, (Fig. B.1) using the experimental data provided by Fenghour et al. [20], providing the result:

$$\mu_\sigma(T, P_{res}) \approx -1.9476 \times 10^{-6} T^3 + 0.0135 T^2 - 9.0436 T + 1.6128 \times 10^3 \quad [\text{Pa}\cdot\text{s}]. \quad \text{(B.1)}$$

The temperature dependent aqueous phase viscosity μ_a [Pa· s] can be approximated by the viscosity of pure water

$$\mu_a \approx \mu_W = -0.0123274 + \frac{27.1038}{T} - \frac{23527.5}{T^2} + \frac{1.01425 \times 10^7}{T^3} - \frac{2.17342 \times 10^9}{T^4} + \frac{1.86935 \times 10^{11}}{T^5} \quad [\text{Pa}\cdot\text{s}]. \quad \text{(B.2)}$$

given in [40]. The relative permeability functions $k_{r\sigma}$ and k_{ra} are considered to be quadratic functions of their respective reduced saturations, *i.e.*,

$$k_{r\sigma} = \begin{cases} 0.95 \left(\frac{s_\sigma - s_{\sigma r}}{1 - s_{ar} - s_{\sigma r}} \right)^2 \\ 0.95 \end{cases}, \; k_{ra} = \begin{cases} 0.5 \left(\frac{s_a - s_{ar}}{1 - s_{ar} - s_{\sigma r}} \right)^2 & \text{for } s_{ar} \le s_a \le 1, \\ 0 & \text{for } \quad s_a < s_{ar}, \end{cases} \quad \text{(B.3)}$$

where s_{ar} is the residual aqueous phase saturation. For simplicity, in this work we put $s_{ar} = 0$ and $s_{\sigma r} = 0$.

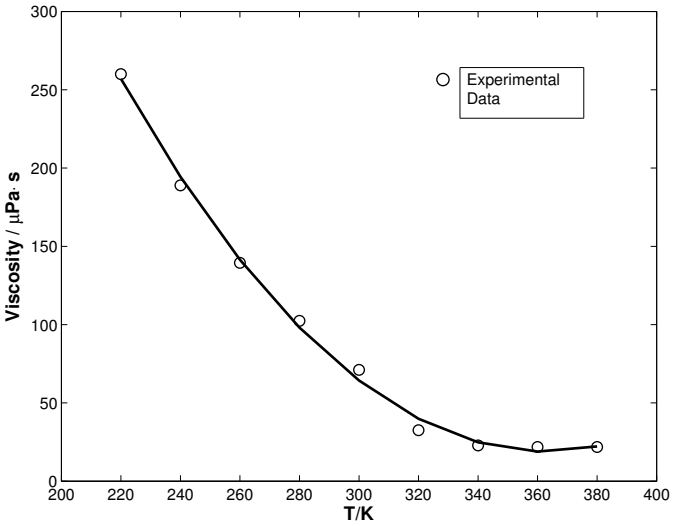

Fig. B.1 Polynomial fit for the experimental data given by Fenghour et al.(1997) [20]. See Table *B*.2 for an approximate value of $\mu_\sigma(T_{res}, P_{res})$.

Table B.1 Reference constants for the model

Expression	*Value*	*Units*
L_{ref}	10	[m]
t_{ref}	L/U_{ref}	[s]
U_{ref}	4.42×10^{-3}	[m^3/(m$^2\cdot$ s)]
ρ_{ref}	998.2	[m^3/kg]
T_{ref}	304.63	[K]
μ_{ref}	3.6874×10^{-5}	[Pa$\cdot$ s]
K_{ref}	20×10^{-12}	[m^2]
h_{ref}	1.3×10^5	[J/m^3 kg]
C_g	4.4215	[-]

Table B.2 Summary of physical input parameters, constants and variables.

Description	*Symbol*	*Value*	*Unit*
Atmospheric Pressure	p_{at}	1.01325×10^5	[Pa]
Reservoir Pressure	P_{res}	1.09×10^7	[Pa]
Absolute Permeability	k	20 (Ch. 3, Ch. 8) 3, (Ch. 6)	[mD]
CO_2's Henry Coefficient at 298.15 [K]	$k_c^{T_\theta}$	29.8×10^2	$[\frac{m^3 Pa}{mol}]$
Universal Gas Constant	R	8.31415	$[\frac{J}{K \cdot mol}]$
Evaporation Heat of Water	$\Lambda_W(T_b^W)$	2.270×10^6	[J/kg]
Partial Darcy velocity	u_σ, u_a	Eq. (2.1)	[m/s]
Total Darcy velocity	u	$u_\sigma + u_a$, Eq. (2.1)	[m/s]
Saturation	s_σ, s_a	Dependent variables.	$[m^3/m^3]$
Phase viscosity	μ_σ, μ_a	Eq. (B.1), Eq. (B.2)	$[Pa \cdot s]$
Fractional flow functions	f_σ, f_a	Eq. (2.3)	$[m^3/m^3]$
Residual supercritical phase saturation	$s_{\sigma r}$	See Eq. (B.3)	$[m^3/m^3]$
Connate water saturation	s_{wc}	See Eq. (B.3)	$[m^3/m^3]$
CO_2 constants for the MSRK EOS	m_c, n_c	0.5809, 0.2727	[-]
H_2O constants for the MSRK EOS	m_w, n_w	0.9499, 0.1633	[-]
Critical temperature for CO_2 and H_2O	T_c	304.2, 647.1	[K]
Critical pressure for CO_2 and H_2O	P_c	73.82×10^5, 221.2×10^5	[Pa]
Accentric factor of CO_2 and H_2O	ω	0.23894, 0.344	[-]
κ_1 (PRSV) for CO_2 and H_2O	κ_1	0.04285, -0.06635	[-]
UCEP for the CO_2-H_2O mixture	T_{ucep}, P_{ucep}	304.63, 74.11×10^5	[K], [Pa]
Pure water density	ρ_W	998.2	$[kg/m^3]$
Fit parameter water enthalpy	C_W	4297	$[J/m^3 \cdot K]$
Water enthalpy reference temperature	$T_{\text{ref}}^{\text{water}}$	274.3775	[K]
Rock enthalpy reference temperature	$T_{\text{ref}}^{\text{rock}}$	273.15	[K]
CO_2 supercritical phase compositions	$\psi_{\sigma c}$	(3.3)	[-]
H_2O aqueous compositions	ψ_{aw}	(3.3)	[-]
CO_2 and H_2O molar masses	M_C, M_W	0.044, 0.018	[kg/mol]
Rock porosity	φ	0.15 (Ch. 3, Ch. 8) 0.38, (Ch. 6)	$[m^3/m^3]$

Table B.3 Physical quantities for Chapter 3

Description	*Symbol*	*Value*	*Unit*
Constant Reservoir Pressure	P_{res}	10.9×10^6	[Pa]
Constant Reservoir Temperature	T_{res}	323.15	[K]
tp mutual solubilities	x_c, y_w	0.0205, 0.0045	[m^3 /m^3]
tp molar volumes	υ_σ, υ_a	1.229×10^{-4}, 1.829×10^{-5}	[m^3/mol]
tp phase densities	ρ_σ, ρ_a	357.068, 1013.2	[kg/m^3]
tp partial supercritical densities.	$\rho_{\sigma c}$, $\rho_{\sigma w}$	356.4089, 0.6591	[kg/m^3]
tp partial aqueous densities	ρ_{ac}, ρ_{aw}	49.3126, 963.8926	[kg/m^3]
Pure aqueous carbon density	ρ_{aC}	1434.8, See Eq. (C.19)	[kg/m^3]
Pure water vapor density	$\rho_{\sigma W}$	1232.5, See Eq. (C.17)	[kg/m^3]
Pure supercritical carbon density	$\rho_{\sigma C}$	356.6	[kg/m^3]
Pure steam density	ρ_{gW}	741.4179	[kg/m^3]
Phase viscosities	μ_σ, μ_a	3.6874×10^{-5}, 5.4308×10^{-4}	[Pa·s]
Mean ascent velocity	G	7.89×10^{-5}	[m^3/(m^2· s)]

Appendix C
Two-Phase Equilibrium for Fixed Temperature and Pressure

Let us place ourselves in the tp configuration. If we assume constant pressure and temperature the number of thermodynamic degrees of freedom is zero. Thus we have constant mutual solubilities for two phases in equilibrium.

Remark C.1. We will omit in this section the superscript ^{TP} used to distinguish quantities taken in the tp-configuration.

Our objective is to describe a method for finding the constant partial densities in the tp configuration $\rho_{\sigma c}$, $\rho_{\sigma w}$, ρ_{ac}, and ρ_{aw}, using the constant mutual solubility data given by Bamberger et al. [5] for the fixed pressure and temperature of the reservoir used in the model of isothermal flow with gravity (Chapter 3; see Table B.3). Using these values we find the pure aqueous CO_2 (constant) density ρ_{aC}. Additionally we find the pure vapor densities: $\rho_{\sigma C}$ and $\rho_{\sigma W}$.

Let $n_{\alpha c}$ and $n_{\alpha w}$ denote the number of moles of carbon dioxide and water present in a unit volume of phase $\alpha = \sigma, a$. We have then

$$\frac{M_C n_{\alpha c}}{M_W n_{\alpha w}} = \frac{\rho_{\alpha c}}{\rho_{\alpha w}}. \tag{C.1}$$

As $n_{\alpha c} + n_{\alpha w} = n_T$, ($n_T$ stands for the total number of moles in phase α), and from the definition of the mole fraction of carbon dioxide (*resp.* water) in the aqueous (supercritical fluid) phase, *i.e.*, x_c (y_w), we obtain

$$\frac{M_C}{M_W}\left(\frac{1-y_w}{y_w}\right) = \frac{\rho_{\sigma c}}{\rho_{\sigma w}}. \tag{C.2}$$

Analogously we obtain,

$$\frac{M_C}{M_W}\left(\frac{x_c}{1-x_c}\right) = \frac{\rho_{ac}}{\rho_{aw}}. \tag{C.3}$$

We need then, two equations in order to find the pairs of densities $\{\rho_{\sigma c}, \rho_{\sigma w}\}$, and $\{\rho_{ac}, \rho_{aw}\}$. They are given by

$$\rho_{\sigma c} + \rho_{\sigma w} = \rho_{\sigma}, \tag{C.4}$$
$$\rho_{ac} + \rho_{aw} = \rho_{a}, \tag{C.5}$$

where ρ_σ (ρ_a) stands for the density of the supercritical fluid (aqueous) phase at the reservoir conditions. From Eqs. (C.2), (C.3), (C.4), and (C.5) we obtain the relations

$$\rho_{\sigma c} = \frac{\rho_\sigma}{1 + \frac{M_W}{M_C}\left(\frac{y_w}{1-y_w}\right)}, \tag{C.6}$$
$$\rho_{ac} = \frac{\rho_a}{1 + \frac{M_W}{M_C}\left(\frac{1-x_c}{x_c}\right)}. \tag{C.7}$$

The mixture densities ρ_σ and ρ_a can be found using the Soave-Redlich-Kwong equation of state (Soave [80]):

$$P = \frac{RT}{\upsilon - b} - \frac{a(T)}{\upsilon(\upsilon + b)}, \tag{C.8}$$

where R is the universal gas constant; the parameters a and b capture the effect of intermolecular attraction and repulsion, respectively. For pure components they are given by

$$b = 0.08664(RT_c)/P_c,$$
$$a(T) = 0.42747\alpha(T)(RT_c)^2/P_c,$$
$$\alpha(T) = (1 + \kappa(1 - \sqrt{T_r}))^2,$$

where

$$\kappa = 0.48 + 1.574\omega - 0.176\omega^2, \tag{C.9}$$

In equation (C.9), P_c and T_c are the critical pressure and temperature and and T_r is the reduced temperature, simply given by T/T_c. Soave (1979) suggested an alternative form for the temperature dependence of the attraction term $\alpha(T)$ of the SRK EOS in order to improve vapor-liquid equilibria and vapor pressure calculations of systems exhibiting strong polar effects, such as the CO_2/water mixture. This extension is commonly called MSRK EOS (the M stands for modified). In this work we use this modification. The alternative form mentioned above is given by

$$\alpha(T) = 1 + (1 - T_r)\,(m + n/T_r)\,,$$

where m and n are empirically-found constants for each component. The numerical values for these constants were taken from the compilation by Sandarusi et al. [74]. This EOS can be used for either liquid and gaseous phases. It may be used to calculate properties for extreme conditions, *i.e.*, supercritical conditions. It can also be used for mixtures, but appropriate modifications must be included:

$$b = \sum \xi_i b_{ii}, \tag{C.10}$$

$$a(T) = \sum\sum \xi_i \xi_k a_{ik}(T). \tag{C.11}$$

Repeated indices denote pure component parameters; the letter ξ stands for the molar fractions of the corresponding phase to be studied. In the case of the CO_2-H_2O system we put,

$$a_{12}(T) = a_{21}(T) = (a_{11}(T)a_{22}(T))^{1/2}(1-k_{12}). \tag{C.12}$$

The parameter k_{12} is found from experimental data fitting. Let υ^σ and υ^a denote the molar volumes of the supercritical fluid and aqueous phases repectively. It is easily verified that

$$\upsilon^\sigma = \frac{M_C + y_w(M_W - M_C)}{\rho_\sigma}, \tag{C.13}$$

$$\upsilon^a = \frac{M_W + x_c(M_C - M_w)}{\rho_a}. \tag{C.14}$$

In order to obtain υ^σ we must solve the MSRK EOS for the CO_2-H_2O system, as a cubic equation in the molar volume:

$$\upsilon^3 - \upsilon^2\left(\frac{RT}{P}\right) - \upsilon\left(\frac{RTb}{P} - \frac{a(T)}{P} + b^2\right) - \left(\frac{a(T)b}{P}\right) = 0. \tag{C.15}$$

The UCEP (Upper Critical End Point) of the CO_2-H_2O system (31.48°C and 74.11 [bar], Wendland et al. [95]) is close to the critical point for pure CO_2 (30.978 ± 0.015°C and 73.773 ± 0.003 [bar] from Span and Wagner [81]). Thus for the reservoir conditions we expect equation (C.15) to have only one root when calculating the molar volume of the supercritical fluid phase. Therefore we can also use the alternative for Cardan's metod for solving the cubic proposed by Nickalls [54] for finding this root. For applying the modifications concerning two-component mixtures, as in our case $y_w \ll 1$ we can make the simplifying assumption $y_w = 0$ in the mixing rules (C.10), (C.11). The values for m and n for each component were provided by Sandarusi et al. [74], see Table B.2. Furthermore, we found the value of ρ_a and υ^a extrapolating experimental values as the ones available in [24]. This was done numerically with Matlab® by performing an orthogonal regression.

For the numerical values of x_c, y_w, υ^σ, υ^a, ρ_σ, ρ_a, $\rho_{\sigma c}$, $\rho_{\sigma w}$, ρ_{ac}, ρ_{aw}, in the tp configuration, which were found by following the procedure above, see Table B.3. The numerical values for the MSRK constants corresponding to pure CO_2 and pure H_2O can also be found in this table.

In order to find the constant value of $\rho_{\sigma C}$, we use the MSRK EOS for pure CO_2 to find the value of the molar volume of pure carbon dioxide, υ_C^σ at the reservoir conditions. Notice now that $\rho_{\sigma C} = M_C/\upsilon_C^\sigma$.

Let's see now how to find the constant value of $\rho_{\sigma W}$. The mixing rules for the supercritical fluid phase are

$$\frac{\rho_{\sigma c}}{\rho_{\sigma C}} + \frac{\rho_{\sigma w}}{\rho_{\sigma W}} = 1, \qquad \rho_{\sigma w} + \rho_{\sigma c} = \rho_{\sigma}. \tag{C.16}$$

In Eq. $(C.16.a)$, $\rho_{\sigma W}$ is the density of pure water vapor in the supercritical fluid phase; this is an artificially introduced variable: it would be the density of the supercritical fluid phase if no solvent (*i.e.*, carbon dioxide) were to be present, but only solute (*i.e.*, H_2O). From these mixing rules we obtain

$$\rho_{\sigma W} = \frac{\rho_{\sigma C}\rho_{\sigma w}}{\rho_{\sigma w} + \rho_{\sigma C} - \rho_{\sigma}}. \tag{C.17}$$

The numerical value of $\rho_{\sigma W}$ is quite surprising; in fact, it has been introduced in order to obtain a consistent thermodynamic model for the supercritical fluid phase. Moreover, is greater than the density of pure water vapor ρ_{gW}! It can be found for the reservoir conditions using the MSRK EOS for pure H_2O.

For finding the numerical value of ρ_{aC}, we may proceed analogously as was done for finding $\rho_{\sigma W}$. The mixing rules for the aqueous phase are

$$\frac{\rho_{ac}}{\rho_{aC}} + \frac{\rho_{aw}}{\rho_{W}} = 1, \qquad \rho_{aw} + \rho_{ac} = \rho_{a}. \tag{C.18}$$

In Eq. $(C.18.a)$, ρ_{aC} is the density of pure carbon dioxide in the aqueous phase; it corresponds to the density of the aqueous phase if no solvent (*i.e.*, water) were to be present, but only solute (*i.e.*, CO_2). From these mixing rules we obtain

$$\rho_{aC} = \frac{\rho_{W}\rho_{ac}}{\rho_{ac} + \rho_{W} - \rho_{a}}. \tag{C.19}$$

For the numerical values of $\rho_{\sigma C}$, $\rho_{\sigma W}$, ρ_{gW} and ρ_{aC} in the tp configuration see Table $B.3$.

C.1 Ideal and Real Mixing

Consider a closed homogeneous multicomponent thermodynamic system (i.e, displaying uniform physical properties throughout, such as a well stirred single-phase fluid, e.g. a CO_2-rich supercritical fluid phase), composed of N chemical components each with n_i number of moles, where $i = 1,\ldots,N$, and let $n_{\mathrm{T}} = \sum_i n_i$ denote the total number of moles in the system.

The molar volume of the mixture at ideal conditions (very low pressures, and large volumes), denoted as $v_{\mathrm{ideal}}^{\mathrm{mix}}$ [m^3/mol] can be calculated by the weighted average of the pure molar volumes of the different components

$$v_{\mathrm{ideal}}^{\mathrm{mix}} = \sum_i \xi_i v_i^{\mathrm{pure}}. \tag{C.20}$$

where $\xi_i = n_i/n_\mathrm{T}$ and v_i^{pure} is the molar volume of pure component i.

Notice that multiplying Eq. (C.20) by n_T we obtain the alternative form

$$V_{\mathrm{ideal}}^{\mathrm{mix}} = \sum_i V_i, \tag{C.21}$$

where $V_{\mathrm{ideal}}^{\mathrm{mix}}$ is the volume of the total system in ideal conditions, and V_i is the volume that the n_i moles of component i occupy in the system. Intuitively, at ideal conditions, the molecules do not "see" each other and thus occupy exclusive volumetric space. Equations (C.20) and (C.21) are called *ideal mixing* rules.

Let M_i denote the molar weight of component i, and $m_i = M_i n_i$ be the mass of component i in the system. Then from Eq. (C.21) we obtain after simple calculations

$$1 = \sum_i \frac{\rho_i}{\rho_I} \tag{C.22}$$

where $\rho_i = m_i/V_{\mathrm{ideal}}^{\mathrm{mix}}$, and $\rho_I = m_i/V_i$. Then intuitively, ρ_i is the *partial density* (also called mass concentration) of component i in the system, and ρ_I is the pure density of component i. This is the form of the mixing rule used in this work.

In real conditions, the ideal mixing rules (C.20) and (C.21) do not hold exactly. Indeed, at high pressures and small volumes, the molecules of different components in a mixture "share" common space. In this case, the molar volume of the system, denoted as $v_{\mathrm{real}}^{\mathrm{mix}}$ is given by the weighted average of the apparent (or *real*) molar volumes $\hat{v}_i$ of the components in the mixture:

$$v_{\mathrm{real}}^{\mathrm{mix}} = \sum_i x_i \hat{v}_i, \tag{C.23}$$

Equation (C.23) is the *real mixing* rule for the system.

Appendix D
Quick Thermo Calculations

In order to derive straightforward methods for calculating approximations to the thermodynamic equilibrium of the CO_2-H_2O system at supercritical conditions, we can use basic thermodynamic principles such as Henry's Law, Raoult's Law, and Clausius-Clapeyron's Law. To calculate P-V-T values of the system, we choose an adequate Equation of State (EOS) that takes into account the binary interaction parameters between carbon dioxide and water, which are appropriate for prediction of the physical properties at supercritical conditions, even for two or more component mixtures. Assumptions such as ideal mixing rules (*i.e.*, volume conservation principles) may be used as a simplifying but good approximation. The generic procedure explained below can be used to calculate approximations to the thermodynamic equilibrium of an arbitrary gas species with water, using appropriate numerical values for Henry's constants (see [75]) for an extensive compilation of these constants).

Carbon capture and sequestration projects have raised interest in thermodynamic computations of complex processes that may include chemical reactions, e.g. the acidification and carbonation of the native brine, caused by the injected CO_2.

The method described below provides good qualitative data for finding analytical solutions of mixed CO_2-H_2O injection in porous media. The first version of the Matlab® package designed for finding the fundamental waves presented in Chapter 6 used the thermodynamic equilibrium data found using the *Quick Thermo* method. Numerical deviations of predicted high pressure phase equilibria data relative to experimental measurements affect quantitatively, rather than qualitatively, the computation of the wave curves found in Chapters 6 and 8, and which are used for the application of the wave-curve method (for a detailed description of this method see [2]).

D.1 Description of the Method

Raoult's Law states a relationship between the vapor pressure of pure water P_{gW}, and its partial vapor pressure P_{gw} in the gaseous phase

$$P_{gw} = x_w P_{gW}, \tag{D.1}$$

where x_w denotes de molar fraction of water in the aqueous phase. For the value of the pure vapor pressure P_{gW} we use the Clausius-Clapeyron Law

$$P_{gW} = p_{at} e^{-\frac{M_W}{R}\Lambda_W(T_b^W)\left(1/T - 1/T_b^W\right)}, \tag{D.2}$$

where $\Lambda_W(T_b^W)$ denotes the evaporation heat of water at its stantard boiling temperature $T_b^W \equiv 373.15\ K$, and p_{at} denotes the atmospheric pressure; for their numerical values see Table B.2 in Appendix B.

For the CO_2-H_2O system at supercritical conditions we assume that the partial vapor pressure of water denoted by $P_{\sigma w}$ can be approximated by P_{gw}.

Henry's Law is used for finding the concentration of a gas dissolved in the liquid in which it is in thermodynamic equilibrium, from its partial pressure in the gaseous phase

$$P_{gc} = y_c P_{res} \tag{D.3}$$

$$= \frac{\rho_{ac}}{M_C}\, k_c^{T_{res}}, \tag{D.4}$$

where Henry's coefficient is approximated by

$$k_c^{T_{res}} = k_c^{T_\theta} e^{-C\left(1/T - 1/T_\theta\right)}. \tag{D.5}$$

The term y_c in Eq. (D.3) corresponds to the molar fraction of carbon in the gas, and P_{res} is the overall reservoir pressure assumed to be constant. We assume that the partial vapor pressure of carbon $P_{\sigma c}$, can be approximated by P_{gc}. The term $k_c^{T_\theta}$ $[\frac{\mathrm{m}^3\cdot\mathrm{Pa}}{\mathrm{mol}}]$ is Henry's coefficient found experimentally at the reference temperature $T_\theta = 298.15\ [K]$ and $C \equiv \Delta H/R$, where ΔH [J/mol] is the molar enthalpy of the solution. For carbon dioxide, $C = 2400\ [K]$. For the numerical value of $k_c^{T_\theta}$ corresponding to carbon dioxide see Table B.2 in Appendix B.

We assume the ideal mixing rules for the aqueous phase

$$\frac{\rho_{ac}}{\rho_{aC}} + \frac{\rho_{aw}}{\rho_W} = 1 \qquad \rho_{ac} + \rho_{aw} = \rho_a, \tag{D.6}$$

where ρ_{ac} and ρ_{aw} are the partial densities of CO_2 and H_2O in the aqueous phase. The artificially introduced unknown ρ_{aC} represents the density of the aqueous solution if it were only composed of carbon dioxide. The density of the aqueous phase, ρ_a can be found approximately using the polar version of the Soave-Redlich-Kwong equation, known as MSRK (the M stands for modified), proposed by Sandarusi et al [74], using the mixing assumption (supported by the experimental data presented in [5]) $x_c \ll 1$; the details of this procedure can be found in Appendix C. Alternatively, we can find ρ_a by extrapolating experimental values as the ones available in [24].This is done numerically with Matlab®

by performing an orthogonal regression. We choose the second possibility, as it fits well with experimental values.

It is straightforward to verify that (see (C.3))

$$\rho_{ac} = \frac{x_c}{x_w}\frac{M_C}{M_W}\rho_{aw}, \tag{D.7}$$

which implies

$$x_c = \frac{M_W \rho_{ac}}{M_W \rho_{ac} + M_C \rho_{aw}}, \tag{D.8}$$

where x_c is the molar fraction of CO_2 in the aqueous phase. We assume that the sum of the partial vapor pressures in the supercritical fluid phase $P_{\sigma c}$ and $P_{\sigma w}$ is equal to the reservoir pressure P_{res}. Using this hypothesis and the relations (D.6)-(D.8) above, after some calculations we obtain the non-linear system for the unknowns ρ_{ac} and ρ_{aC}

$$a\rho_{ac}^2 - b\rho_{ac} + c = 0 \tag{D.9}$$

$$\rho_{aC} = \rho_W \left(\frac{\rho_{ac}}{\rho_{ac} + \rho_W - \rho_a} \right), \tag{D.10}$$

where the coefficients of Eq. (D.9) are

$$\begin{aligned} a &= \frac{k_c^{res}}{M_C}\left(M_W \rho_{aC} - M_C \rho_W\right) \\ b &= P_{gW} M_C \rho_W - k_c^{res} \rho_{aC} \rho_W + P_{res}(M_W \rho_{aC} - M_C \rho_W) \\ c &= (P_{gW} - P_{res}) M_C \rho_{aC} \rho_W . \end{aligned}$$

We solve the system of nonlinear equations (D.9) and (D.10) using Matlab® fsolve function. We can proceed now to calculate the remaining unknowns, *i.e.*, ρ_{aw}, (using (D.6.b)), $P_{\sigma w}$ (one may use Raoult's Law (D.1), Eq. (D.8) and the identity $x_c + x_w = 1$; rather we use Henry's Law (D.4) to approximate $P_{\sigma c}$). We calculate the concentrations of carbon dioxide and water in the supercritical fluid phase $\rho_{\sigma c}$ and $\rho_{\sigma w}$ in a three-step procedure. First, from (D.3) we can find y_c and y_w. Second, from the MSRK EOS we find the molar volume υ_σ, and subsequently the phase density ρ_σ; for the details of this procedure see Appendix C. Using Eq. (C.6), we find the partial density $\rho_{\sigma c}$, and from Eq. (C.4) we obtain $\rho_{\sigma w}$. The pure supercritical CO_2 density $\rho_{\sigma C}$ can be found by using the MSRK EOS for pure carbon dioxide to find the corresponding molar volume $\upsilon_{\sigma C}$. The artificially introduced density $\rho_{\sigma W}$ is found using the mixing rule $C.16.a$.

In the figures below we show the most relevant results of the Quick thermodynamic calculations for the two-phase equilibria of carbon dioxide and water. The mutual solubilities of CO_2 and H_2O in the aqueous and supercritical fluid phase, x_c and y_w, are depicted in Fig. D.1. Next, in Fig. D.2.a and Fig. D.2.b we show the partial concentrations ρ_{ac} and $\rho_{\sigma w}$; the supercritical fluid composition $\psi_{\sigma c}$, Fig. D.3.a and the aqueous composition

ψ_{aw}, Fig. D.3.b, establish boundaries for regions of single phase equilibria. Finally, in Fig. D.4, we see the results for $\rho_{\sigma C}$, ρ_{aC} and $\rho_{\sigma W}$.

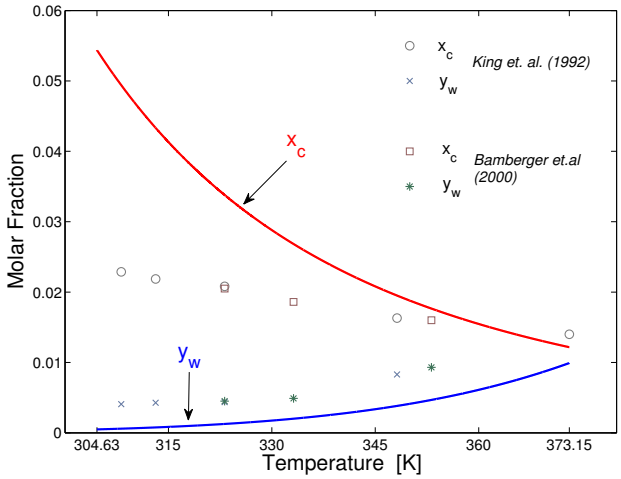

Fig. D.1 Mutual solubilities of the CO_2-H_2O system at $P = 10.09\ MPa$ from the range of values starting from the upper critical temperature $T_{ucep} = 304.63\ [K]$ of the CO_2-H_2O system (See [95]) and ending in the boiling temperature of water at normal atmospheric pressure $T_b^W = 373.15\ [K]$, found with the method above. We also show the experimentally found discrete values given by King et al (1992) [33] and Bamberger et al (2000) [5]. The measurements in [33] are performed at 10.13 MPa.

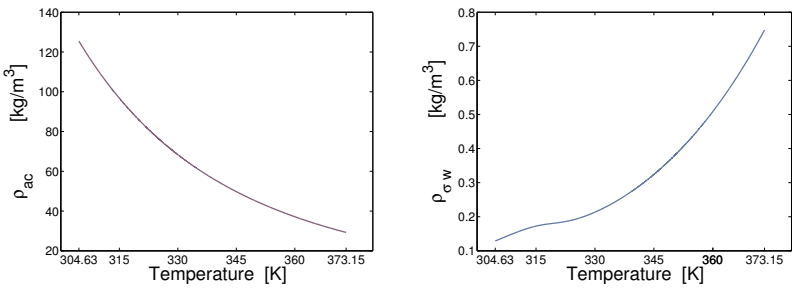

Fig. D.2 Left: Partial concentration of carbon dioxide dissolved in the aqueous phase at different temperatures, and at constant pressure $P = 10.09\ MPa$. Right: Partial concentration of water dissolved in the supercritical fluid at different temperatures, and constant pressure $P = 10.09\ MPa$.

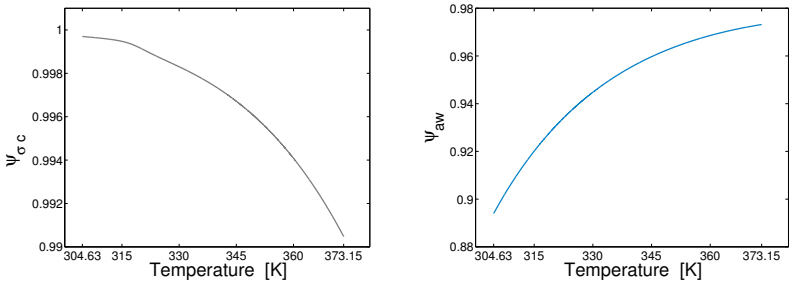

Fig. D.3 Left: Supercritical fluid phase composition $\psi_{\sigma w}$. Right: Aqueous phase composition ψ_{aw}.

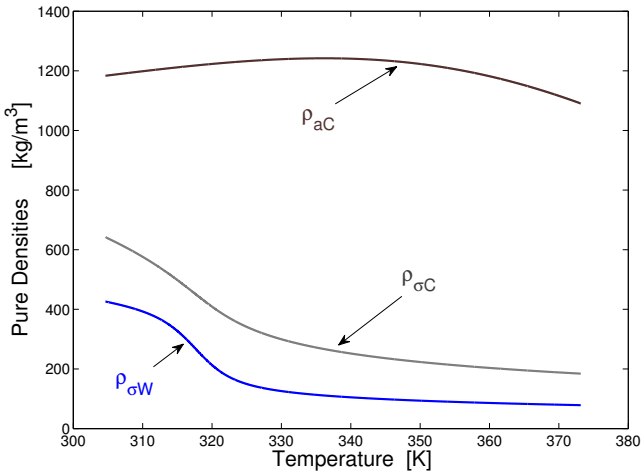

Fig. D.4 Pure supercritical CO_2 density as calculated from the MSRK EOS [74], and the artificially introduced pure densities ρ_{aC} and $\rho_{\sigma W}$.

Appendix E
Analytical expressions for the model

E.1 Vertical Migration

In this section we include auxiliary expressions appearing in the model for vertical migration (Chapter 3):

$$
\begin{aligned}
n_1 &= f^+(\rho^+_{\sigma c} - \rho^+_{ac}) + \rho^+_{ac} \\
d_1 &= s^+(\rho^+_{\sigma c} - \rho^+_{ac}) + \rho^+_{ac} - \rho^-_{\sigma c} \\
n_2 &= f^+(\rho^+_{\sigma w} - \rho^+_{aw}) + \rho^+_{aw} \\
d_2 &= s^+(\rho^+_{\sigma w} - \rho^+_{aw}) + \rho^+_{aw} - \rho^-_{\sigma w} \\
d_3 &= s^+(\rho^+_{\sigma c} - \rho^+_{ac}) + \rho^+_{ac} - \rho^-_{ac} \\
d_4 &= s^+(\rho^+_{\sigma w} - \rho^+_{aw}) + \rho^+_{aw} - \rho^-_{aw} \\
g_1 &= f^+ g^*(\rho^+_{\sigma c} - \rho^+_{ac}) \\
g_2 &= f^+ g^*(\rho^+_{\sigma w} - \rho^+_{aw}) \\
g^* &= k m^+_a (\rho_a - \rho_\sigma) g_\beta .
\end{aligned}
$$

E.2 Details for the Riemann Solution: Slanted Isothermal Flow

E.2.1 Case $\beta = 0$

We can look for a point $W^{\text{TP},\alpha}$ (where $\alpha = \in, \ni$) in the tp-configuration as in (3.46) where the Buckley-Leverett characteristic speed coincides with the discontinuity speed v_α, *i.e.*,

$$
f'(s^{\text{TP},\alpha}) = \frac{f^{\text{TP},\alpha} - C_\alpha}{s^{\text{TP},\alpha} - C_\alpha}. \tag{E.1}
$$

We solve Eq. (E.1) writing it as a 4-th degree polynomial in $s := s_\sigma$:

$$\mathbb{P}_e(s, C_\alpha) = a_4 s^4 + a_3 s^3 + a_2 s^2 + a_1 s + a_0,$$

whose coefficients depend on C_α:

$$\begin{aligned}
a_4 &= \big(C_\sigma + C_a\big)\big(C_\sigma - C_\alpha(C_\sigma + C_a)\big) \\
a_3 &= 4C_\alpha C_a(C_\sigma + C_a) \\
a_2 &= -C_a\,(C_\sigma + 4C_\alpha C_\sigma + 6C_\alpha C_a) \\
a_1 &= 2C_\alpha C_a(C_\sigma + 2C_a) \\
a_0 &= -C_\alpha C_a^2,
\end{aligned}$$

where $C_\sigma = 0.95/\mu_\sigma$, $C_a = 0.5/\mu_a$.

E.2.2 Case $\beta = \pi/2$

In this case, the coincidence between the characteristic speed in the tp configuration, *i.e.*, the derivative of the fractional flow with gravity function, and the speed of the discontinuity betweeen regions can be written as

$$\mathrm{F}'(s^{\mathrm{TP},\alpha}) = \frac{\mathrm{F}(s^{\mathrm{TP},\alpha}) - \big(u^{\mathrm{TP}}/\varphi\big)C_\alpha}{\big(s^{\mathrm{TP},\alpha} - C_\alpha\big)}, \tag{E.2}$$

where $\alpha = \mathrm{c}, \mathrm{e}$.

Equation (E.2) can be written in the form

$$u^{\mathrm{TP}} = \frac{(fg^*)^{\mathrm{TP},\alpha} - \big(\frac{d}{ds}(fg^*)\big)^{\mathrm{TP},\alpha} \times (s^{\mathrm{TP},\alpha} - C_\alpha)}{\left(\big(\frac{d}{ds}f\big)^{\mathrm{TP},\alpha} \times (s^{\mathrm{TP},\alpha} - C_\alpha)\right) - (f^{\mathrm{TP},\alpha} - C_\alpha)}. \tag{E.3}$$

For the vapor-liquid displacement problem we know that

$$u^{\mathrm{TP}} = \frac{u^{\mathrm{L}}\rho^{\mathrm{L}}_{\sigma c} - g_1 + \big(\frac{d}{ds}(fg^*)\big)^{\mathrm{TP},\mathrm{e}} d_1}{n_1 - \big(\frac{d}{ds}f\big)^{\mathrm{TP},\mathrm{e}}}. \tag{E.4}$$

From equations (E.3) for $\alpha = \mathrm{e}$ and (E.4) we obtain the non-linear equation (which is in fact a polynomial!) in $s := s_\sigma$

$$\mathbb{T}_{\mathrm{e}}(s,u^{\mathrm{L}},\rho^{\mathrm{L}}_{\sigma c}) = \left((fg^*)^{\mathrm{TP},\alpha} - \left(\frac{d}{ds}(fg^*)\right)^{\mathrm{TP},\alpha} \times (s^{\mathrm{TP},\alpha} - C_\alpha)\right)\left(n_1 - \left(\frac{d}{ds}f\right)^{\mathrm{TP},\mathrm{e}}\right) - \left(u^{\mathrm{L}}\rho^{\mathrm{L}}_{\sigma c} - g_1 + \left(\frac{d}{ds}(fg^*)\right)^{\mathrm{TP},\mathrm{e}} d_1\right)\left(\left(\frac{d}{ds}f\right)^{\mathrm{TP},\alpha} \times (s^{\mathrm{TP},\alpha} - C_\alpha) - (f^{\mathrm{TP},\alpha} - C_\alpha)\right) = 0. \tag{E.5}$$

In the vapor-liquid displacement problem, we look for a zero of $\mathbb{T}_{\mathrm{e}}$ inside of the interval $[0,1]$ such that the construction of the Riemann problem satisfies Oleinik entropy condition. Using the result, $s^{\mathrm{TP},\mathrm{e}}$, we use Eq. (E.3) or (E.4) to find u^{TP}.

The wave that follows in the construction is a s_σ-rarefaction along the fractional flow with gravity, ending at the first point $s^{\mathrm{TP},\mathrm{C}}$ where condition (E.2) is satisfied, for $\alpha = \mathrm{C}$ and $C_{\mathrm{C}} = C_{\mathrm{C}}(\rho^{\mathrm{R}}_{aw})$. The saturation $s^{\mathrm{TP},\mathrm{C}}$ is found by solving Eq. (E.3) for $s^{\mathrm{TP},\mathrm{C}}$, setting $\alpha = \mathrm{C}$, $C_{\mathrm{C}} = C_{\mathrm{C}}(\rho^{\mathrm{R}}_{aw})$ and using the value of u^{TP} previously calculated. In other words, we find the zeros of a polynomial equation $\mathbb{Q}_{\mathrm{C}}(\cdot, u^{\mathrm{TP}})$ in $s = s_\sigma$ (found after some calculations on Eq. (E.3)) inside of the interval $[0,1]$ and choose the root satisfying the requirements.

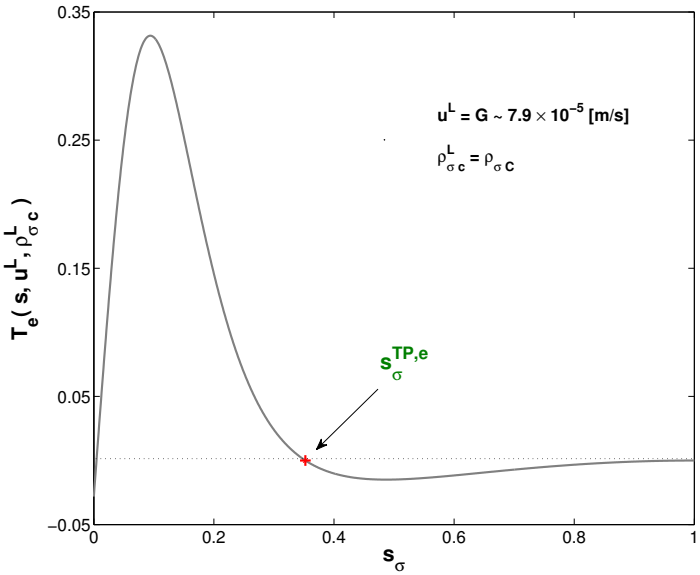

Fig. E.1 Plot of $\mathbb{T}_{\mathrm{e}}$. The largest zero corresponds to $s^{TP,\mathrm{e}}_\sigma$. For this example $u^{\mathrm{L}} = G$, where G is the mean ascent velocity for our problem, defined in Section 3.4 of Chapter 3.

From the value of u^{TP}, $s^{\mathrm{TP},c}$ and ρ^{R}_{aw} we can find u^{R} using Eq. (3.28) in the form

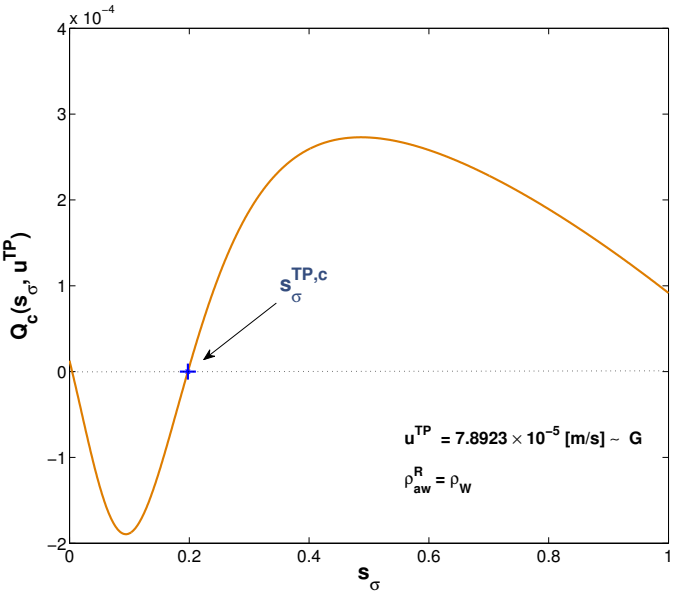

Fig. E.2 Plot of $\mathbb{Q}_{\mathrm{c}}$. The largest zero corresponds to $s_{\sigma}^{TP,\mathrm{e}}$. For this example $u^{\mathrm{L}} = G$, where G is the mean ascent velocity for our problem, defined in Section 3.4 of Chapter 3, see also Table B.2 in Appendix B.

$$u^{\mathrm{R}} = \frac{u^{\mathrm{TP}}\left(n_2 - \left(\frac{d}{ds}f\right)^{\mathrm{TP,C}} d_4\right) + g_2 - \left(\frac{d}{ds}\left(fg^*\right)\right)^{\mathrm{TP,C}} d_4}{\rho_{aw}^{\mathrm{R}}} \tag{E.6}$$

In Figures E.1-E.2 we show the plot of $\mathbb{T}_{\mathrm{e}}$ and $\mathbb{Q}_{\mathrm{c}}$ as functions of s_σ, together with the values of $s_\sigma^{\mathrm{TP,e}}$ and $s_\sigma^{\mathrm{TP,C}}$ found for the vapor-liquid displacement problem given by $\rho_{\sigma c}^{\mathrm{L}} = \rho_{\sigma C}$ with injection velocity $u^{\mathrm{L}} \equiv G$, and $\rho_{aw}^{\mathrm{R}} = \rho_W$.

References

1. Arnold, K., Gosling, J., Holmes, D.: The Java Programming Language 4th Ed. Prentice Hall (2005)
2. Azevedo, A., de Souza, A., Furtado, F., Marchesin, D., Plohr, B.: The Solution by the Wave Curve Method of Three-Phase Flow in Virgin Reservoirs. Transport in Porous Media **83**(1), 99-125 (2010)
3. Bachu, S.: Sequestration of CO_2 in geological media in response to climate change: road map for site selection using the transform of the geological space into CO_2 phase space. Energy Conversion and Management **35**, 87-102 (2002)
4. Baker, L.E., Pierce, A.C., Luks, K.D.: Gibbs Energy Analysis of Phase Equilibria. SPE Journal **22**, 731-742 (1982)
5. Bamberger, A., Sieder, G., Maurer, G.: High-pressure (vapor liquid) equilibrium in binary mixtures of (carbon dioxide water or acetic acid) at temperatures from 313 to 353 K. J. Supercritical Fluids **17**(2), 97-110 (2000)
6. Beattie, J. A.: The Computation of The Thermodynamic Properties of Real Gases And Mixtures Of Real Gases, Symposium on Thermodynamics and Molecular Structure of Solutions. 114th Meeting of the American Chemical Society, Portland, Oregon, Sept. 13-14 (1948)
7. Beek, W. J., Mutzall, M. K.: Transport Phenomena. Wiley, New York (1975)
8. Bird, R. B., Stewart, W. E., Lightfoot, E. N.: Transport Phenomena, Wiley, New York (1960)
9. Boor, C. de: A Practical Guide to Splines. Springer-Verlag (1978)
10. Bruining, J., Marchesin, D.: Analysis of Nitrogen and steam injection in a porous medium with water. Transport in Porous Media **62**(3), 251-281 (2006)
11. Bruining, J., Marchesin, D.: Maximal oil recovery by simultaneous condensation of alkane and steam. Physical Review E, Statistical, Nonlinear and Soft Matter Physics **3**, 036312 (2007)
12. Bruining, J., Marchesin, D., Van Duijn, C. J.: Steam injection into water-saturated porous rock, Comput. App. Math. **22**(3), 359-395 (2003)
13. Buckley, S.E., Leverett, M.C.: Mechanism of fluid displacement in sands. Trans AIME **146**, 107-116 (1942)
14. Dafermos, C.: Hyperbolic Conservation Laws in Continuum Physics, 3rd Edition, Springer, Heidelberg (2010)
15. Dahl, S., Michelsen, M.: High-pressure vapor-liquid equilibrium with a UNIFAC-based equation of state. AIChE journal **36**(12), 1829-1836 (1990)
16. Darcy, H.: Les Fountaines Publiques de la Ville de Dijon. Dalmont, Paris (1856)
17. http://www.dofmaster.com/steam.html
18. Eftekhari, A.A., Bruining, J., Wahanik, H., Marchesin, D.: CO2 Injection in Sub-salt Water Layers at 7000m Depth. SPE Reservoir Simulation Symposium, The Woodlands, Texas, USA, 21-23 Feb (2011)

19. Farajzadeh, P.R., Zitha, P.L.L., Bruining, J.: The effect of heterogeneity on the character of density-driven natural convection of CO2 overlying a brine layer. Proceedings: Canadian Unconventional Resources and International Petroleum Conference. 19-21 Oct. Calgary, Alberta, Canada. 19-21 Oct, SPE 138168 (2010)
20. Fenghour, A., Wakeham, W.A., Vesovic, V.: The Viscosity of Carbon Dioxide. Journal of Physical and Chemical Reference Data **27**, 31-44 (1998)
21. Fermi, E.: Thermodynamics. Dover Publication Inc (1956)
22. Furtado, F.: Structural Stability of Nonlinear waves for conservation laws. PhD. Thesis, Courant Institute of Mathematical Sciences, NYU, October (1989)
23. Gibbs, J.W.: Scientific Papers. Longmans, Green and Company, New York **I**, 155-8 (1906)
24. Gmelin Inst. for Inorganic Chemistry of the Max-Planck-Society for the Advancement of Science, Founded by: Gmelin, L.: Gmelin Handbook of Inorganic and Organometallic Chemistry, Elservier (1772-1995)
25. Hayek, M., Mouche, E., Mügler, C.: Modeling vertical stratication of CO2 injected into a deep layered aquifer, Advances in Water Resources **32**, 450-462 (2009)
26. Hebach, A., Oberhof, A., Dahmen, N.: Density of water + carbon dioxide at elevated pressures: measurements and correlation. J. Chem. Eng. Data **49**(4), 950-953 (2004)
27. Holloway, Sam: Carbon dioxide capture and geological storage. Phil. Trans. R. Soc. A **365**, 1095-1107 (2007)
28. Huang, H., Sandler, S.: Prediction of vapor-liquid equilibria at high pressures using activity coefficient parameters obtained from low-pressure data: a comparison of two equation of state mixing rules. Industrial & Engineering Chemistry Research **32**(7), 1498-1503 (1993)
29. Huron, M., Vidal, J.: New mixing rules in simple equations of state for representing vapour-liquid equilibria of strongly non-ideal mixtures. Fluid Phase Equilibria **3**(4), 255-271 (1979)
30. Isaacson, E., Marchesin, D., Plohr, B.: Transitional Waves for Conservation Laws. Siam, J. Math. Anal. **21**(4), 837-866 (1990)
31. Isaacson, E., Marchesin, D., Plohr, B., Temple, J. B.: Multiphase flow models with singular Riemann problems. Mat. Apl. Comput. **11**(2), 147-166 (1992)
32. Kaasschieter, E.F.: Solving the Buckley Leverett equation with gravity in a heterogeneous porous medium. Computational Geosciences **3**, 23-48 (1999)
33. King M.B., Mubarak A., Kim J.D., Bott T.R.: The mutual solubilities of water with supercritical and liquid carbon dioxide. J. Supercrit. Fluids **5**, 296-302 (1992)
34. Kongsjorden, H., Karstad O., Torp, T.: Saline aquifer storage of carbon dioxide in the Sleipner project. Waste management **17**(5-6), 303-308 (1998)
35. Koschel, D., Coxam, J., Rodier, L., Majer, V.: Enthalpy and solubility data of CO2 in water and NaCl (aq) at conditions of interest for geological sequestration. Fluid Phase Equilibria **247**(1-2), 107-120 (2006)
36. Lake, L. W.: Enhanced Oil Recovery. Prentice Hall (1989)
37. Lambert, W.: Doctoral thesis: Riemann solution of balance systems with phase change for thermal flow in porous media. IMPA, www.preprint.impa.br (2006)
38. Lambert, W., Marchesin, D.: The Riemann problem for compositional flows in porous media with mass transfer between phases. IMPA, www.preprintimpa.br (2009)
39. Lambert, W., Marchesin, D.: The Riemann problem for multiphase flows in porous media with mass transfer between phases. Journal of Hyperbolic Differential Equations **6**(4), 735-751 (2009)
40. Lambert, W., Marchesin, D., Bruining, J.: The Riemann solution for the injection of steam and nitrogen in a porous medium. Transport in Porous Media **81**(3), 505-526 (2010)
41. Lauwerier, H.: The transport of heat in an oil layer caused by the injection of hot fluid. Applied Scientific Research **5**(2), 145-150 (1955)
42. Lax, P.D.: Hyperbolic systems of conservation laws. Comm. Pure Appl. Math. **10**, 537-566 (1957)

43. Lewis, G.N., Randall, M.: Thermodynamics. McGraw-Hill Book Company, Inc., New York (1923)
44. Lide, D.R.: CRC Handbook of Physics and Chemistry. The Chemical Rubber Company, Cleveland, OH (2003)
45. Lima, E.L.: Curso de análise. Rio de Janeiro, IMPA, Projeto Euclides, 10 ed. (2009)
46. Liu, T. P.: The Riemann problem for general 2 X 2 conservation Laws. Transactions of A.M.S., **199**, 89-112 (1974)
47. Liu, T. P.: The Riemann problem for general systems of conservation laws. J. Diff. Equations **18**, 218-234 (1975)
48. Liu, T. P.: The entropy condition and the admissibility of shocks. J. Math. Anal. Appl. **53**, 218-234 (1976)
49. Marchesin, D., Plohr, B.: Wave Structure in WAG Recovery. SPE Journal **6**(2), 209-219 (1999)
50. Michelsen, M.: The isothermal flash problem. Part I. Stability. Fluid Phase Equilibria **9**(1), 1-19 (1982)
51. Michelsen, M.: The isothermal flash problem. Part II. Phase-split calculation. Fluid Phase Equilibria **9**(1), 21-40 (1982)
52. Moore, W.J.: Physical Chemistry. Prentice Hall, (1962)
53. Nichita, D. V., Gomez, S., Luna, E.: Multiphase equilibria calculation by direct minimization of Gibbs free energy with a global optimization method. Computer and Chemical Engineering **26**, 1703-1724 (2002)
54. Nickalls, R. W. D.: A new approach to solving the cubic: Cardan's solution revealed. Mathematical Gazette **77**, 354-359 (1993)
55. Noh, M., Lake, L.W., Bryant, S.L. Araque-Martinez, A.: Implications of Coupling Fractional Flow and Geochemistry for CO_2 Injection in Aquifers. SPE Reservoir Evaluation & Engineering **10**(4), 406-414 (2007)
56. Nordbotten, M., Celia, M., Bachu, S.: Injection and Storage in Deep Saline Aquifers: Analytical Solution for CO_2 Plume Evolution During Injection. Transport in Porous Media **58**, 339-360 (2005)
57. Oleinik, O. A.: On the uniqueness of the generalized solution of the Cauchy problem for a nonlinear system of equations occurring in mechanics. Uspekhi Mat. Nauk **12**, 169-176 (1957)
58. Orbey, H, Sandler, S.: Modeling vapor-liquid equilibria: cubic equations of state and their mixing rules. Cambridge University Press (1998)
59. Orr, F.M., Jr.: Storage of Carbon Dioxide in Geologic Formations. Distinguished Author Series, Journal of Petroleum Technology **56**(9) Sept (2004)
60. Orr, F.M., Jr.: Theory of Gas Injection Processes. Tie-Line Publications (2007)
61. Pèneloux, A., Rauzy Richard, E.: A consistent correction for Redlich-Kwong-Soave volumes. Fluid Phase Equilibria **8**(1), 7-23 (1982)
62. Peng, D.-Y., Robinson, D. B.: A new two-constant equation of state. Ind. Eng. Chem. Fundament. **15**, 59-64 (1981)
63. Prausnitz, J. M., Lichtenthaller, R. N., De Azedevo, E. G.: Molecular Thermodynamics of Fluid Phase Equilibria. Prentice Hall, New York (1986)
64. Pritchett, J.W.: On the relative effectiveness of H_2O and CO_2 as reservoir working fluids for EGS heat mining. Transactions, Geothermal Resources Council **33**, 211-216 (2009)
65. Proskurowski, W.: A note on solving the Buckley Leverett equation in the presence of gravity. J. Computational Physics **41**(1), 136-141 (1981)
66. Pruess, K.: On production behavior of enhanced geothermal systems with CO2 as working fluid. Energy Conversion and Management **49**(6), 1446-1454 (2008)
67. Redlich, O., Kwong, J. N. S.: On the thermodynamics of solutions. V. An equation of state. Fugacities of gaseous solutions. Chem. Rev. **44**, 233-244 (1949)
68. Reinsch, C.: Smoothing by Spline Functions. Numerische Mathematik **10**, 177-183 (1967)

69. Renon, H., Prausnitz, J.: Local compositions in thermodynamics excess functions for liquid mixtures. AIChE journal **14**(1), 135-144 (1968)
70. Renon, H., Prausnitz, J.: Estimation of parameters for the NRTL equation for excess Gibbs energies of strongly nonideal liquid mixtures. Industrial & Engineering Chemistry Process Design and Development **8**(3), 413-419 (1969)
71. Riaz, A., Tchelepi, H.A.: Dynamics of vertical displacement in porous media associated with CO2 sequestration. SPE Journal **13**(3), 305-313 (2008)
72. Riddiford, F., Wright, I., Bishop, C., Espie, T., Tourqui, A.: Monitoring geological storage: the In Salah gas CO2 Storage Project.
73. Rodríguez, P.: Buoyancy Driven Three-Phase Flow in Porous Media. Ph.D Thesis, IMPA (2010)
74. Sandarusi, J. A., Kidnay, A. J., Yesavage, V. F.: Compilation of parameters for a polar fluid Soave-Redlich-Kwong equation of state. Ind. Eng. Chem. Process Des. Dev. **25**(4), 957-963 (1986)
75. Sander, R.: Compilation of Henrys Law Constants for Inorganic and Organic Species of Potential Importance in Environmental Chemistry. Version 3 Webpage http://www.mpch-mainz.mpg.de/ sander/res/henry.html (1999)
76. Shearer, M., Schaeffer, D.G., Marchesin, D., and Paes-Leme, P.J.: Solution of the Riemann Problem for a Prototype $2\times$ 2 System of Non-strictly Hyperbolic Conservation Laws, Arch. Rat. Mech. Anal. **97**, 299-320 (1987)
77. Silin, D., Patzek, T., Benson, M.: A Model of Buoyancy-Driven Two-Phase Countercurrent Fluid Flow. Transp. Porous. Med. **76**, 449-469 (2009)
78. Smith, J.M., Van Ness, H. C. Abbott, Michael, M. Introduction to Chemical Engineering Thermodynamics. 7th ed. McGraw-Hill, Boston (2005)
79. Smoller, J.: Shock Waves and Reaction-Diffusion Equations. Springer-Verlag (1983)
80. Soave, G.: Equilibrium constants from a modified Redlich-Kwong equation of state. Chem. Eng. Sci. **27**(6), 1197-1203 (1972)
81. Span, R., Wagner, W.: A new equation of state for carbon dioxide covering the fluid region from the triple-point temperature to 1100K at pressures up to 800 MPa. J. Phys. Chem. Ref. Data **25**(6), 1509-1596 (1996)
82. Spycher N., Pruess K., Ennis-King J.: CO2-H2O mixtures in the geological sequestration of CO2. I. Assessment and calculation of mutual solubilities from 12 to 100C and up to 600 bar. Geochim. Cosmochim. Acta **67**, 3015-3031 (2003)
83. Spycher N., Pruess K.: CO2-H2O mixtures in the geological sequestration of CO2. II. Partitioning in chloride brines at 12100C and up to 600 bar. Geochimica et Cosmochimica Acta **69**(13), 3309-3320 (2005)
84. Stoer, J., Bulirsch, R.: Introduction to Numerical Analysis. Springer-Verlag, New York (1980)
85. Stroustrup, B.: The C++ Programming Language. Addison-Weasley (1986)
86. Stryjek, R., Vera, J.: PRSV: An improved Peng-Robinson equation of state for pure compounds and mixtures. The Canadian Journal of Chemical Engineering **64**(2), 323-333 (1986)
87. Temple, B.: Systems of conservation laws with coinciding shock and rarefaction waves. Contemporary Mathematics, **17**, 141-151 (1983)
88. Trangenstein, J.A.: Customized minimization techniques for phase equilibrium computations in reservoir simulation. Chem. Eng. Sc. **42**(12), 2847-2863 (1987)
89. Trefethen, L.N., Bau, David III.: Numerical Linear Algebra. SIAM, Philadelphia (1997)
90. Valtz, A., Chapoy, A., Choquelet, C., Paricaud, P., Richon, D.: Vapour-liquid equilibria in the carbon dioxide-water system, measurement and modelling from 278.2 to 318.2 K. Fluid Phase Equilibria **226**, 333-344 (2004)
91. Van Der Waals, J.D.: The equation of state for gases and liquids. Nobel Lectures in Physics 254265 (1910)
92. Wahanik, H., Eftekhari, A., Bruining, J., Marchesin, D., Wolf, K-H.: Analytical solutions for mixed CO2-water injection in geothermal reservoirs. Proceedings: Canadian Unconventional

Resources and International Petroleum Conference. 19-21 Oct. Calgary, Alberta, Canada, SPE 138154 (2010)
93. Walas, S.: Phase equilibria in Chemical Engineering. Butterworth Boston (1985)
94. Welge, H.J.: A simplified method for computing oil recovery by gas or water drive. Trans, 91-98 (1952)
95. Wendland, M., Hasse, H., Maurer, G.: Experimental pressure temperature data on three- and four-phase equilibria of fluid, hydrate, and ice phases in the system carbon dioxide-water. J. Chem. Eng. Data **44**(5), 901-906 (1999)
96. Wendroff, B.: The Riemann problems for materials with non-convex equations of state II. J. Math. Anal. Appl. **38**, 454-466 (1972)
97. Wiebe, R., Gaddy, V.: The solubility in water of carbon dioxide at 50, 75 and 100, at pressures up to 700 atmospheres. Journal of the American Chemical Society **61**(2), 315-318 (1939)
98. Wilson, G.M.: A Modified Redlich-Kwong Equation of State, Application to General Physical Data Calculation. Paper15C, presented at the 1969 AIChE 65th National Mtg., Cleveland, OH (1969)
99. Zweigel, P, Arts, R., Lothe A., Lindeberg, E.: Reservoir geology at the Utsira Formation at the first industrial-scale underground CO2 storage site (Sleipner area, North Sea). Geological storage of carbon dioxide **233**, 165-180 (2004)